공학석사 학위논문

Electrochemical Investigations into the Influence of the Outer Helmholtz Plane towards the Oxygen Reduction Reaction on Non-Precious Metal Catalysts in Alkaline Mediums

알칼리 전해질에서 비귀금속 촉매의

산소환원반응에 대한 외부 헬름홀츠면

영향의 전기화학적 조사

2015년 2월

서울대학교 대학원

공과대학 화학생물공학부

Stanfield Youngwon Lee (이영원)

Abstract

Electrochemical Investigations into the Influence of the Outer Helmholtz Plane towards the Oxygen Reduction Reaction on Non-Precious Metal Catalysts in Alkaline Mediums

Stanfield Youngwon Lee

School of Chemical & Biological Engineering

Seoul National University

The continuous decrease in the amount of fossil fuels combined with the increasing energy demands of our society has fueled the rapid growth in research for alternative energy sources. Although these energy devices possess ample potential to supply these energy demands, most of these devices require rare and/or expensive materials to operate at highly efficient rates. No electrochemical energy device exemplifies this more than fuel cells. Fuel cells, which harness the chemical energy released from redox reactions and converts it to electrical energy, offer a clean, renewable, and non-toxic

energy source and can potentially play a major role in supplying the energy demands of the future. However, the oxygen reduction reaction, which occurs at the cathode, suffers from a high overpotential and is often viewed as the biggest obstacle to fuel cell commercialization. Therefore, research into an affordable and durable catalyst to lower the overpotential and increase the efficiency of fuel cells has been and continues to be a major area of research.

Recent reports have shown metal ions coordinated to nitrogen compounds having high catalytic activity for the oxygen reduction in alkaline mediums. Remarkable, even though heat treatment likely destroys these coordinated structures, improvements in catalytic activity are seen after heat treatment. Although these catalysts provide great promise as an alternative to platinum, the active sites or how the oxygen reduction reaction proceeds remains a mystery. In addition, controversies exist in regards to where the active sites are in these non-precious metal catalysts. Therefore, optimization of these catalysts remains impossible until this information is known.

This work focused on investigating the active site as well as the possible pathways for the oxygen reduction reaction using copper, cobalt, and iron metal phthalocyanines. Due to differing oxygen adsorption energies between these metal ions, different ORR activities were observed. In addition, poisoning experiments showed a significant decrease in activity, further proving that before heat treatment, the M^+-N-C structure is the active site and whether the ORR proceeds via the 2 electron or 4 electron pathway

is dependent on the oxygen adsorption strength.

However, these structures are bound to decompose during heat treatment and, as a result, the ORR pathway likely does not proceed through the same pathway. Electrochemical measurements using LiOH, NaOH, KOH, and CsOH electrolytes were done on the phthalocyanine catalysts before and after heat treatment to confirm this hypothesis. Changes in the ORR activity trends for cobalt and iron phthalocyanine before and after heat treatment show that different pathways are favored. To determine the changes after heat treatment, physical characterization measurements, such as x-ray diffraction (XRD), x-ray photoelectron spectroscopy (XPS), and ultraviolet-visible absorbance (UV-Vis) were conducted. The results of this study show that after heat treatment, oxygen is first converted to a superoxide via the outer Helmholtz plane reaction and is completely reduced at nitrogen doped sites created during heat treatment. These conclusions offer a viable explanation for the high level of activity observed after heat treatment as well as a possibility why this high activity is only observed in alkaline mediums.

Table of Contents

List of Tables

List of Figures

Chapter 1: Introduction

1.1 Fuel Cells

1.1.1 Fuel Cell Fundamentals

Fuel cells are electrochemical devices that operate by converting the chemical energy released from redox reactions occurring at the anode and cathode and converting it into electrical energy. Benefits, such as high efficiency, lack of mechanical parts, use of non-toxic reactants, and production of environmentally friendly byproducts during operation, are the main reasons that fuel cells have been and continue to be one of the most promising alternative energy sources to supply society's growing energy demands.

As shown in figure 1.1, fuel cells, like all electrochemical energy devices, consist of an anode, cathode, electrolyte, and an external circuit.[1] Oxidation of the fuel at one of the electrodes leads to the release of electrons which then travel through the opposite electrode via the external circuit. Meanwhile, the fuel, in its oxidized form, simultaneously diffuses to the opposite electrode, where, along with the electrons, becomes part of the reactants for the reduction reaction. However, fuel cells differ from other devices in that it is a thermodynamically open system. Therefore, whereas closed systems, such as batteries, are limited by the specific capacity of the active material, fuel cells con continuously produce electricity for as long as a continuous supply of fuel is provided.[1]

Due to the performance of fuel cells being linked to many different factors, each type of fuel cell has their own distinct pros and cons. Like the name suggests, high operating temperature fuel cells such as molten
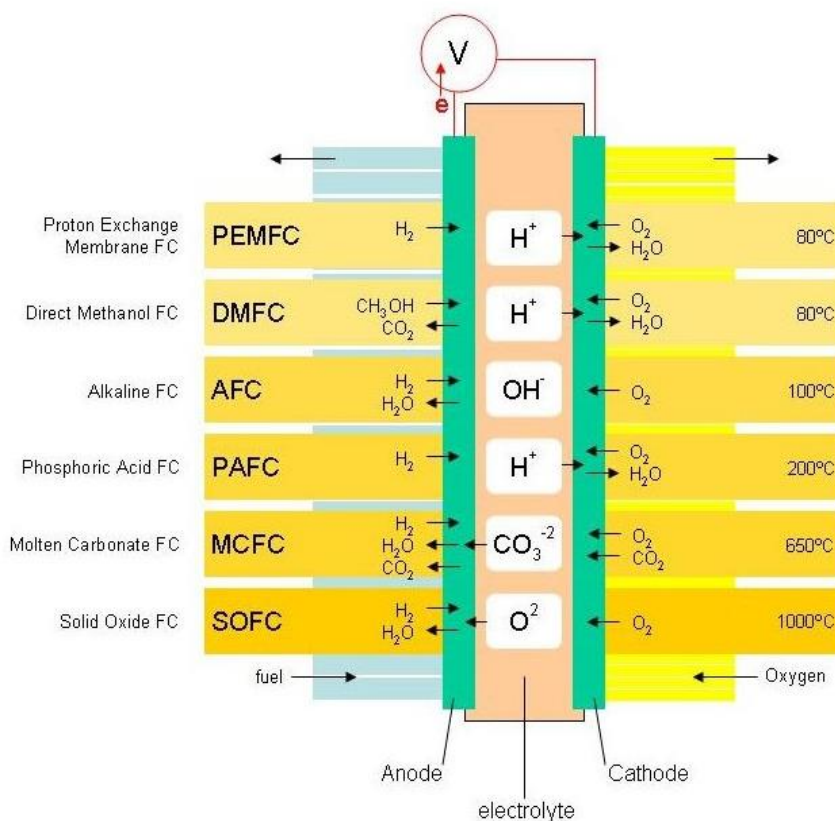
Figure 1.1. Schematic diagram of the operating principles of a fuel cell. Taken from http://www.jobsinfuelcells.com/.

carbonate fuel cells and solid oxide fuel cells, operate at high temperatures, which helps lower the overpotential of the overall process.[2] However, material corrosion/destruction occurs at these high operating temperatures, which leads to durability issues.   On the other hand, low operating temperature fuel cells such as polymer electrolyte membrane fuel cells and phosphoric acid fuel cells offer a less destructive and dangerous environment. However, low operating temperature fuel cells usually require the use of a liquid electrolyte.   Although theoretically, this is not a problem, practical prolonged use can lead to electrolyte leakage/evaporation issues.

1.1.2 Acid vs Alkaline Fuel Cells

Table 1.1 shows the electrochemical reactions that occur at the anode and cathode for polymer electrolyte fuel cells (PEMFC) and alkaline fuel cells (AFC).   Although the half-cell reactions are slightly different, the net reactants, products, and voltage are the same.[3]

Figure 1.2 shows the operating principles of an acidic polymer electrolyte membrane fuel cell (PEMFC).   Hydrogen enters the anode and is oxidized to H^+ ions and electrons.   The electrons are transferred to the cathode through an external circuit connected to an external load, while the H^+ ions reach the cathode by diffusing through the electrolyte.   At the cathode, the ions and electrons combine with oxygen to produce water.   Along with having a high voltage output of 1.2 V, PEMFC's are appealing from a commercial point of view because they operate at low temperatures (approximately 60-70^{0}C) and can operate using a solid electrolyte.   As mentioned above, the use of a liquid electrolyte can lead to leakage and/or evaporation issues after prolonged use.   However, PEMFC's can operate with relatively high efficiency using Nafion (figure 1.3), a solid electrolyte similar in structure to Teflon.   Nafion provides high ionic diffusivity and conductivity for H^+ ions, which in turn, leads to improved overall

Type	Anode Reaction	Standard Potential	Cathode Reaction	Standard Potential	Net Potential
PEMFC	$2H_2 \rightarrow 4H^+ + 4e^-$	0 V	$O_2 + 4H^+ + 4e^- \rightarrow 2H_2O$	1.229 V	1.229 V
AFC	$4OH^- + 2H_2 \rightarrow 2H_2O$	.828 V	$O_2 + 2H_2O + 4e^- \rightarrow 4OH^-$	.401 V	1.229 V

Table 1.1. Comparison of electrochemical reactions occurring at the anode and cathode of PEMFC's and AFC's. Taken from reference [2].
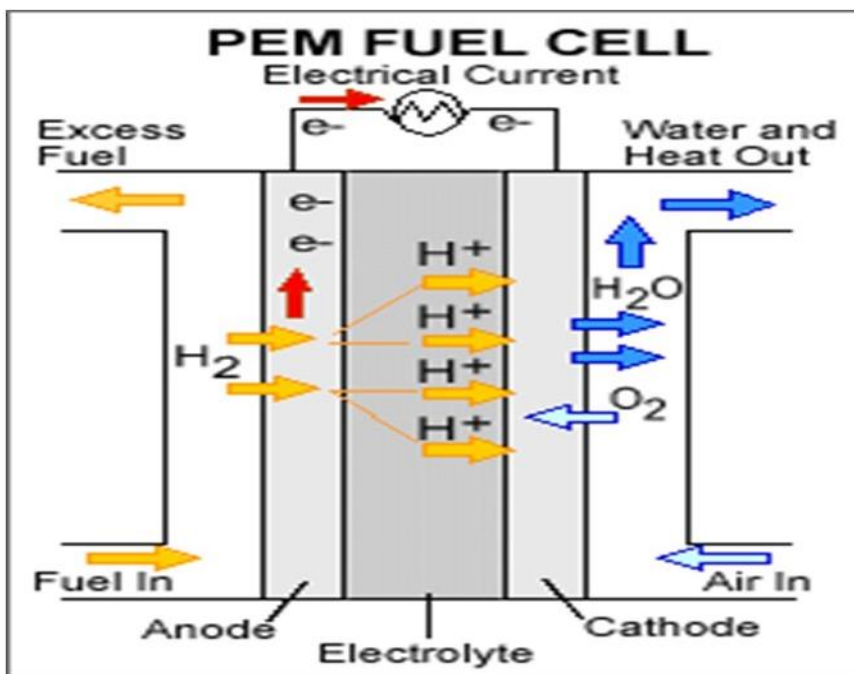
Figure 1.2. Schematic diagram of an acidic polymer electrolyte fuel cell Taken from http://www.forbes.com/sites/tomkonrad/2013/12/11/twelve-hydrogen-and-fuel-cell-stocks/.

$$[(CF_2CF_2)_m - (CF\text{-}CF_2)]_n$$
$$|$$
$$O$$
$$|$$
$$CF_2$$
$$|$$
$$F-C \longrightarrow OCF_2CF_2 \longrightarrow SO_3^-H^+$$
$$|$$
$$CF_3$$
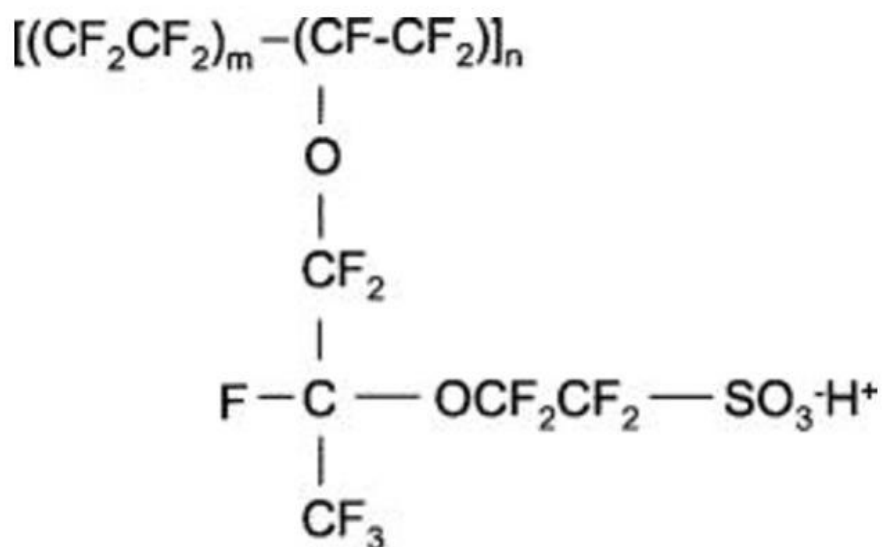
Figure 1.3. Polymeric structure of Nafion, a solid electrolyte used in polymer electrolyte membrane fuel cells. Taken from reference [4].

performance.[4]

Alkaline fuel cells (AFC) operate in a similar manner to that of acidic polymer electrolyte membrane fuel cells. Figure 1.4 shows the operating principles of an alkaline polymer electrolyte membrane fuel cell. Although like PEMFC's, hydrogen is still oxidized at the anode and oxygen is reduced at the cathode, AFC's are different in that the reduced OH$^-$ ions diffuse across the electrolyte and water is produced at the anode rather than the cathode. A lack of a solid electrolyte that can allow OH- diffusion has prevented AFC's from commercialization and is the main reason why PEMFC's instead of AFC's have been further developed so far. However, due to faster oxygen reduction kinetics in alkaline mediums, a more diverse selection of catalysts can be utilized in alkaline mediums and thus, AFC's still remain an active area of research.[1]

1.1.3 Factors Affecting Fuel Cell Performance

Figure 1.5 shows the major factors that influence the overpotential for fuel cells during operation. At low current outputs, the reaction kinetics govern the current density output and is governed by the Butler-Volmer equation:

$$j = j^o \left(\frac{C_R^*}{C_R^{O*}} e^{\frac{\alpha nFn}{RT}} - \frac{C_P^*}{C_P^{O*}} e^{-\frac{(1-\alpha)nFn}{RT}} \right)$$

where j, j^0, C_R^*, C_R^{O*}, C_P^*, C_P^{O*}, α, n, F, n, R, and T are current density, exchange current density at standard conditions, concentration of reactants at the catalyst surface, initial concentration of reactants, concentration of products at the catalyst surface, initial concentration of products, charge
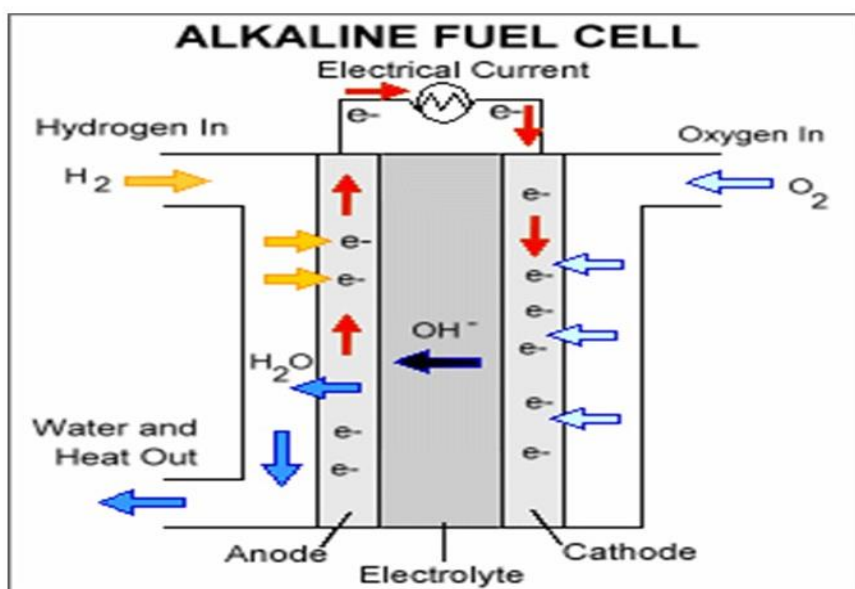
Figure 1.4. Schematic diagram of an alkaline polymer electrolyte fuel cell Taken from http://www.forbes.com/sites/tomkonrad/2013/12/11/twelve-hydrogen-and-fuel-cell-stocks/.

transfer coefficient, number of electrons transferred, Faraday's constant, overpotential, ideal gas constant, and temperature.   For acidic and alkaline polymer electrolyte fuel cells, the main source of overpotential at low current densities originates from the kinetics of the oxygen reduction reaction.   Therefore, catalysts that facilitate oxygen reduction kinetics are often employed to lower the overpotential and increase the overall current density output.[2]

As the overpotential increases, fuel cell performance is increasingly affected by Ohmic resistance rather than oxygen reduction kinetics. Ohmic resistance can be defined as resistance that occurs due to diffusion across the electrolyte as well as the resistance that occurs during electron charge transport.   For the most part, ionic diffusion dominates and is the major contribution to the overall Ohmic resistance.[2]

Finally, at high overpotentials, mass transport from the bulk electrolyte to the catalyst surface is the limiting factor in overall performance. High overpotentials can overcome the oxygen reduction kinetics as well as ion resistance.   Therefore, reactants are converted to products as soon as they reach the catalyst surface, making transport to the catalyst surface the limiting step at high overpotentials.[2]

1.2 The Oxygen Reduction Reaction (ORR)

1.2.1 The Role of Catalysts

Oxygen electrochemistry is an integral part in many electrochemical devices.   The complete reduction of oxygen to water is vital for operation in PEMFC's [5] and lithium air batteries [6] while the oxygen evolution reaction is part of the water splitting reaction powered by solar energy [7].

As figure 1.6 shows, the oxygen reduction can occur through two different pathways.[8]   Both these pathways occur simultaneously and the
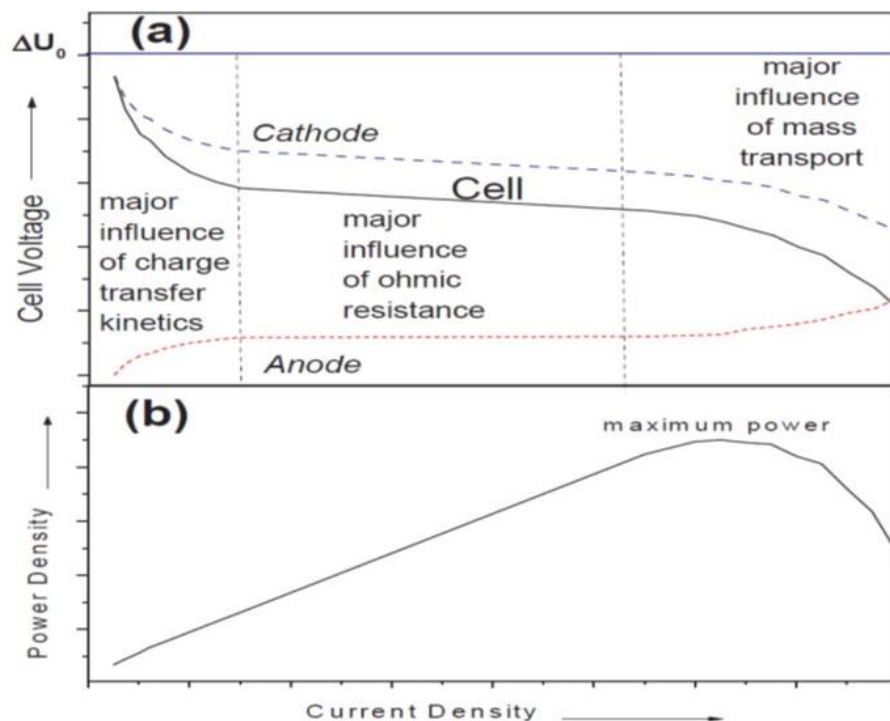
Figure 1.5. Current density curves (a) and power density curves (b) for fuel cells showing the major factors influencing the overpotential at operating voltages. Taken from reference [1].

favored pathway is determined by the catalyst, oxygen adsorption strength, and the applied overpotential.[8]   The dissociative mechanism occurs if the adsorption strength is strong enough to break the oxygen double bond whereas the associative mechanism occurs through hydrogen being attached to the adsorbed oxygen and progressive disassociation (figure 1.7).[9]

Figure 1.8 shows the how the activation barrier for a chemical reaction changes in the presence of a catalyst. For the oxygen reduction reaction, the first electron transfer step is often viewed as the rate determining step. [8] Therefore, when catalysts with an oxygen adsorption energy that is not too strong or too weak are used, the activation overpotential can be significantly mitigated.   Using density functional theory, Norskov et al. calculated the catalytic activity of all the transition metals based off each metal's d-band center. [8]   The results, as shown in figure 1.9, is a volcano plot with the metals near the peak having the highest catalytic activity, the transition metals on the left hand side of the peak having too strong of an oxygen adsorption energy and the transition metals on the right hand side of the peak having too weak of an oxygen adsorption energy.   Figure 1.9 shows platinum near the peak of the volcano plot and as expected, platinum has been shown to be the most active electrocatalyst for the oxygen reduction reaction.

Some recent reports have refuted the results published by Norskov et al. saying that the d-band center that Norskov et al. based their catalytic activity calculations on does not correlate to general catalytic activity. [10, 11]   Indeed, Norskov et al. responded to these reports by saying that using the d-band center only works when the matrix elements are the same and minimization of these types of errors can be done by using the binding energy of adsorbents rather than the d-band center. [12].   To confirm this, Yu et al. used photoelectron spectroscopy data as well as density functional theory calculations to determine the catalytic activity of transition metals for the oxygen reduction reaction based off of O_2 and OH binding energies.[9]
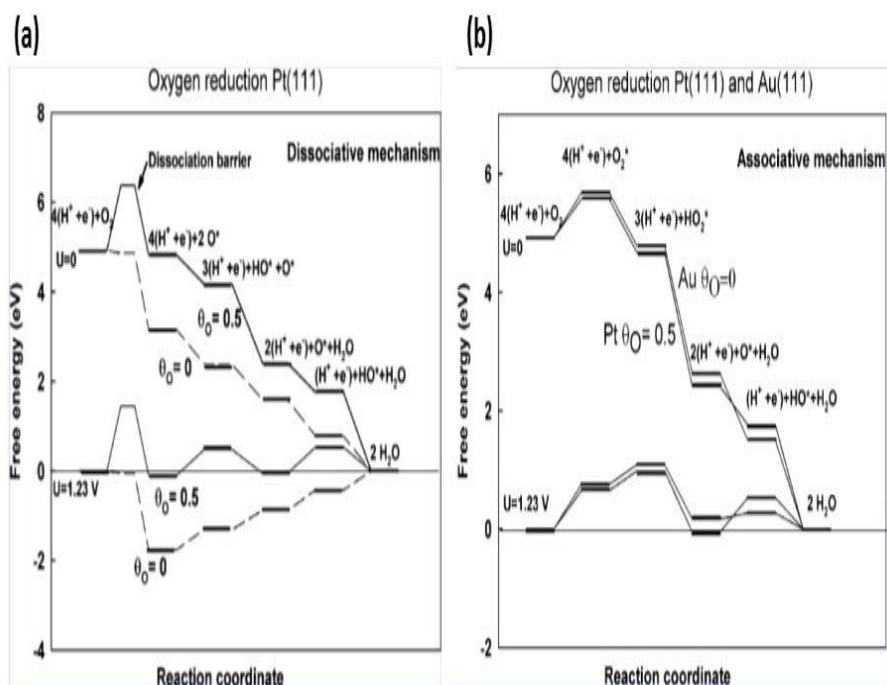
Figure 1.6. The dissociative (a) and associative (b) mechanism for the oxygen reduction reaction occurring on Pt and Au (111). Taken from reference [8].

ORR Reaction Mechanism Scheme
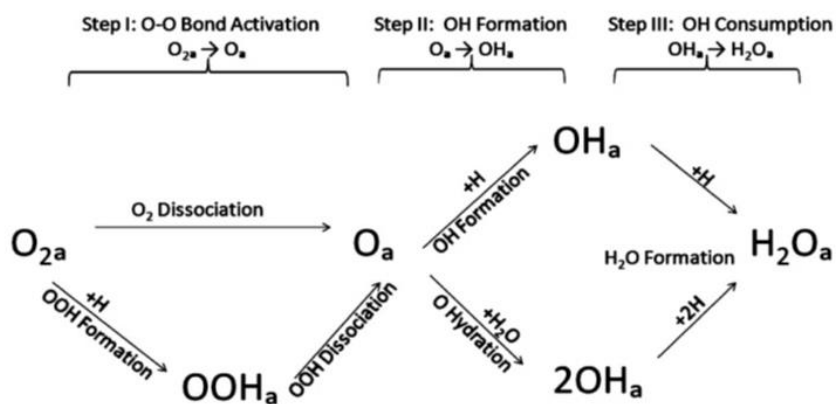
Figure 1.7. The steps involved in the dissociative (top) and associative (bottom) pathway for oxygen reduction reaction. Taken from reference [9].
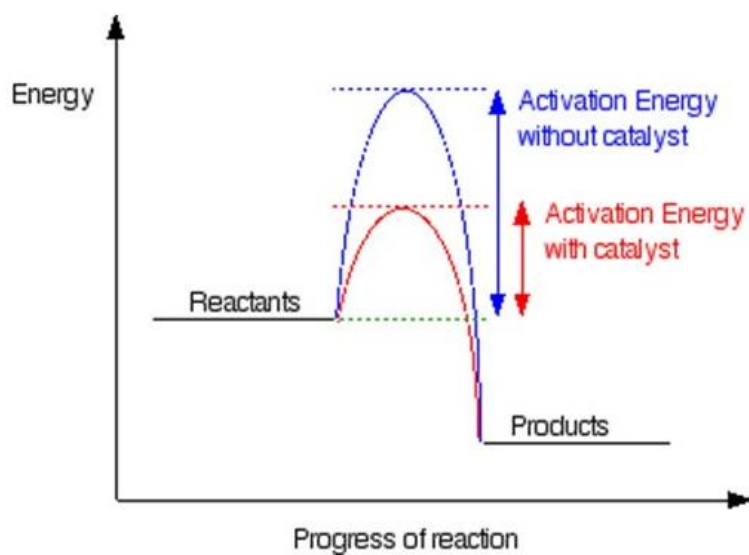
Figure 1.8. Schematic showing the how catalysts affect the affect the activation energy of a reaction. Taken from reference [2].
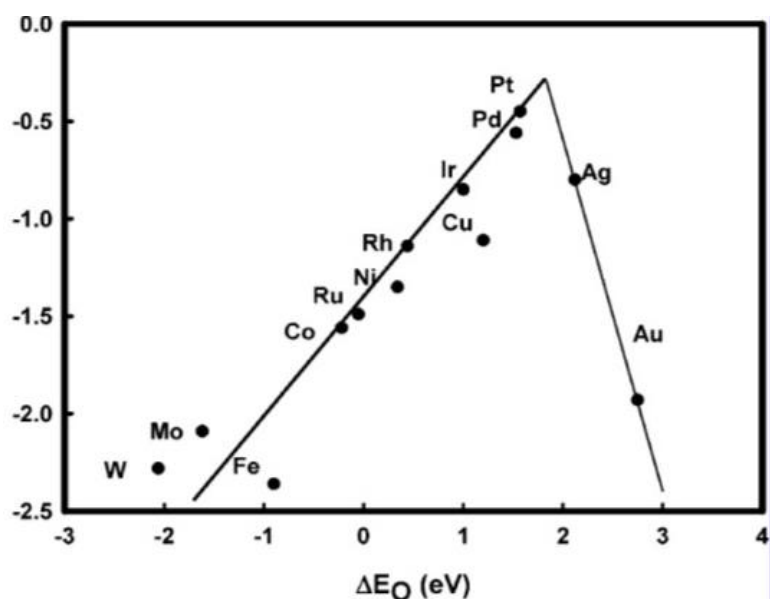
Figure 1.9. Volcano plot showing the catalytic activity of transition metals toward the oxygen reduction reaction. Elements on the left hand side have too strong of an adsorption energy whereas elements on the right hand side have too weak of an adsorption energy. Taken from reference [8].
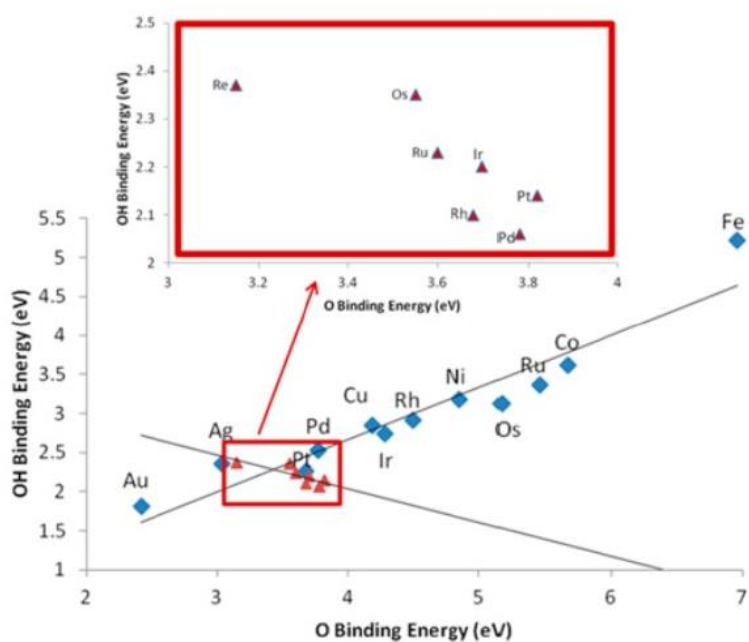
Figure 1.10. Catalytic activity for the oxygen reduction reaction based of O_2 and OH binding energies. Taken from reference [9].

Their results (figure 1.10) correlated well with results found by Norskov et al. and also showed that alloying platinum with other alloys can further increase the catalytic activity.

1.2.2 Acidic vs Alkaline Electrolytes

Table 1.2 shows the reduction potential for the oxygen reactions that can occur in acid and alkaline mediums.　As alluded to in the previous section, the oxygen binding energy to the catalyst surface plays a major role in whether oxygen is partially reduced (2 e^- pathway) to peroxide or completely reduced (4 e^-) to water.　To date, platinum and platinum based alloys have the best catalytic activity in acidic electrolytes.　The high electrode potential, rapid hydration upon electron transfer and requirement of very high oxygen adsorption energies to bind the relatively neutral oxygen molecule are all reasons why only a limited number of catalysts are effective in acidic mediums.

　Contrary to acidic mediums, a diverse number of catalysts show oxygen reduction activity in alkaline mediums.　For example, gold shows almost no activity in acidic mediums but significantly higher activity is observed in alkaline electrolytes.[13]　Blizanac et al. explained the significantly difference in activity by using the Nernst equation and pH influences.[14]　They showed through a modified Pourbaix diagram (figure 1.11) that the overpotential for the oxygen reduction reaction decreases with increasing pH.[14]　In addition, other reports explain the higher activity by arguing that the lower electrode potential in alkaline mediums allows superoxide ions to be more stable in solution. [15, 16]　This, in turn, may facilitate the oxygen reduction reaction since adsorption and reduction of superoxide is easier than that of oxygen molecules.[15, 17]

Electrolyte	ORR Reactions	Thermodynamic Reduction Potentials at Standard Conditions (V)
Acidic Aqueous Solution	$O_2 + 4H^+ + 4e^- \longrightarrow H_2O$	1.229
	$O_2 + 2H^+ + 2e^- \longrightarrow H_2O_2$	.70
	$H_2O_2 + 2H^+ + 2e^- \longrightarrow 2H_2O$	1.76
Alkaline Aqueous Solution	$O_2 + H_2O + 4e^- \longrightarrow 4OH^-$	.401
	$O_2 + H_2O + 2e^- \longrightarrow HO_2^- + OH^-$	-.065
	$HO_2^- + H_2O + 2e^- \longrightarrow 3OH^-$	.867

Table 1.2. The reduction potentials of reactions that can occur in acid and alkaline electrolytes. Taken from reference [2].
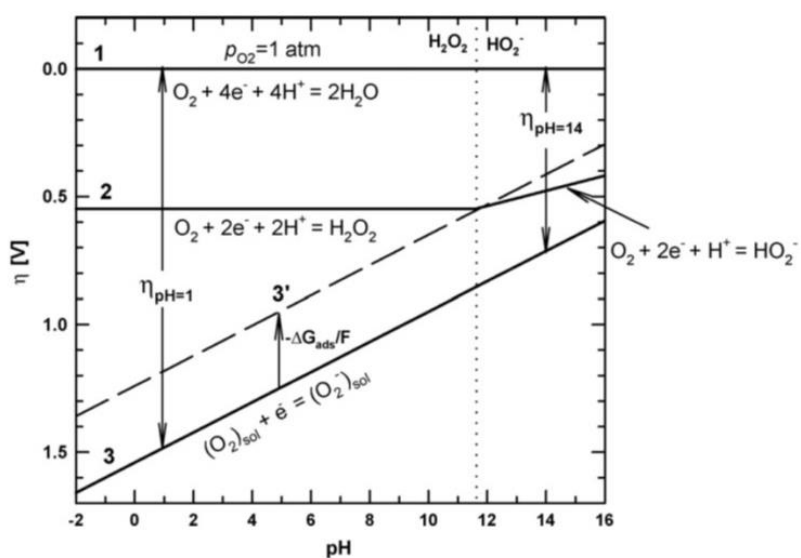
Figure 1.11. A modified Pourbaix diagram showing how the overpotential decreases with increasing pH. Taken from reference [14].

1.2.3 Inner and Outer Helmholtz Planes

As figure 1.12 shows, dependent on the electrode potential, several layers exist in the solution at the electrode surface.[18]   Solvent molecules and other ions or molecules that are able to directly adsorb onto the catalyst surface are what compose the closest layer to the electrode.   Within this inner layer, the plane passing through the center of these adsorbed molecules is called the inner Helmholtz plane (IHP).[18]   For solvated ions, solvent molecules prevent the direct adsorption onto the electrode surface.   Instead, the closest distance these ions can approach is marked by x_2 in figure 1.12. These solvated ions compose the secondary layer and the plane passing through the center of these solvated ions is thus called the outer Helmholtz plane (OHP).[18]

The reduction potential of a reaction is determined using the Nernst equation:

$$E = E^O + \frac{RT}{nF} \ln \frac{A^a B^b}{C^c D^d}$$

where E. E^O, R, T, n, F, are reduction potential, standard reduction potential, ideal gas constant, temperature, number of electrons transferred, and Faraday constant respectively. A^a, B^b, C^c, and D^d are the concentrations of reactants and products for a chemical reaction in the form of:

$$aA + bB \leftrightarrow cC + dD$$
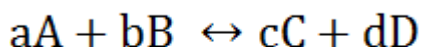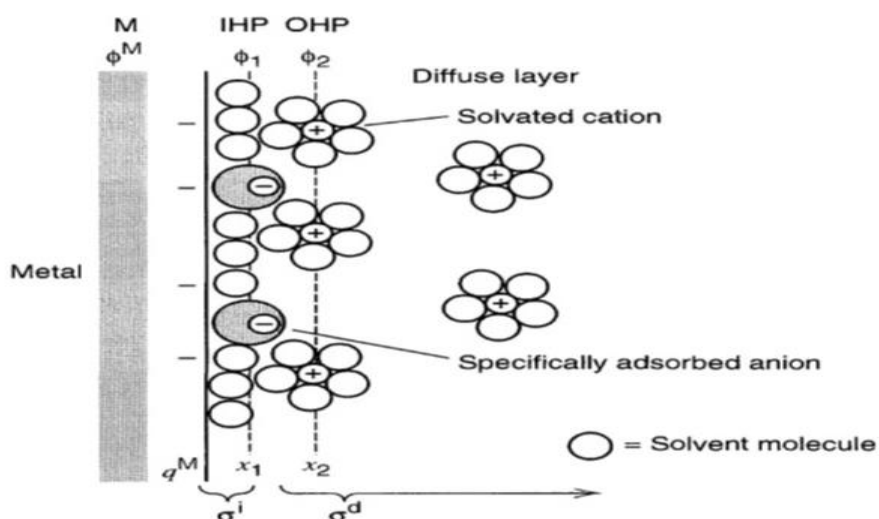
Figure 1.12. Schematic diagram showing the multiple layers that exist on the solution side of the electrode-surface interface. Taken from reference [18].

Therefore, application of the Nernst equation to the oxygen reduction reaction:

$$O_2 + 4H^+ + 4e^- \leftrightarrow 2H_2O$$
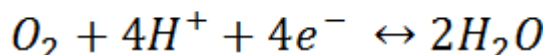
results in: (assuming that the fugacity of oxygen = 1, the concentration of electrons = 1 and the activity of water = 1):

$$E = E^O + \frac{RT}{F} \ln a^{H^+}$$

Since pH can be defined as:

$$pH = -\log a^{H^+}$$

$$\ln a^{H^+} = 2.303 \log a^{H^+}$$

Substitution back into the Nernst equation yields the final equation in the form of:

$$E = E^O - .059(pH)$$

As can be seen from the above equation, an inverse relationship exists between the electrode potential and pH. Therefore, when compared to acidic environments, the electrode potential is significantly lower in alkaline mediums. This allows for lower repulsion of the solvated cations, which in turn, allows for the outer Helmholtz plane to be closer to the

electrode surface.   This closer distance may allow for phenomena, such as electron transfer, that are not possible in acidic mediums to occur in alkaline mediums.[15]

1.2.4 Non-Precious Metal Catalysts

Although platinum shows the highest activity for the oxygen reduction reaction, many obstacles still exist. In addition to its scarcity and high cost,[19] it is well known that platinum is very susceptible to carbon monoxide poisoning, which, in turn, leads to fuel cells requiring ultra-pure reactants.[20, 21]   Platinum also shows significantly less catalytic activity in sulfuric acid due to the HSO_4^- and SO_4^{2-} ions adsorbing onto Pt (111) facets and blocking oxygen adsorption.[22, 23] This is a problem because Nafion contains sulfate groups and performance decline with the presence of Nafion have been observed.[24, 25]   As a result, catalysts that show catalytic activity competitive to platinum but are cheaper and less susceptible to poisoning are necessary for commercialization of fuel cells.

The Dai group pioneered the concept of non-precious metal catalysts by reporting the high electrocatalytic activity of nitrogen doped nanotubes in alkaline mediums.[26]   Since then, a spate of reports have been published that show doped carbons with or without metal ion coordination having high catalytic activity, especially in alkaline mediums.[27, 28]   These carbon based materials show great potential and hope for a viable catalyst for fuel cell commercialization, but due to the infancy of this research area, there are still many aspects that are unknown and thus prevent optimization.

Surprisingly, the high activity of non-precious catalysts have been reported numerous times but the pathway or the mechanism upon which the oxygen reduction reaction proceeds on these catalysts has yet to be found. As a result, there remains a controversy in this field, where some researchers stress the need of a non-precious metal, such as iron or cobalt [27, 29], while

other researchers argue that these non-precious metal catalysts only exist to help facilitate the creation of active sites in nitrogen-doped carbons [30].   In addition, although the products may seem similar at the end, the steps taken to synthesize the products lead to very different catalytic activity for the oxygen reduction reaction.   Clearly, though non-precious metal catalysts possess an immense amount of potential, unless a clearer understanding of how the electrochemical reactions are occurring is achieved, carbon based catalysts cannot be optimized and, in turn, not be used as a substitute for platinum in fuel cell operations.

1.2.5 Metal Phthalocyanines for the ORR

Due to their intense colors, phthalocyanines are often used in paints and dyes.   However, as figure 1.13 shows, the fact that these structures already contain an M^+-N-C coordinated structure makes them a suitable material upon which the ORR mechanism on non-precious materials can be studied.

Copper, cobalt, and iron phthalocyanines were chosen to study the oxygen reduction reaction for a variety of reasons.   In general, oxygen can adsorb in one of two ways: the side on or end on method (figure 1.14).[31] Accordingly, different adsorption methods lead to different adsorption energies and therefore, comparisons between a catalysts adsorbing oxygen in the side on method cannot be made with catalysts adsorbing oxygen in the end on method.   For copper, cobalt, and iron phthalocyanines however, the side-on adsorption method is unstable and only the end on adsorption method is favored.[32, 33]   In addition, density functional theory calculations show that copper, cobalt and iron phthalocyanines all have different oxygen binding energies, which can help determine if these M^+-N-C sites are indeed the active sites.   From this, the role of the inner Helmholtz plane in the oxygen reduction reaction can be assessed.[32, 33]
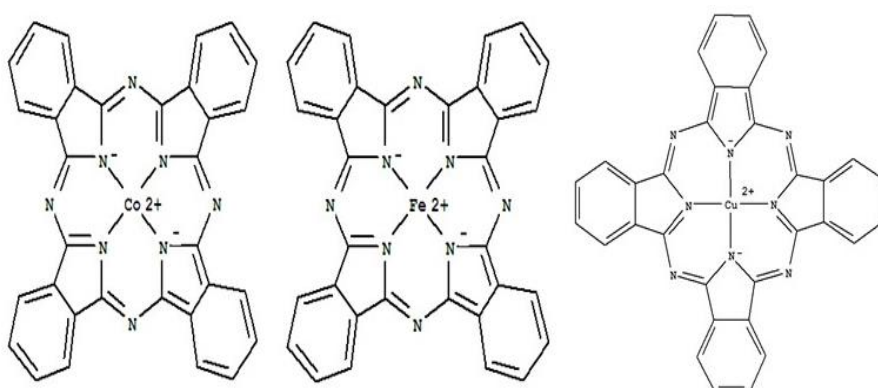
Figure 1.13. Metal phthalocyanine structures.
Taken from http://www.sigmaaldrich.com/.
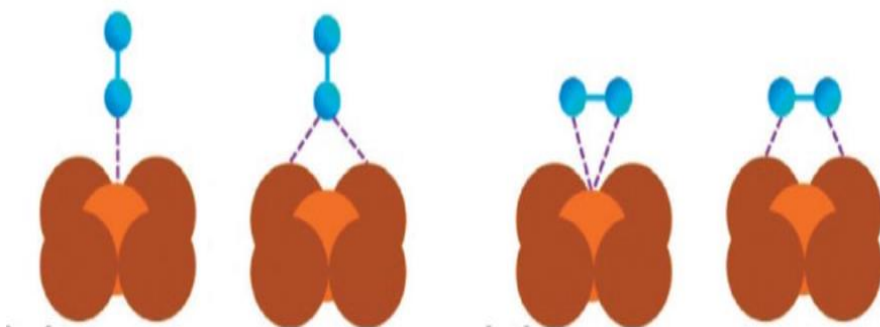
Figure 1.14. Schematic drawing showing the oxygen end on adsorption method and the side on adsorption method on a catalyst surface. Taken from reference [32].

1.3 Research Objectives of this Dissertation

This study was conducted with the goal of elucidating a clearer understanding of the active sites as well as the mechanism/pathway the oxygen reduction reaction proceeds through on non-precious metal catalysts in alkaline mediums. Specifically, the concept that multiple pathways for the oxygen reduction reaction could exist and whether different pathways could be favored by different conditions was explored.

Currently, the general synthesis methods for non-precious metal catalysts involve heat treating a mixture of nitrogen, carbon, and metal ion containing precursors. This process, though resulting in high activity, presents problems since it allows for a multitude of possibilities for how the electrochemical reactions occur. Proponents of the concept that M^+-N-C coordinated structures being the active site have no rebuttal for why heat treatment leads to improved activity since the heat treatment temperature is bound to destroy the coordinated structure. Similarly, proponents of nitrogen doped metal free catalysts can't agree on whether pyridinic, pyrrolic, or graphitic nitrogen is the active site and again, why heat treatment leads to increased activity since heat treatment leads to a loss of overall nitrogen content as well as conversion of pyridinic and pyrrolic nitrogen to graphitic nitrogen.[34]

In this study, metal phthalocyanines with different oxygen binding energies were loaded onto a carbon support and heat treated at 800^0C. ORR activities in different electrolytes and physical characterizations were taken and compared before and after in an attempt to determine what scenarios could lead to heat treatment improving activity for some catalysts while decreasing activity in others. Studies using different electrolytes to determine reaction mechanisms have been done on platinum, gold and some other rare transition metal catalysts [35-38], but this technique has yet to be applied to non-precious metal catalysts.

Chapter 2: Experimental

2.1 Preparation and Synthesis

2.1.1 Chemicals and Materials

Commercial carbon supported platinum (Johnson-Matthey, 40 weight % Pt/C) was purchased from Alfa Aesar (Alfa Aesar, Ward Hill, MA, USA).   Gold (III) chloride ($AuCl_3$, 99.99%), perchloric acid ($HClO_4$, 70% solution, 99.999%), sulfuric acid (H_2SO_4, 95-98%), N,N-Dimethylformamide ($HCON(CH_3)_2$, 99.8%), sodium borohydride ($NaBH_4$, 99.99%), iron (II) phthalocyanine ($C_{32}H_{16}FeN_8$, 90%), cobalt (II) phthalocyanine ($C_{32}H_{16}CoN_8$, 97%), copper (II) phthalocyanine ($C_{32}H_{16}CuN_8$, 90%), lithium hydroxide monohydrate ($LiOH*H_2O$, 98%), potassium hydroxide (KOH, 45% solution), cesium hydroxide monohydrate ($CsOH*H_2O$, 99.5%), sodium citrate tribasic dihydrate ($HOC(COOONa)CH_2COONa)_2*2H_2O$, 99%), potassium cyanide (KCN, 96%), 2-propanol (($CH_3)_2CHOH$, LC-MS Chromasolv, 99.9%), and Nafion perfluorinated resin solution (5 weight % in lower alipathic alcohols and water) were all purchased from Sigma-Aldrich Inc. (Sigma-Aldrich, St. Louis, MO, USA).   Sodium hydroxide (NaOH, 98%) was purchased from Samchun Chemicals (Samchun Chemicals, Seoul, Korea) and Vulcan XC-72 carbon was purchased from the Cabot Corporation (Boston, MA, USA). All chemicals were used as is without further purification.   38 x 8 mm octahedral PTFE stirring bars were purchased from Cowie Technology (Cowie Technology, Middlesbrough, United Kingdom).   Cellulose acetate membrane filter papers with a pore size of 45μm was purchased from Advantec (Advantec MFS Inc., Dublin, CA, USA).   All aqueous solutions were made using deionized (DI) water that was purified using a Milli-Q

system (18.2 MΩ cm, Millipore, Bedford, MA, USA). Ultra-pure hydrogen (99.995%), argon (99.995%) and oxygen (99.95%) gas were supplied by Daesung Industrial Gases (Daesung Industrial Gases Co., Ltd, Seoul, Korea).

2.1.2 Synthesis of Au Nanoparticle on Vulcan XC-72

Synthesis of Au nanoparticles on Vulcan XC-72 was done following a previously reported method and outlined in figure 2.1.[39]   800 mL of DI water and a magnetic stir bar were added to a 1000 mL beaker and stirred at 800 RPM.   While stirring, .0517 g of $AuCl_3$ was added and a minute later, .1 g of sodium citrate tribasic dihydrate was added.   After another minute of stirring, a mixture of .1 g sodium citrate tribasic dihydrate and .03 g sodium borohydride was added to the stirring solution.   The solution immediately turned a pinkish-red color, which confirmed the reduction of gold (III) chloride to gold nanoparticles.   The solution was stirred at 800 RPM for an additional 30 minutes, after which .07 g of Vulcan XC-72 was added.   The solution was then stirred for 24 hours and then filtered with 4 L of DI water.   The final sample was then placed in a vacuum oven and dried overnight at room temperature.

2.1.3 Preparation of Metal Phthalocyanines on Vulcan XC-72

Copper, cobalt, and iron phthalocyanines were dispersed on Vulcan XC-72 following the procedure outlined in figure 2.2.   .02 g of metal phthalocyanine was dispersed in .010 L of concentrated H_2SO_4.   .1 g of Vulcan XC-72 was then added and the solution underwent sonication for two hours.   The solution was then filtered with 2 L of DI water and then vacuum dried overnight at room temperature.

2.1.4 Heat Treatment of Metal Phthalocyanines on Vulcan XC-72

A quartz tube furnace (Ajeon Heating Industrial Co. Ltd, Gyeonggi-do, Korea) was used to heat treat all the samples at 800^0C in an argon atmosphere.   First, the phthalocyanine sample was placed in the furnace and purged with argon for 1 hour.   The temperature was then raised from room temperature to 800^0C at 5^0C/minute.   The sample was placed just outside of the furnace while the temperature was raised.   When the furnace reached 800^0C, the sample was quickly placed inside the center of the furnace and heat treated for 20 minutes.   The sample was then allowed to cool for three hours and then slid out from the center of the furnace and allowed to cool to room temperature.   Pure Vulcan XC-72 was also heat treated following this procedure.

2.2 Physical Characterization

Ultraviolet-Visible spectroscopy measurements were taken using a Jasco V-670 UV-Vis-NIR Spectrophotometer (Jasco International Co. Ltd., Tokyo, Japan).   Samples were dispersed in *N, N*-Dimethylformamide (DMF) and measurements were taken from 800-300 nm.   Baseline corrections were calculated by taking transmission measurements with pure DMF.

TEM measurements were taken at the Research Institute for Advanced Materials' (RIAM) Center for Materials Analysis (Seoul National University, Seoul, Korea) using a Tecnai F20 analytical TEM (FEI, Hillsboro, Oregon, USA) at 200 kV.

X-ray diffraction (XRD) measurements were taken using a Rigaku D/MAX 2500 (Rigaku Corporation, Tokyo, Japan) from $20^0 < 2\theta < 80^0$ with Cu Kα radiation (.1541 nm) at 40 kV and 200 mA.   All measurements were taken at a speed of 2^0 min^{-1}.

1. Gold (III) Chloride
2. Distilled H_2O

1. Sodium Citrate
Tribasic Dihydrate

1. Sodium Borohydride
2. Sodium Citrate
Tribasic Dihydrate

Distilled
H_2O

Stirring for
1 minute

Stirring for
1 minute

Stirring
Overnight

Vacuum
Filtration

Vacuum Drying
Overnight
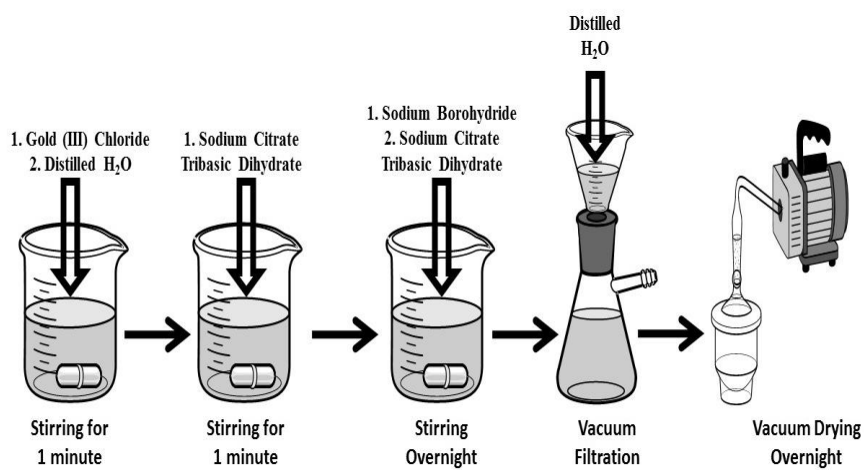
Figure 2.1. Schematic outline for the synthesis of gold nanoparticles loaded on Vulcan XC-72.

1. Metal Phthalocyanine
2. Vulcan Carbon XC-72

Distilled H$_2$O

Sulfuric Acid

Sonication

Vacuum Filtration

Vacuum Drying Overnight

Brief Heat Treatment @ 800^{0}C
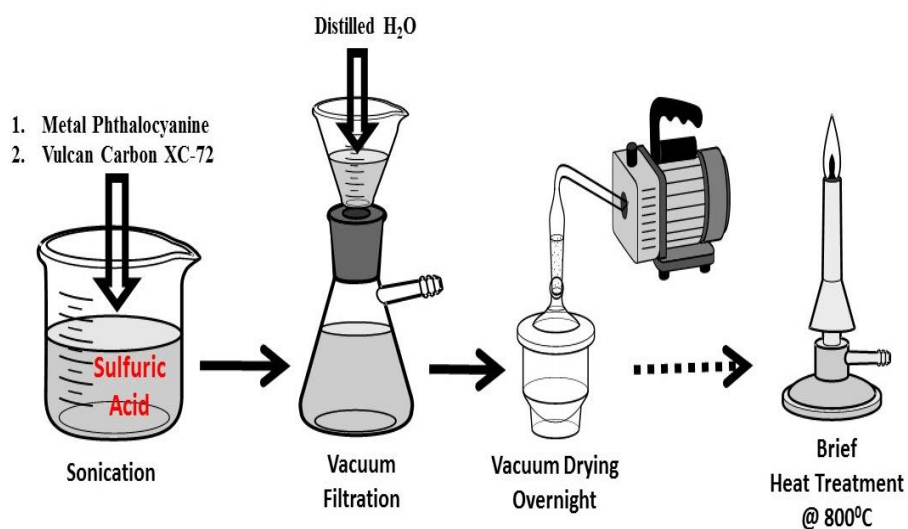
Figure 2.2. Schematic outline for the metal phthalocyanine loading on Vulcan XC-72 and subsequent heat treatment for heat treated samples.

Elemental analysis for the weight percent of carbon and nitrogen present in the samples was conducted at the Seoul National University School of Chemical and Biological Engineering's Center for Materials Analysis (Seoul National University, Seoul, Korea) using a CHNS-932 elemental analyzer (LECO Corporation, St. Joseph, MI, USA).

X-ray photoelectron spectroscopy (XPS) measurements were taken at the 8A1 line at the Pohang Accelerator Laboratory (Pohang, Korea) (figure 2.3).   Measurements included survey, carbon 1s, and nitrogen 1s spectra and were taken at 700 eV.   All spectra were calibrated to the gold 4f orbital (86.4 eV) using a gold foil.   Spectra peaks were fitted using the XPSPEAK 4.1 software package.

2.3 Electrochemical Measurements

Three electrode half-cell measurements were conducted using a rotating ring-disk electrode (RRDE) (Pine Research Instrumentation, Durham, NC, USA) and connected to an Echochemie Inc. PGSTAT302N bipotentiostat running GPES version 4.9 software (Metrohm Autolab, Utrecht, Netherlands).   A platinum wire was used as the counter electrode. For the reference electrode, an Ag/AgCl electrode calibrated to the reversible hydrogen electrode (RHE) was used for all alkaline measurements and a saturated calomel electrode (SCE) electrode calibrated to the RHE was used for all acid measurements.   The working electrode consisted of an ink solution of the catalyst loaded onto a glassy carbon electrode.   All measurements were conducted at 20^0C.

Calibration for conversion to the RHE scale was performed using a platinum working electrode.   The cell was initially purged with hydrogen for 25 minutes.   A linear sweep of the potential from -1 V to 1 V was performed and the potential shift value was the voltage at which the current equaled zero.   Table 2.1 lists the potential shifts required to calibrate to the

reversible hydrogen electrode for all the electrolytes used in the electrochemical measurements.

Preparation of the catalyst ink was done by adding .01 g of the catalyst to 20 μL if DI water, 60 μL of Nafion and 700 μL of 2-propanol. The solution then underwent sonication for two minutes and then stirred at 350 RPM for 10 minutes. The solution then underwent sonication for an additional two minutes. 7 μL of the catalyst ink was then loaded onto a glassy carbon working electrode possessing a diameter of .2475 cm^2. The electrode was then allowed to dry in an oven at 60^{0}C for 15 minutes.

All measurements were made using a .1 M salt concentration electrolyte. The electrolytes used were LiOH, NaOH, KOH, CsOH, and HClO$_4$. Before all measurements, the cell was purged with argon gas for a minimum of 20 minutes followed by 40 pretreatment cycles from .05-1.05 V vs RHE at a scan rate of 50 mV/s. Argon atmosphere cyclic voltammograms (CV) were taken from .05-1.05 V at scan rates of 50 mV/s and 5 mV/s. After completion of the cyclic voltammograms, the cell was purged for 25 minutes with ultra-pure oxygen gas. Measurements for iR compensation were then taken from 10,000 Hz to 1 Hz at the open circuit voltage using the Frequency Response Analyzer (FRA) version 4.9 software. Following this, CV measurements under the previously mentioned conditions were then conducted with the exception being under an oxygen atmosphere rather than an argon atmosphere. Oxygen reduction reaction (ORR) polarization curve measurements were taken at a scan rate of 5mV/s from .05-1.05 V vs RHE and at a rotation rate of 1600 RPM. The 5mV/s argon CV measurement was then subtracted from this measurement to negate the capacitive contribution, leaving only the activity due to the catalyst. All measured currents were normalized by the electrode surface area (.2475 cm^2). ORR polarization curves for the Koutecky-Levich measurements followed the same protocol except the rotation rate was varied (400, 600, 900, 1200, 1600, 2200, and 2400 RPM) for each measurement.
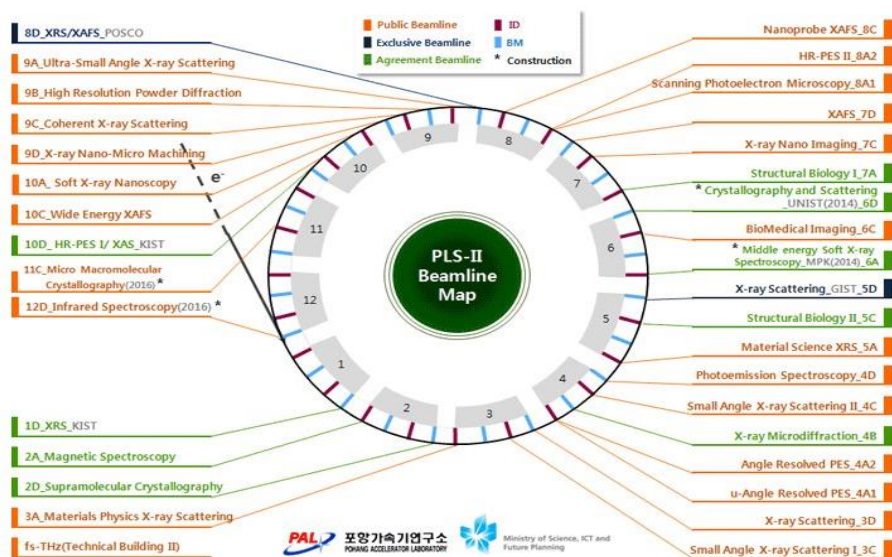
Figure 2.3. Map of the beam lines present at the Pohang Acceleration Laboratory (PAL). Taken from http://pal.postech.ac.kr/.

Electrolyte	Reference Electrode	RHE Potential Shift (V)
.1M HClO$_4$	Saturated Calomel Electrode (SCE)	.318
.1M LiOH	Ag/AgCl	.925
.1M NaOH	Ag/AgCl	.924
.1M KOH	Ag/AgCl	.930
.1M CsOH	Ag/AgCl	.934

Table 2.1. Potential shifts to calibrate for the reversible hydrogen electrode (RHE) for the electrolytes used in electrochemical measurements.

Chapter 3: Results and Discussion

3.1 Gold and Platinum Nanoparticles

3.1.1 Structural Characterization

Figure 3.1 shows the TEM images of the commercial Johnson-Matthey platinum nanoparticles loaded onto a carbon support.   As the images show, the particles are well dispersed throughout the carbon matrix and have a uniform size of approximately 3-5 nm.

Figure 3.2 shows the TEM images of the synthesized gold nanoparticles on carbon support.   Similar to the commercial Pt/C catalyst, the synthesized Au/C catalyst showed uniform dispersion throughout the carbon matrix as well as a similar particle size of approximately 3-5 nm. Similar particle sizes are important when comparing catalysts as the size of the nanoparticle can lead to differences in electrochemical performance.[40]

As seen from the x-ray diffraction (XRD) profiles (figure 3.3), the diffraction peaks observed within the catalyst samples align well with that of reference platinum (JCPDS PDF # 04-0802) and gold (JCPDS PDF # 04-0784) diffraction peaks. In addition, X-ray photoelectron spectroscopy (XPS) spectra of the Pt 4f and Au 4f orbitals showed visible peaks, which can lead to the conclusion that platinum and gold nanoparticles exist on the surface of the catalyst.   This is crucial since, as previously mentioned, electrochemical reactions for catalysts such as platinum, are based on reactant adsorption to the catalyst surface.[41, 42]
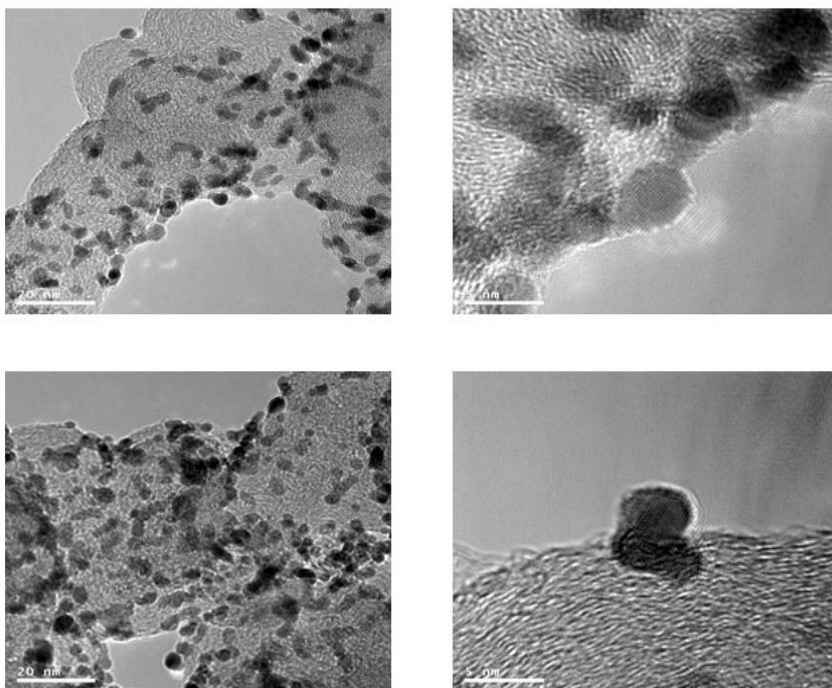
Figure 3.1. TEM images of Johnson-Matthey 40% Pt/C. The images show that the Pt particles are uniform in size and well dispersed throughout the carbon matrix.
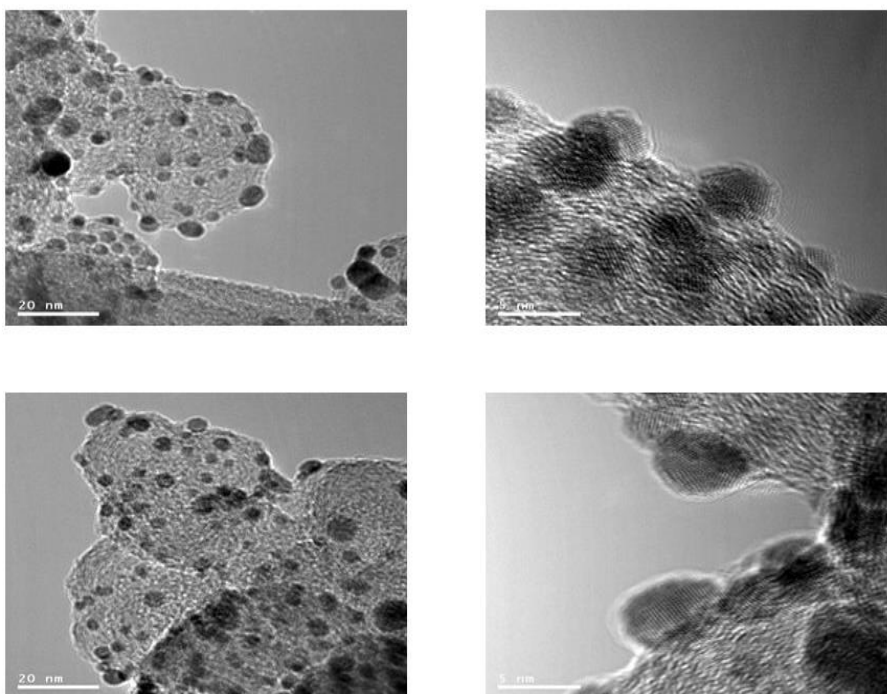
Figure 3.2. TEM images of gold nanoparticle supported on Vulcan XC-72. The images show that the Au particles are uniform in size and well dispersed throughout the carbon matrix.
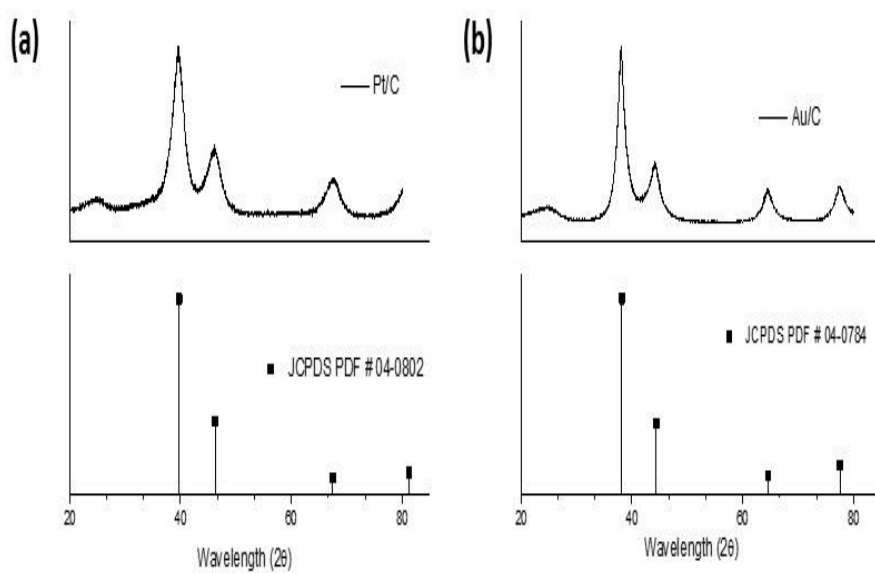
Figure 3.3. XRD images confirming the presence of platinum (a) and gold (b) on the carbon matrix.
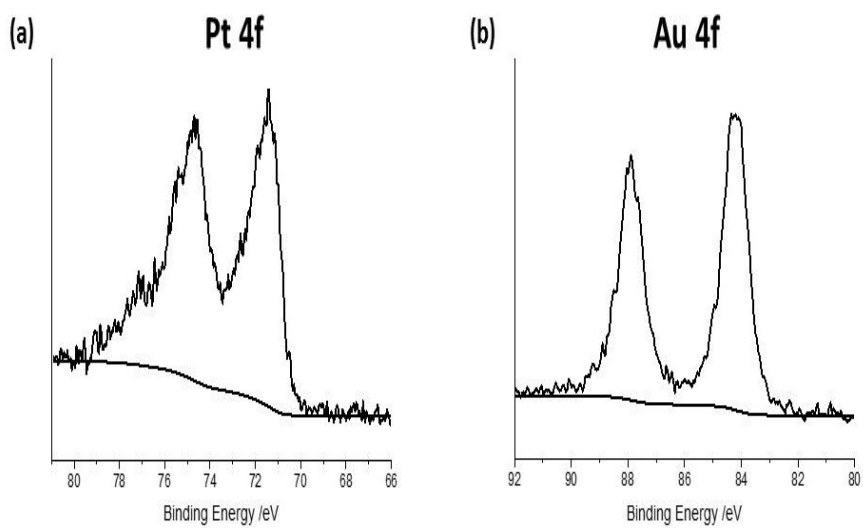
Figure 3.4. XPS images confirming the presence of platinum (a) and gold (b) on the surface of the carbon matrix.

3.1.2 Electrochemical Measurements

The cyclic voltammetry profile (CV) of platinum (figure 3.5(a)) matches well with the typical profile for platinum catalysts.[35, 43]   The CV can be easily explained by separating it into four regions.   From .05-.4 V (region 1), reversible hydrogen ion adsorption/desorption ($H^+ + e^- \leftrightarrow H_{upd}$) occurs, as evidenced by the two adsorption and desorption peaks.   Double layer charging (region II) occurs next followed by reversible adsorption/desorption of hydroxide anions ($OH^- \leftrightarrow OH_{ad} + e^-$) (region III) in the potential range of .4-.85 V.   Finally, the irreversible adsorption of hydroxide ions, also known as oxide formation, occurs at potentials greater than .85 V (region IV).[35]   As can be seen in figure 3.5, the use of different electrolytes lead to changes in both the shape of the CV profiles (figure 3.5(a)) as well as in ORR performance (3.5(b)).

The shift of the hydrogen adsorption/desorption regions to higher potentials when comparing the CV's taken in alkaline and acid electrolytes is one of the most prominent differences. The Koper group explained this difference by pointing out that acidic electrolytes contain an ample amount of H^+ ions while alkaline electrolytes do not.   Therefore, hydrogen adsorption/desorption is much slower in alkaline mediums since the H^+ ion must be stripped from a water molecule, rather than an H_3O^+ ion in acidic mediums.[43, 44]   Likewise, for similar reasons (OH^- ions being more bountiful in alkaline mediums), the hydroxide anion adsorption occurs at lower potentials in alkaline electrolytes.

Although the differences in concentrations of H^+ and OH^- can plausibly explain the differences in CV profiles, differences in both the shape of CV's and ORR performance were seen when electrolytes containing the same anion but different metal cations were used.   A close examination of the cyclic voltammetry profiles show that for peaks
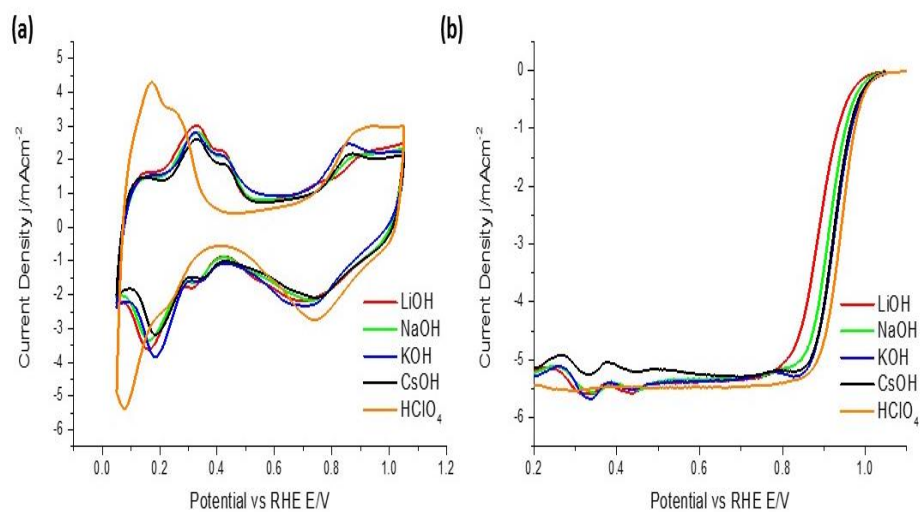
Figure 3.5. Cyclic voltammetry in an argon atmosphere (a) as well as ORR polarization curves (b) for Johnson Matthey Pt/C using different electrolytes.

attributed to reversible adsorption/desorption, the peak intensities seem to increase in the order of (CsOH < KOH < NaOH < LiOH).   In contrast, for the irreversible, oxide formation peaks above .82 V, the peak intensity seems to increase in the inverse order (LiOH < NaOH < CsOH <KOH).

The ORR polarization curves using alkaline electrolytes with different cations also showed several distinct and interesting characteristics. With the exception of the measurement taken in CsOH, similar ORR polarization curves are seen until approximately .7 V.   After .7 V, the catalytic performances began to deviate with measurements taken in LiOH electrolytes showing the worst catalytic activity and increasing in the order of (LiOH < NaOH < KOH ≤ CsOH < $HClO_4$).

The Markovic group explained this anomaly by theorizing that these differences were due to the lower working electrode potential in alkaline mediums allowing for the outer Helmholtz plane, and consequently the metal cations, to be closer in distance to the catalyst surface.[35]   The solvated metal cations can then be stabilized through a non-covalent interaction between the solvated metal cation and a oxidized or OH_{ad} catalyst surface (OH_{ad}-M^+(H_2O)$_x$).[35]   Since oxygen reduction reaction occurs upon the platinum surface, the Markovic group hypothesized that the closer cation distance to the catalyst surface could hinder oxygen diffusion to the surface of the catalyst.[35]   They further found a correlation between the hydration of the energy of the metal cation and ORR performance, and from this, they concluded that a higher hydration energy ($Li^+ > Na^+ > K^+ > Cs^+$) leads to greater concentrations of solvated metal ion clusters at the outer Helmholtz plane.[35]   This leads to increased inhibition of oxygen diffusion and, as can be seen in figure 3.5(b), lower ORR performance. Thus, an inverse relationship was found to exist between hydration energy of the metal cations and ORR performance.   These conclusions correlate very well to the experimental data.   As previously mentioned, hydroxide adsorption/oxide formation does not start on platinum surfaces until

approximately .65-.7 V (figure 3.5(a)). As expected, no differences in ORR performance were observed before this voltage (figure 3.5(b)). The differences in ORR performance were only observed at voltages where oxides or hydroxides would be present on the platinum surface. This phenomena does not occur in acidic mediums because a greater charge repulsion due to the electrode potential being much higher in acid electrolytes (1.229 V vs .401) repels any solvated cations far away from the catalyst surface. As a result, as figure 3.5(b) shows, the oxygen reduction reaction performed the best in acid mediums. Although this groundbreaking study was performed Pt single crystals, the data shown in figure 3.5 as well as the research done by Katsounaros and Mayrhofer [37] show that this trend also exists on polycrystalline platinum surfaces.

The discrepancies using CsOH electrolytes (having less irreversible OH^- adsorption than KOH when it should be higher and having an ORR polarization curve different from the measurements in other electrolytes) were probably due to the poorer purity of the electrolyte itself rather than the result of the Cs^+ cation. Similar discrepancies and conclusions using CsOH electrolytes were reported in other published manuscripts as well.[37, 45, 46]

Figure 3.6 shows the cyclic voltammetry (3.6(a)) and ORR polarization curves (3.6(b)) for the as synthesized Au/C catalysts. When viewing the volcano plot of oxygen adsorption strength (figure 1.9), gold is theorized to have too weak of an oxygen adsorption energy. Thus, peaks correlating to the OH^- adsorption/oxide formation were only seen at potentials higher than 1.1 V (figure 3.6(b)). However, this potential is right outside the potential scan range used for ORR polarization measurements, and as can be seen in figure 3.6(b), the absence of adsorbed OH and/or oxides led to no significant changes in performance when different electrolytes were used. These patterns correlate very well with studies that were done on gold single crystals.[36] Once again, the CsOH
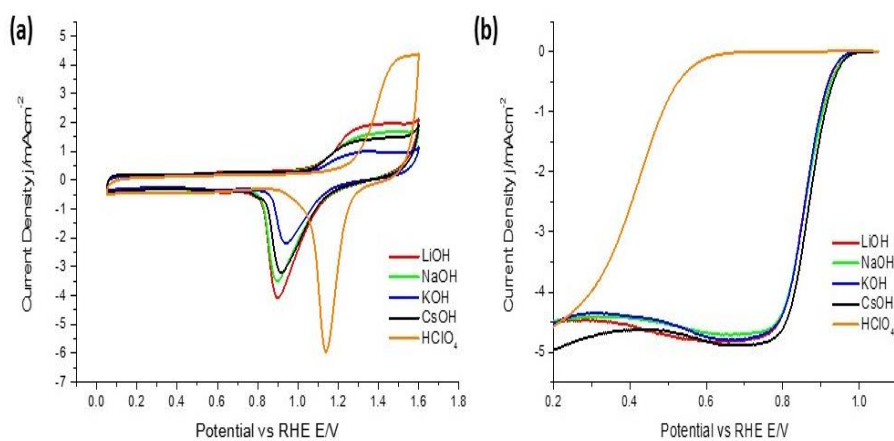
Figure 3.6. Cyclic voltammetry in an argon atmosphere (a) as well as ORR polarization curves (b) for as synthesized Au/C using different electrolytes.

electrolyte was the exception, and as was the case with platinum, the lower purity of the electrolyte itself rather than the Cs^+ cation probably led to this anomaly.

Interestingly, opposite of what was observed with platinum catalysts, vast improvements in the ORR performance were seen when acidic electrolytes were replaced with alkaline ones (figure 3.6(b)). Although hypotheses explaining the reason for this occurrence have been published [13], it is still unknown what exactly causes this enormous discrepancy between alkaline and acid electrolytes. However, no change in ORR performance using different electrolytes seems to imply that whatever pathway the oxygen reduction reaction takes in alkaline mediums is not dependent on oxygen diffusion to the inner Helmholtz plane and thus, may not rely on direct adsorption of oxygen to the catalyst surface. The Mukerjee group reported on the possibility of electron tunneling from the electrode to the outer Helmholtz plane and the creation of superoxide anions as being possible in alkaline mediums.[15] Indeed, Blizanac et al. also calculated that these superoxide anions, though unstable in acidic mediums due to rapid protonation by H^+ ions, are considerably more stable in alkaline mediums.[14] These superoxide ions, as previously mentioned in the introduction, may play a role in the increased performance of gold catalysts in alkaline mediums. To conclude, the use of electrolytes containing different cations can be a useful and effective technique toward determining which reaction pathway is favored for different catalysts in different conditions.

3.2 Metal Phthalocyanines on Vulcan XC-72

3.2.1 Structural Characterization

Due to the low solubility properties of phthalocyanines, common

solvents such as ethanol or isopropyl alcohol could not be used to disperse the phthalocyanines on carbon support.[47]   Fortunately, dispersion of phthalocyanines was possible using concentrated sulfuric acid (H_2SO_4) and its use as a solvent has been reported in previous publications.[48, 49] However, due to the high acidity and corrosive nature of sulfuric acid, experiments to confirm that the (M^+-N-C) coordinated structures were preserved during loading onto Vulcan XC-72 were undertaken.

Even after loading of metal phthalocyanines onto Vulcan XC-72, only XRD diffraction peaks associated to Vulcan XC-72 were seen (figure 3.7). Other reports have published similar results and the lack of diffraction peaks are more than likely due to the metal phthalocyanines existing in an amorphous state on the carbon support.[50]   However, successful loading of the metal phthalocyanines onto Vulcan XC-72 was confirmed through UV-Vis absorption measurements.   As figure 3.8 shows, the UV-Vis spectra peaks associated to each metal phthalocyanine remain present even after loading onto the carbon support.   Thus, UV-Vis and XRD measurements, confirmed the presence of M^+-N-C coordination structures even after loading onto Vulcan XC-72.

3.2.2 Electrochemical Measurements

Copper, cobalt and iron phthalocyanines were chosen due to oxygen binding onto the metal ion occurring through the same end on method and also because the varying oxygen adsorption strengths of these three phthalocyanines could confirm that the ORR occurs through reactions in the inner Helmholtz plane.[32, 33]   Density functional theory calculations concluded that copper phthalocyanine would not bind oxygen at all, cobalt phthalocyanine would bind and facilitate the two electron reduction reaction to peroxide and iron phthalocyanine would bind and complete the four electron reduction of oxygen.[32, 33]
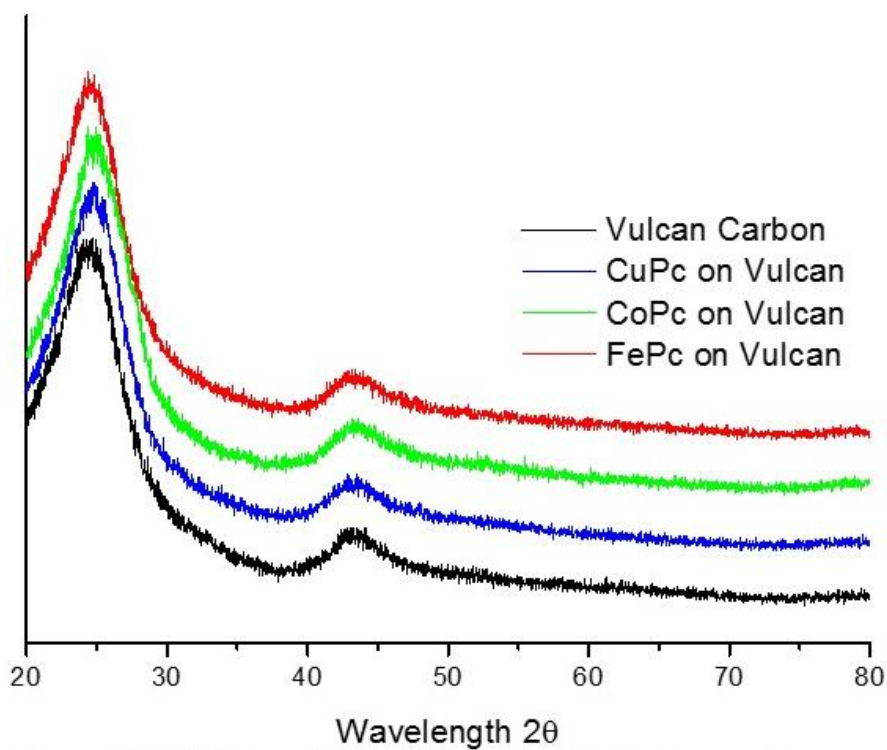
Figure 3.7. XRD profiles of the metal phthalocyanines loaded on Vulcan XC-72.
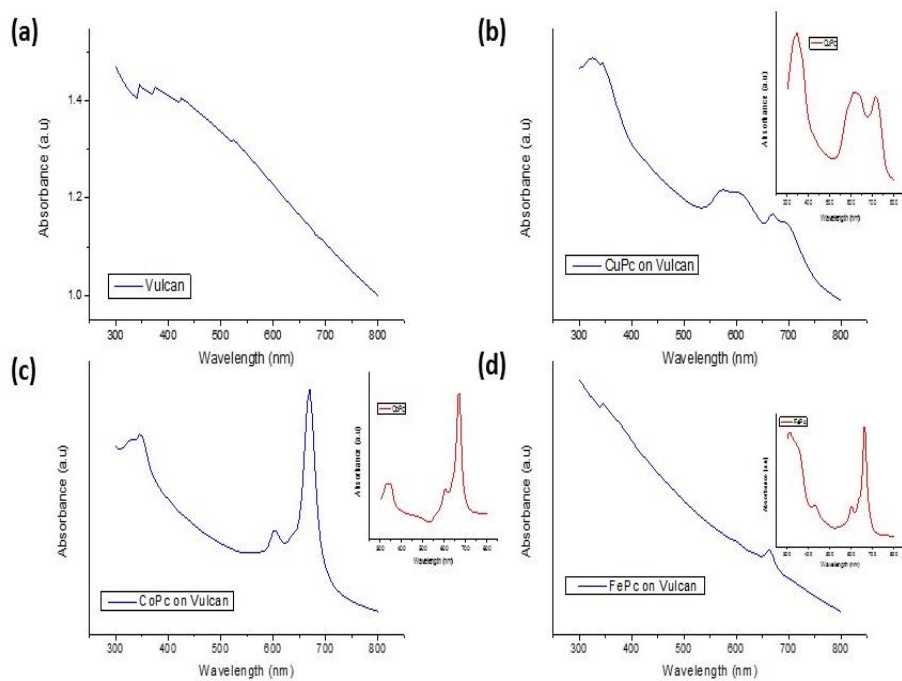
Figure 3.8. UV-Vis absorbance spectra for Vulcan XC-72, (a) copper phthalocyanine, (b) cobalt phthalocyanine (c), and iron phthalocyanine (d).

Since all the metal phthalocyanines were loaded onto a carbon support, electrochemical measurements of the carbon support itself were initially taken.   Although the exact mechanism is currently not known, as figure 3.9 shows, carbon materials do possess some ORR activity. Differing theories involving the stability of the superoxide [51], presence of unsaturated carbons at crystallite edges [52] and/or the presence of oxygen containing surface groups [53] have all been published and provide plausible explanations for how carbon based materials catalyze the ORR.   However, all of these theories were in agreement that carbon catalysts proceed mostly through the two electron reduction pathway, which results in oxygen reduction to peroxide.   In addition, differences in ORR performance were seen when different electrolytes were used.   The ORR performance for Vulcan XC-72 increased in the order of LiOH $\leq$ NaOH < CsOH < KOH.

To confirm that Vulcan XC-72 behaved like other carbon materials, the Koutecky-Levich equation was used to calculate the number of electrons transferred.   The Koutecky-Levich equation:

$$\frac{1}{j} = \frac{1}{j_k} + \frac{1}{j_L} = \frac{1}{jk} + \frac{1}{(B\omega^{1/2})}$$

where j, j_k, j_L, and ω are current density at a certain potential, kinetic current density and limiting current density, and rotation rate respectively and B can be defined as:

$$B = .62nFC_0(D_0)^{2/3} \nu^{-1/6}$$

where n, F, C0, D0, and ν are number of electrons transferred, Faraday's constant, reactant diffusion coefficient, and kinetic viscosity of the solution
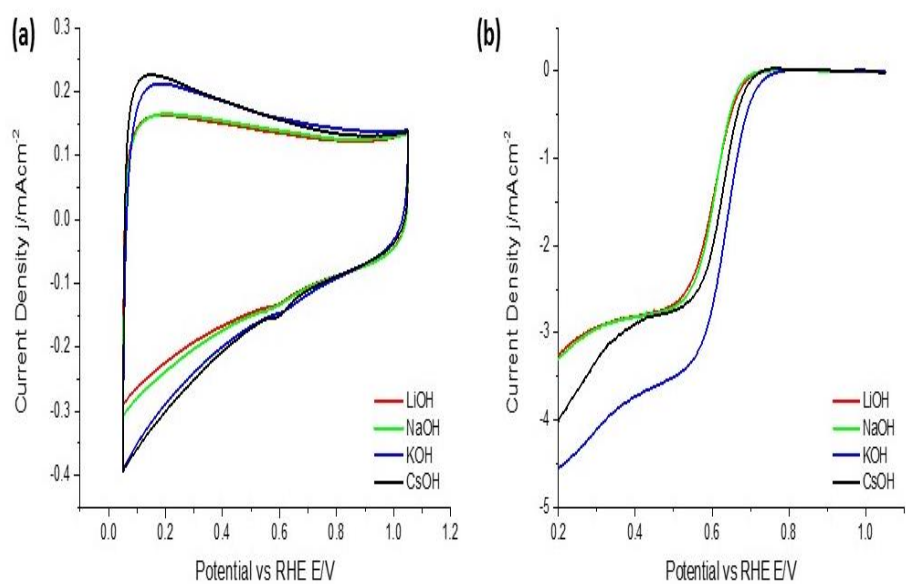
Figure 3.9. Cyclic voltammetry in an argon atmosphere (a) as well as ORR polarization curves (b) for Vulcan XC-72 using different electrolytes.

respectively.   This equation can be rewritten as:

$$\frac{j^{-1}}{\omega^{-.5}} = \frac{1}{j_k} + \frac{1}{B}$$

Therefore, when a Koutecky-Levich graph (1/j vs $\omega^{-.5}$) graph is drawn, the y-intercept of the resulting line becomes $1/j_k$ and the slope (*m*) is equal to 1/B.[54-57]   Substituting the value of B into the equation and resulting reordering to solve for the number of electrons transferred (n) leads to the final equation:

$$n = \frac{1}{.62FC_0D_0{}^{2/3}v^{-1/6}m}$$

ORR polarization curves taken at different rotation rates and the resulting Koutecky-Levich graphs (figures 3.10 and 3.11) were used to calculate the number of electrons transferred for Vulcan XC-72.   Although at high overpotentials, electron transfer numbers as high as 3 were possible, as table 3.1 shows, ORR on Vulcan XC-72 at higher potentials, which are closer to practical fuel cell conditions, favored the two electron pathway rather than the four electron pathway.

The ORR polarization curves for copper phthalocyanine on Vulcan XC-72, gave the appearance as if the copper phthalocyanine compounds possess some oxygen reduction activity (figure 3.12(b)).   However, when comparing this activity with that of the carbon support (figure 3.12(c-f)), it
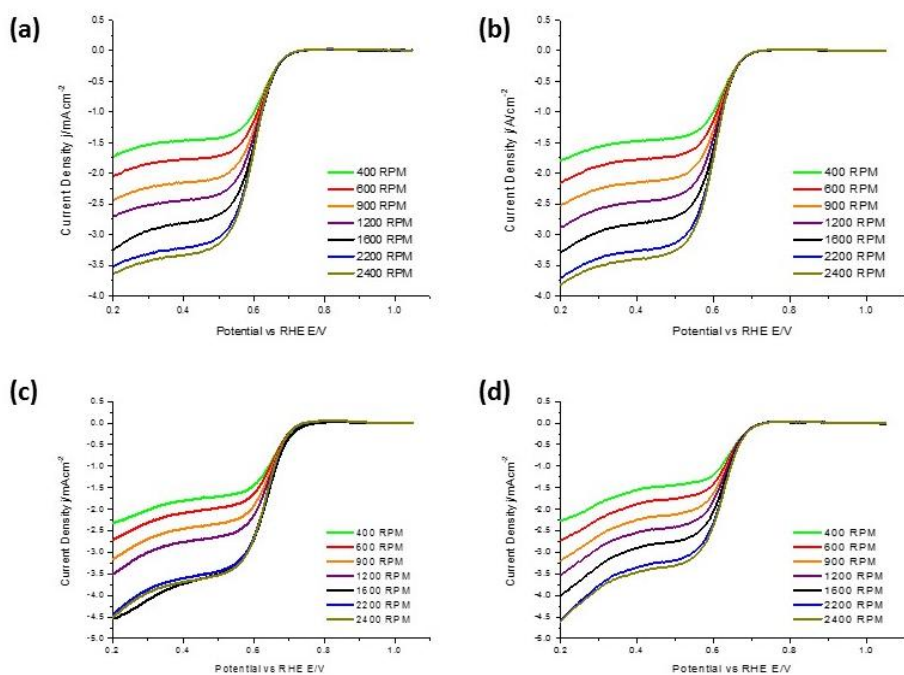
Figure 3.10. ORR polarization curves taken at different rotation rates for Vulcan XC-72 in LiOH (a), NaOH (b), KOH (c), and CsOH (d).
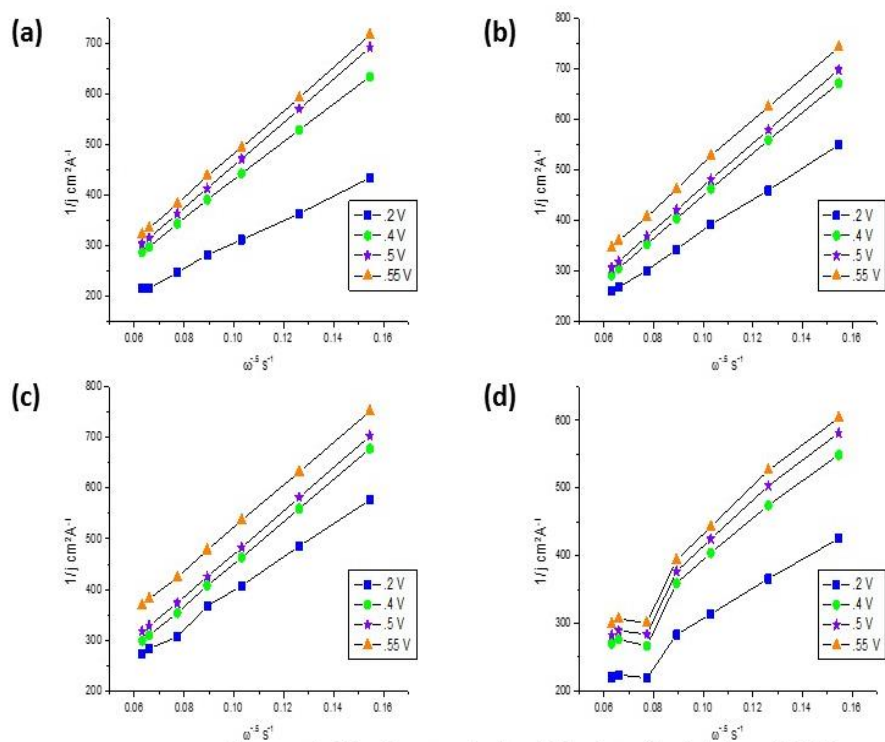
Figure 3.11. Koutecky-Levich plots for Vulcan XC-72 in LiOH (a), NaOH (b), KOH (c), and CsOH (d).

(a)	Voltage	# of Electrons Transferred
	.2	2.710
	.4	2.189
	.5	2.153
	.55	2.169

(b)	Voltage	# of Electrons Transferred
	.2	2.856
	.4	2.182
	.5	2.118
	.55	2.086

(c)	Voltage	# of Electrons Transferred
	.2	3.839
	.4	2.794
	.5	2.613
	.55	2.559

(d)	Voltage	# of Electrons Transferred
	.2	3.781
	.4	2.393
	.5	2.139
	.55	2.112

Table 3.1. Number of electrons transferred for Vulcan XC-72 at different voltages in LiOH (a), NaOH (b), KOH (c), and CsOH (d).

can be concluded that the observed activity was mostly from the carbon support rather than the phthalocyanine compound.   These results correlated well with previously reported density functional theory calculations.   The ORR performance was found to increase in the order of LiOH $\leq$ NaOH < KOH $\leq$ CsOH.   Resulting Koutecky-Levich calculations (figures 3.13, 3.14 and table 3.2) show that the oxygen reduction reaction was favored along the two electron reduction pathway, further confirming that the observed ORR activity was from the carbon support.

Cyclic voltammetry scans of the cobalt phthalocyanine loaded on Vulcan XC-72 (figure 3.15(a)) show the $Co^{+2/+3}$ redox peak at approximately .3 V [58] and further confirmed the successful loading of cobalt phthalocyanine onto Vulcan XC-72.   The ORR polarization curves (3.15(b)) showed that although both Vulcan XC-72, copper phthalocyanine loaded on Vulcan XC-72, and cobalt phthalocyanine loaded on Vulcan XC-72 favor the two electron reduction pathway, cobalt phthalocyanine on Vulcan XC-72 exhibited some noticeable differences.   The ORR polarization curves for cobalt phthalocyanine loaded on Vulcan XC-72 have a longer limiting current region and a higher onset potential.   In addition no clear trend in activity can be made other than the use of different electrolytes caused changes in ORR performance.   Corresponding Koutecky-Levich calculations (figures 3.16, 3.17 and table 3.3) proved that this catalyst does proceed mostly through the two electron pathway, but the improved kinetics and overall performance suggests that a different pathway is utilized.   Thus, these conclusions give further credence to previous density functional theory calculations [32, 33, 59] since oxygen adsorption and consequent reduction could be occurring on the metal phthalocyanine surface itself, a phenomena that is not possible with copper phthalocyanines loaded on Vulcan XC-72.

Analysis of the iron phthalocyanines loaded on Vulcan XC-72 electrochemical data provided the most conclusive evidence that the oxygen reduction reaction occurs through an inner Helmholtz plane reaction on the
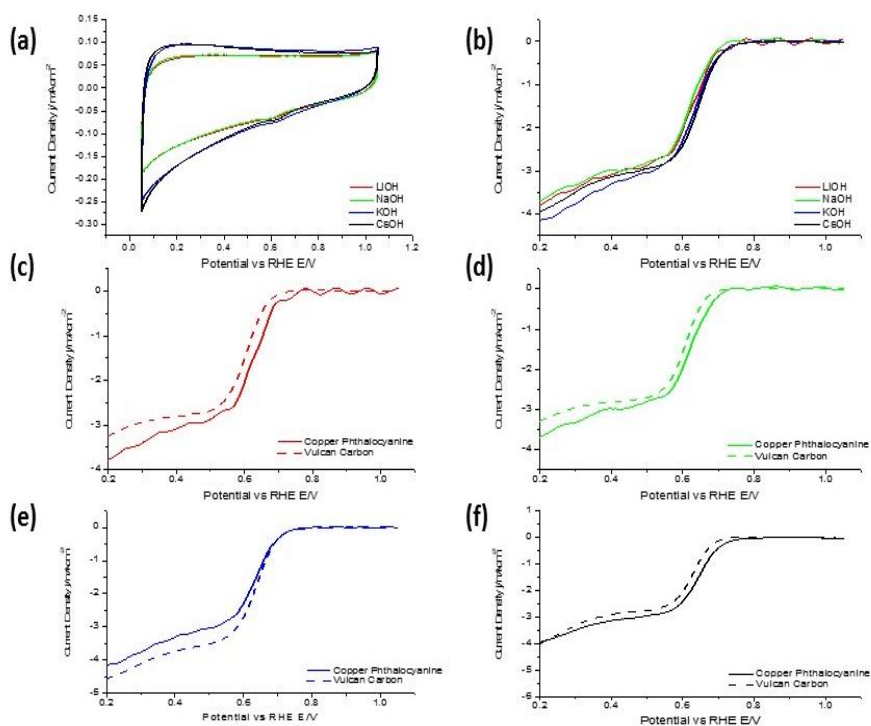
Figure 3.12. Cyclic voltammetry in an argon atmosphere (a) as well as ORR polarization curves (b) for copper phthalocyanine loaded on Vulcan XC-72 using different electrolytes and ORR comparisons to Vulcan XC-72 in LiOH (c), NaOH (d), KOH (e), and CsOH (f).
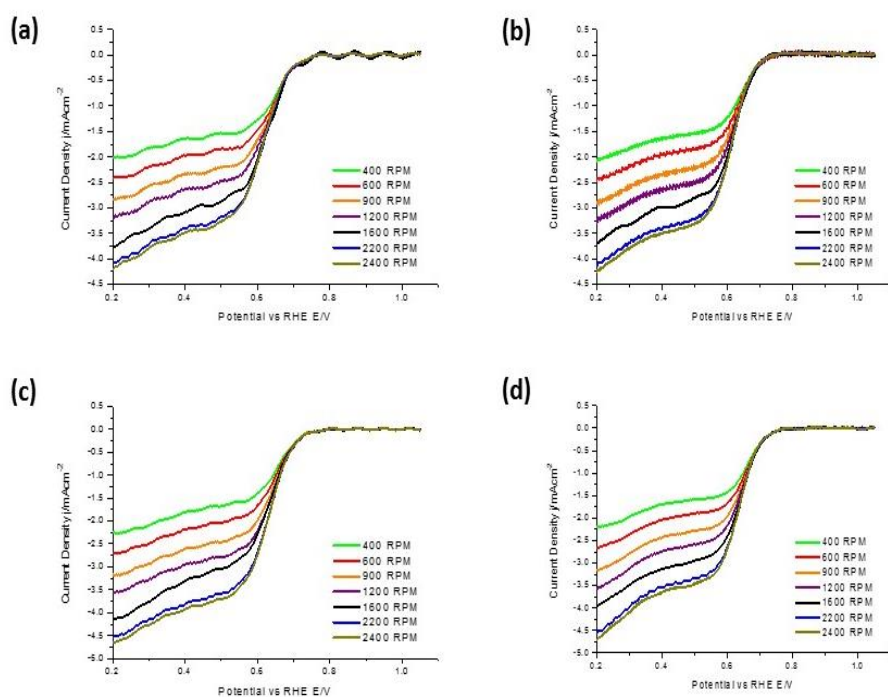
Figure 3.13. ORR polarization curves taken at different rotation rates for copper phthalocyanine loaded on Vulcan XC-72 in LiOH (a), NaOH (b), KOH (c), and CsOH (d).
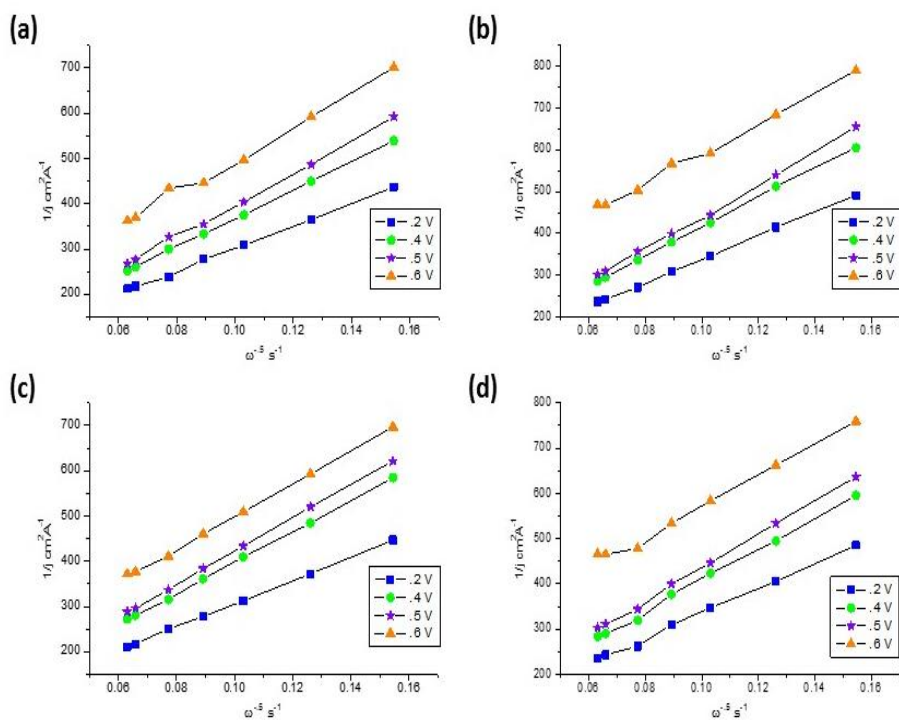
Figure 3.14. Koutecky-Levich plots for copper phthalocyanine loaded on Vulcan XC-72 in LiOH (a), NaOH (b), KOH (c), and CsOH (d).

(a) Voltage	# of Electrons Transferred
.2	3.305
.4	2.642
.5	2.463
.6	2.726

(b) Voltage	# of Electrons Transferred
.2	3.226
.4	2.588
.5	2.361
.6	2.557

(c) Voltage	# of Electrons Transferred
.2	3.668
.4	2.903
.5	2.588
.6	2.490

(d) Voltage	# of Electrons Transferred
.2	3.540
.4	2.654
.5	2.478
.6	2.529

Table 3.2. Number of electrons transferred for copper phthalocyanine loaded on Vulcan XC-72 at different voltages in LiOH (a), NaOH (b), KOH (c), and CsOH (d).
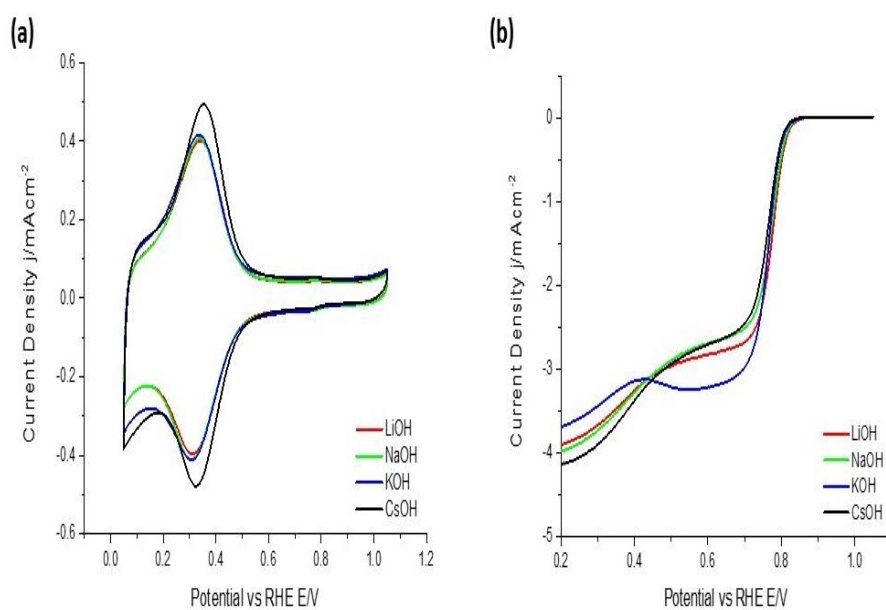
Figure 3.15. Cyclic voltammetry in an argon atmosphere (a) as well as ORR polarization curves (b) for cobalt phthalocyanine loaded on Vulcan XC-72 using different electrolytes.
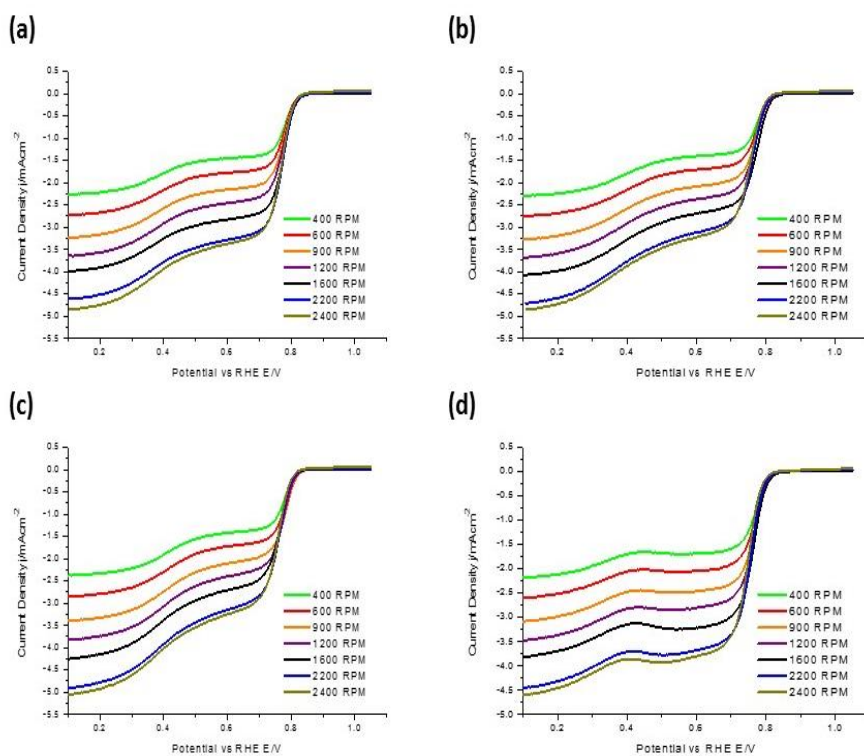
Figure 3.16. ORR polarization curves taken at different rotation rates for cobalt phthalocyanine loaded on Vulcan XC-72 in LiOH (a), NaOH (b), KOH (c), and CsOH (d).
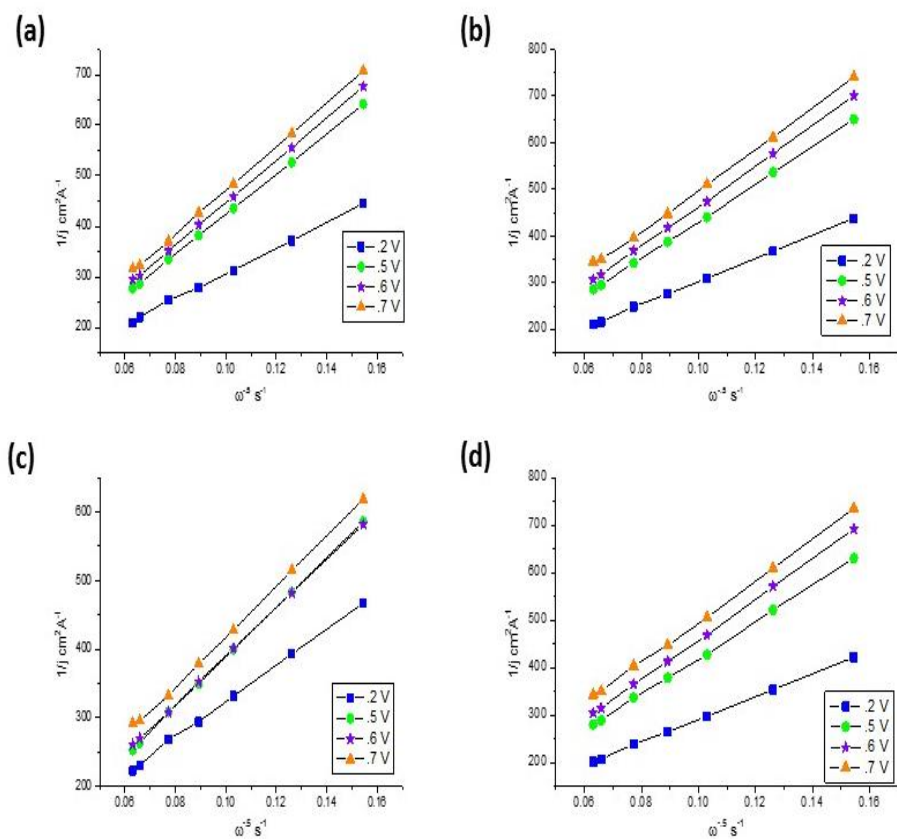
Figure 3.17. Koutecky-Levich plots for cobalt phthalocyanine loaded on Vulcan XC-72 in LiOH (a), NaOH (b), KOH (c), and CsOH (d).

(a)	Voltage	# of Electrons Transferred
	.2	3.584
	.5	2.282
	.6	2.168
	.7	2.106

(b)	Voltage	# of Electrons Transferred
	.2	3.650
	.5	2.278
	.6	2.114
	.7	2.078

(c)	Voltage	# of Electrons Transferred
	.2	3.423
	.5	2.250
	.6	2.580
	.7	2.512

(d)	Voltage	# of Electrons Transferred
	.2	3.778
	.5	2.376
	.6	2.147
	.7	2.115

Table 3.3. Number of electrons transferred for cobalt phthalocyanine loaded on Vulcan XC-72 at different voltages in LiOH (a), NaOH (b), KOH (c), and CsOH (d).

catalyst surface.   To start, two distinct redox peaks correlating to the $Fe^{+1/+2}$ and $Fe^{+2/+3}$ redox reactions were present at approximately .25 V and .8 V (figure 3.18(a).[60]   Of the two, the $Fe^{+2/Fe+3}$ peak seemed to play an integral role in ORR kinetics.   Based off of how hemoglobin transports oxygen within our own bodies, Fe^{+2} ions are thought to be able to bind and release oxygen with relative ease while Fe^{+3} ions have too strong of a binding energy, and thus prevent detachment of the final product.[61, 62] Although the conditions within a human body and electrochemical measurement conditions are drastically different, adaptations of this concept could explain how the ORR is proceeding on iron phthalocyanine and why it had the highest activity of the three metal phthalocyanines being compared in this study.   As figure 3.18(c) shows, the ORR activity curve sharply rises from the limiting current value to a nearly zero current value at a potential close to where the Fe^{+2}/Fe^{+3} redox reaction occurs.   This sharp incline is in contrast to what is seen for Pt/C catalysts.   As mentioned in section 3.1.2 and can be seen from figure 3.18(c), no redox peaks are present for Pt/C and ORR activity is likely gradually deactivated due to the blocking of active sites by OH ion adsorption or platinum oxide formation.   This explains the gradual incline from the limiting current value to zero current value observed in the mixed kinetics region; deactivation of the active sites gradually occurs as an increasing number of active sites are blocked.   However, this gradual rise is not observed in iron phthalocyanines because if the ORR only proceeds when the Fe ion are in the Fe^{+2} state, complete, instantaneous deactivation of all the active sites would occur when the Fe^{+2} ions oxidize to the Fe^{+3} state.   As a result, a nearly instantaneous decrease in reduction activity should be seen near the redox peak potential, which appears to be the case in figure 3.18(c).   Both density functional theory calculations and in-situ experimental data supporting this theory have been reported.[63-65]

When comparing the ORR performance across different electrolytes (figure 3.18(b)), no significant differences are seen.   Slight differences are
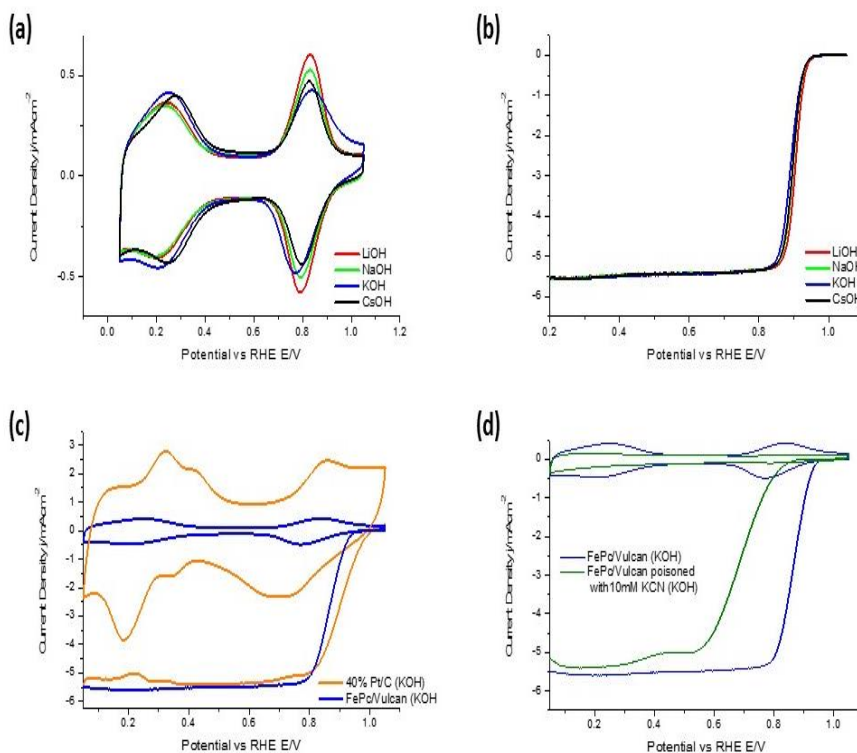
Figure 3.18. Cyclic voltammetry in an argon atmosphere (a) as well as ORR polarization curves (b) for iron phthalocyanine loaded on Vulcan XC-72 using different electrolytes. Cyclic voltammetry and ORR polarization curve comparisons for iron phthalocyanine loaded on Vulcan XC-72 and 40% Pt/C in KOH (c) and the effect of KCN poisoning on iron phthalocyanine loaded on Vulcan XC-72 (d).

seen after .8 V which may be attributed to changes that occur after the Fe ion has oxidized to the Fe^{+3} state.   However, as per density functional theory calculations, Fe^{+2}-N-C coordinated structures seem to have the appropriate oxygen binding energy to adsorb and release oxygen and oxygen intermediates, which leads to high catalytic activity.   Resulting Koutecky-Levich calculations confirmed the transfer of four electrons and subsequent complete four electron reduction (figure 3.19, 3.20 and table 3.4).

In order to confirm the integral role that Fe^{+2}-N-C coordinated sites play in the ORR, 10 mM of KCN was introduced into the electrolyte and electrochemical measurements were subsequently taken.   Cyanide ions (CN^-) are known to strongly attach to iron and iron ions and consequently block the active site surface.[27, 48, 66]   As expected, the ORR performance was significantly lower when cyanide ions were introduced and observation of the CV profile showed the disappearance of both redox peaks (figure 3.18(d)).   These results confirm that iron ions are vital to the ORR and that the Fe^{+2}-N-C coordinated structures are the active sites, from which it can be concluded that the ORR is proceeding through an inner Helmholtz plane reaction on the catalyst surface.

When comparing the catalytic activity for the ORR for Vulcan XC-72 and the three metal phthalocyanines used in this study (figure 3.21), the ORR performance increased in the order of. Vulcan XC-72 = copper phthalocyanine on Vulcan XC-72 $\leq$ cobalt phthalocyanine on Vulcan XC-72 $\leq$ iron phthalocyanine on Vulcan XC-72.   This trend correlates very well with density functional theory calculations that found the same pattern with oxygen binding energy.   When different electrolytes were used, Vulcan XC-72 showed increasing performance in the order of LiOH $\leq$ NaOH < CsOH < KOH.   Copper phthalocyanine on Vulcan XC-72 increased in performance in the order of LiOH $\leq$ NaOH < KOH $\leq$ CsOH and cobalt phthalocyanine on Vulcan XC-72 showed different performances throughout.   Meanwhile, iron phthalocyanine loaded on Vulcan XC-72 showed similar activity
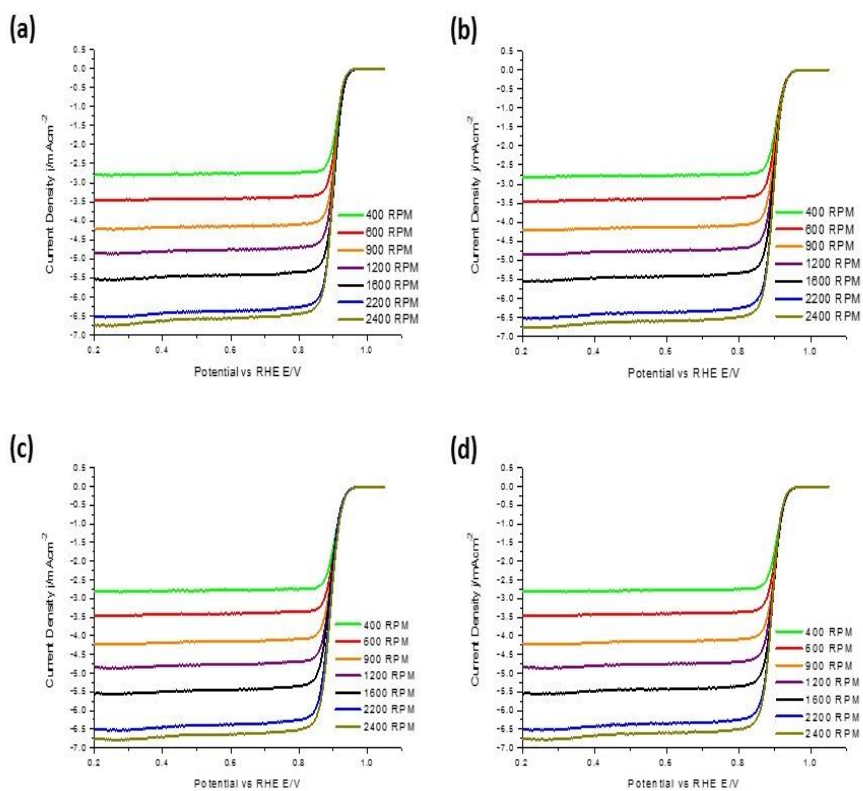
Figure 3.19. ORR polarization curves taken at different rotation rates for iron phthalocyanine loaded on Vulcan XC-72 in LiOH (a), NaOH (b), KOH (c), and CsOH (d).
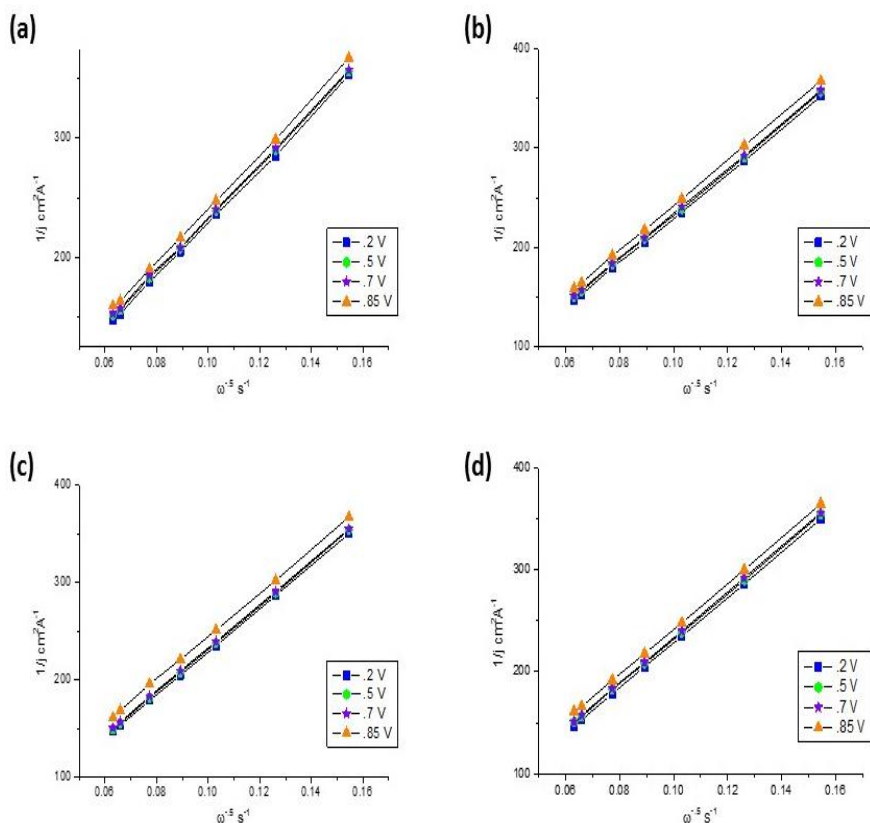
Figure 3.20. Koutecky-Levich plots for iron phthalocyanine loaded on Vulcan XC-72 in LiOH (a), NaOH (b), KOH (c), and CsOH (d).

(a)	Voltage	# of Electrons Transferred
	.2	4.064
	.5	4.062
	.7	4.063
	.85	3.992

(b)	Voltage	# of Electrons Transferred
	.2	4.058
	.5	4.037
	.7	4.029
	.85	3.976

(c)	Voltage	# of Electrons Transferred
	.2	4.091
	.5	4.067
	.7	4.068
	.85	4.058

(d)	Voltage	# of Electrons Transferred
	.2	4.102
	.5	4.082
	.7	4.058
	.85	4.073

Table 3.4. Number of electrons transferred for iron phthalocyanine loaded on Vulcan XC-72 at different voltages in LiOH (a), NaOH (b), KOH (c), and CsOH (d).
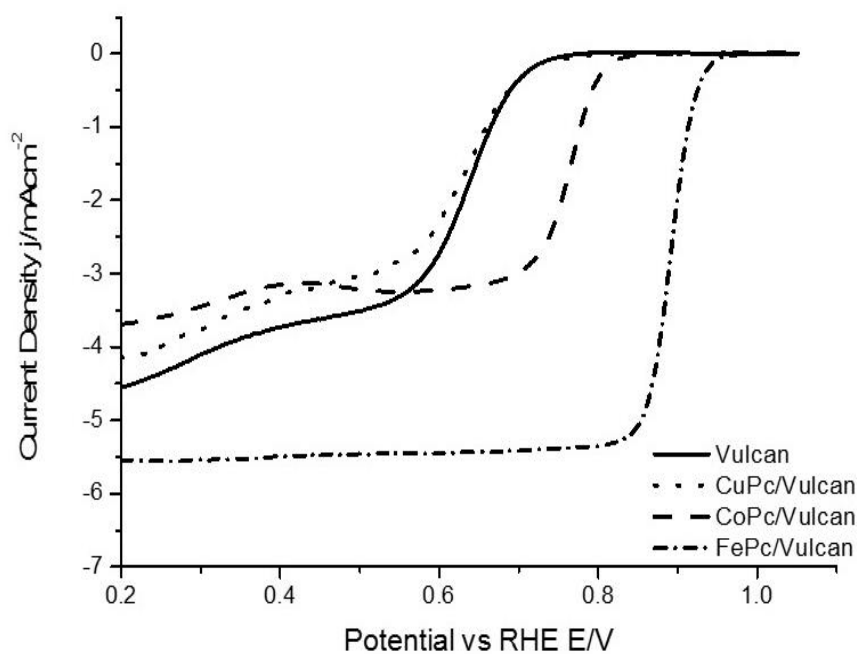
Figure 3.21. ORR polarization curves for Vulcan XC-72, copper phthalocyanine, cobalt phtalocyanine, and iron phthalocyanine loaded on Vulcan XC-72. The trend in increasing ORR performance correlated well with density functional calculations of oxygen binding energies for metal phthalocyanines

throughout all the electrolytes.   The importance of these patterns will be shown and explained further in the next section.   To conclude, before heat treatment, reactions seem to be occurring through the inner Helmholtz plane. Therefore, factors such as oxygen adsorption/binding energy are likely to play a major role in determining the overall ORR catalytic activity.

3.3 Heat Treated Metal Phthalocyanines

3.3.1 Structural Characterization

For most non-precious metal catalysts, heat treatment leads to improvements in catalytic activity. Thus, a multitude of reports have been published to try and explain this phenomena [67-70] but currently, no exact reason or explanation has been determined.

Although graphitization of carbon with heat treatment is usually well agreed upon, what happens to the M^+-N-C coordination sites still remains a controversy.   Some researchers argue that heat treatment stabilizes the catalyst and although some of the M^+-N-C coordinated structures do decompose, the sites that survive heat treatment continue to facilitate the ORR.   However, though the idea that some active sites surviving the heat treatment is plausible, a lower number of active sites should lead to a decrease in catalytic activity.   Figure 3.22 shows the XRD diffraction profiles of the phthalocyanines on Vulcan XC-72 before and after heat treatment.   As previously mentioned, due to the phthalocyanines existing in an amorphous state on the carbon support, only the diffraction peaks associated to Vulcan XC-72 were present before heat treatment (figure 3.22(a)).   In contrast, heat treatment led to the appearance of minor peaks throughout the entire scan range of the metal phthalocyanines.   These peaks were too small to characterize but most likely are associated to the formation of metal oxides.[50]   Therefore, a scenario in which the high temperatures
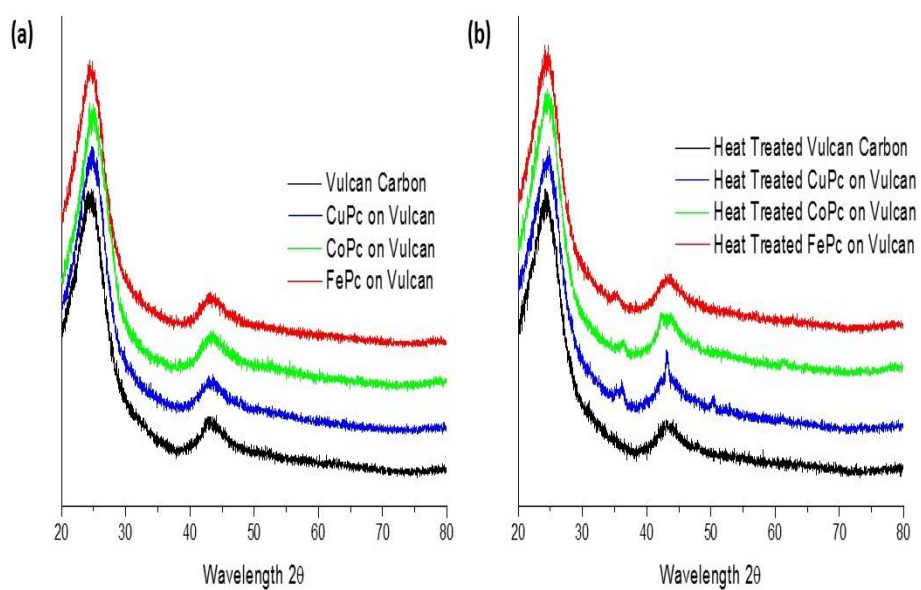
Figure 3.22. XRD diffraction peaks for metal phthalocyanines loaded on Vulcan XC-72 before (a) and after (b) heat treatment.

destroy the M^+-N-C coordinated structures and the metal ions are either reduced to the metal form or are oxidized to the oxide form during cooling to room temperature seems plausible.

UV-Vis absorbance spectra after heat treatment of the metal phthalocyanines on Vulcan XC-72 provided further support against the notion that the existing coordinated sites after heat treatment remain the active sites. As seen in figure 3.23, none of the absorbance peaks attributed to the metal phthalocyanines are present after heat treatment. Thus, even though some M^+-N-C coordinated sites could realistically survive the heat treatment process and consequently continue to catalyze the ORR through an inner Helmholtz plane/adsorption to catalyst surface reaction, the lack of absorbance peaks and formation of oxide diffraction peaks suggest that most of these sites are destroyed during heat treatment and the surviving sites only provide a minor contribution to the overall ORR performance.

3.3.2 Electrochemical Measurements

CV profiles of the heat treated Vulcan XC-72 showed no noticeable changes. However, a loss in ORR activity is seen after heat treatment (figure 3.24(a), (c)) of Vulcan XC-72. The ORR activity followed the same trend as before heat treatment in that catalytic activity increased in the order of LiOH ≤ NaOH <CsOH < KOH. Corresponding Koutecky-Levich calculations showed that though the heat treated Vulcan XC-72 can reach electron numbers close to 4 in some electrolytes at high overpotentials, at potentials likely found in fuel cell operating conditions, it catalyzed the ORR mostly via the two electron method (figures 3.25, 3.26, and 3.27).

When comparing the electrochemical data before and after heat treatment, certain hypotheses can be made. As mentioned earlier, numerous plausible theories exist for oxygen reduction to peroxide on carbon based catalysts. One of these theories involves oxygen functional
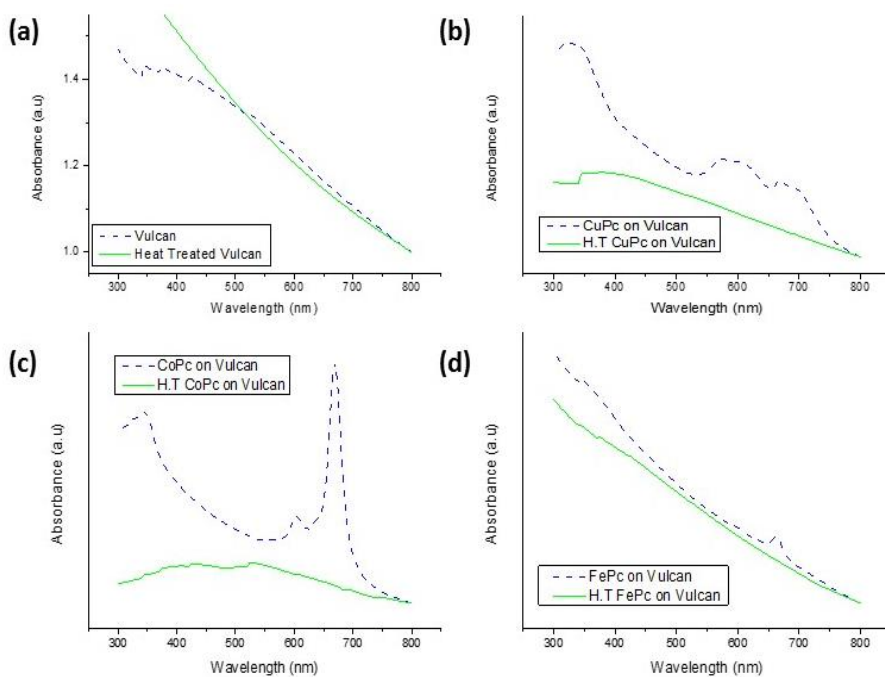
Figure 3.23. UV-Vis absorbance spectra before and after heat treatment for Vulcan XC-72 (a), copper phthalocyanine on Vulcan XC-72 (b), cobalt phthalocyanine on Vulcan XC-72 (c), and iron phthalocyanine on Vulcan XC-72 (d).
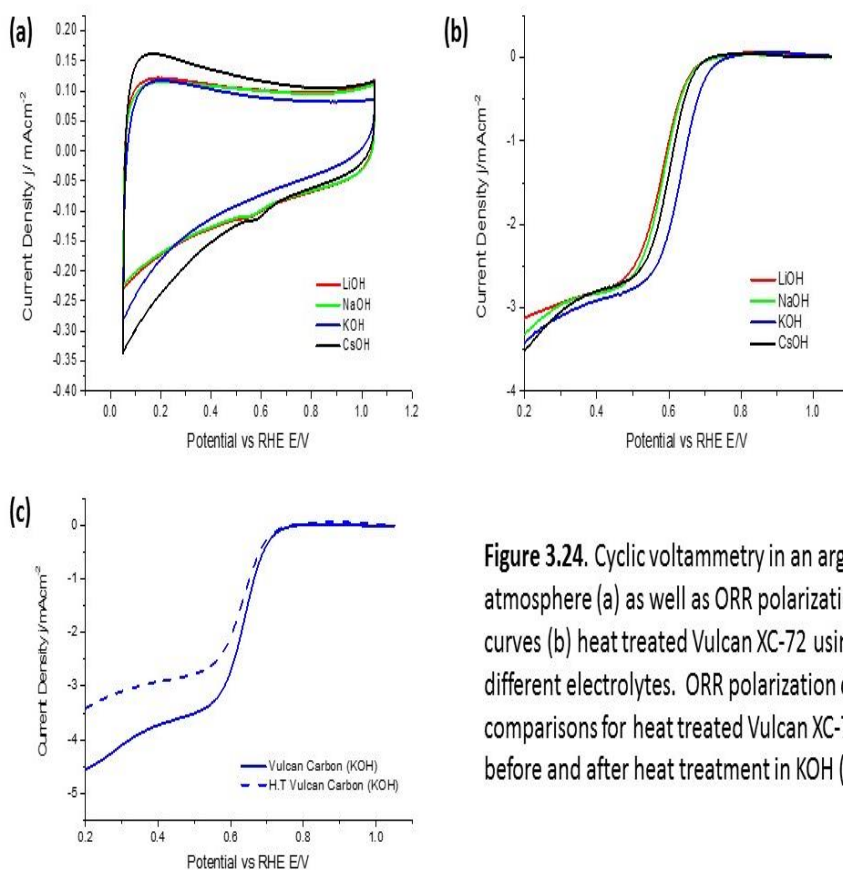
Figure 3.24. Cyclic voltammetry in an argon atmosphere (a) as well as ORR polarization curves (b) heat treated Vulcan XC-72 using different electrolytes. ORR polarization curve comparisons for heat treated Vulcan XC-72 before and after heat treatment in KOH (c)
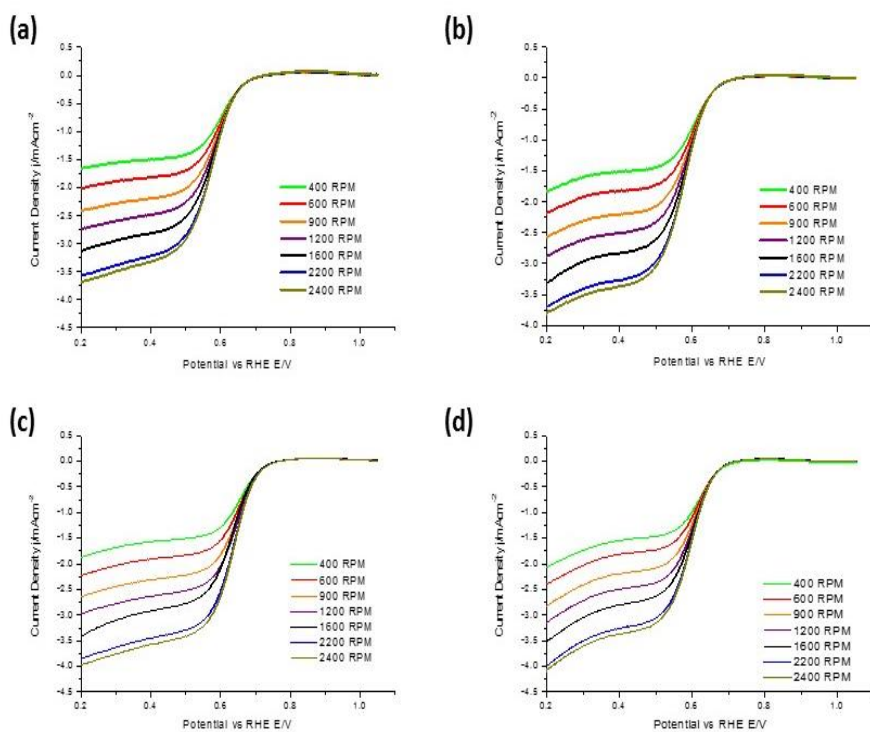
Figure 3.25. ORR polarization curves taken at different rotation rates for heat treated Vulcan XC-72 in LiOH (a), NaOH (b), KOH (c), and CsOH (d).
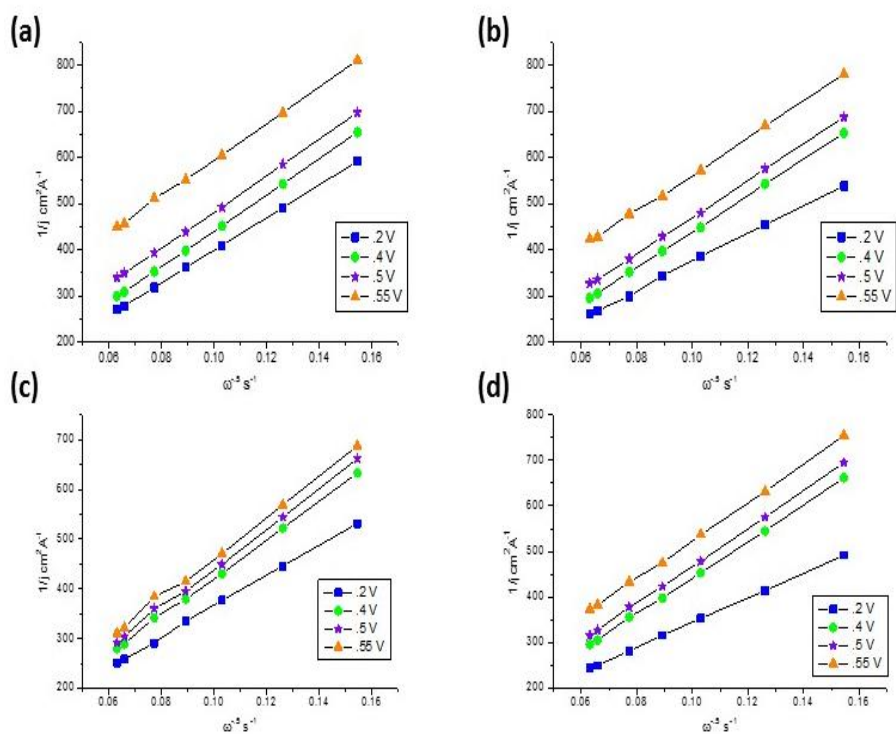
Figure 3.26. Koutecky-Levich plots for heat treated Vulcan XC-72 in LiOH (a), NaOH (b), KOH (c), and CsOH (d).
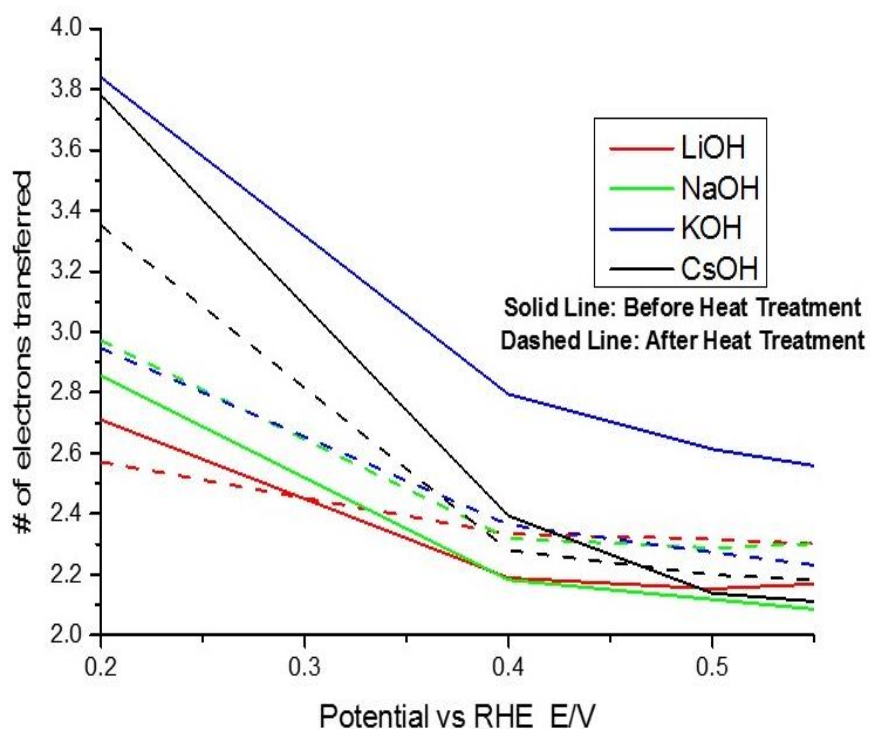
Figure 3.27. Number of electrons transferred for heat treated Vulcan XC-72 at different voltages and in different electrolytes before (solid lines) and after (dashed lines) heat treatment.

groups present on the surface altering the surface properties of the carbon material, and thus easing the reaction kinetics.[53, 71]   The experimental data supports this idea since heat treatment usually leads to a loss of surface functional groups.[52]   Heat treatment is actually even one of the methods used to eliminate the oxide functional groups on graphene oxide, resulting in reduced graphene sheets.[72, 73]   The experimental data supports this theory since the loss of oxygen functional groups could explain the loss in activity seen after heat treatment.   In addition, the fact that the same pattern in performance with different electrolytes is seen before and after heat treatment implies that the ORR is proceeding along the same pathway.

Unlike heat treated Vulcan XC-72, heat treatment of copper phthalocyanine showed a remarkable jump in catalytic activity.   A cursory glance of the CV profile showed no disappearance or formation of new peaks after heat treatment (figure 3.28(a)).   However, a comparison of the ORR performance (figure 3.28(c)) showed drastic differences.   Heat treatment led to both a stable limiting current region and a significant improvement in the onset potential.   In addition, corresponding Koutecky-Levich calculations showed a shift from the electron transfer number of two before heat treatment to four after heat treatment (figures 3.29, 3.30, and 3.31).   Interestingly, with the exception of CsOH, the performance patterns across different electrolytes (LiOH $\leq$ NaOH $\leq$ KOH) remained the same before and after heat treatment.   The discrepancies with CsOH could be due to the generally lower purity of CsOH, as mentioned earlier.[37, 45, 46] These results suggest that the, like Vulcan XC-72, the ORR pathway remains the same, but formation of a new active site to catalyze the peroxide intermediates to water could possibly be responsible for the improvements in catalytic performance.   This concept will be explained and further supported in the following section (section 3.4).

Differences were also found when cobalt phthalocyanines on
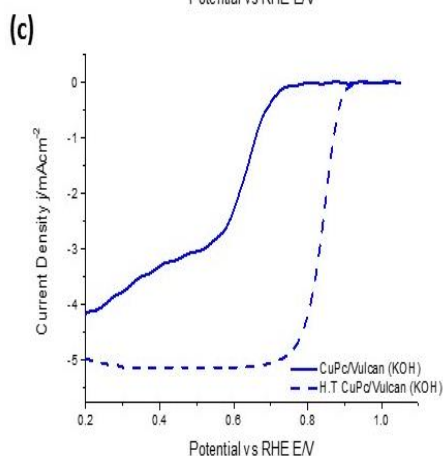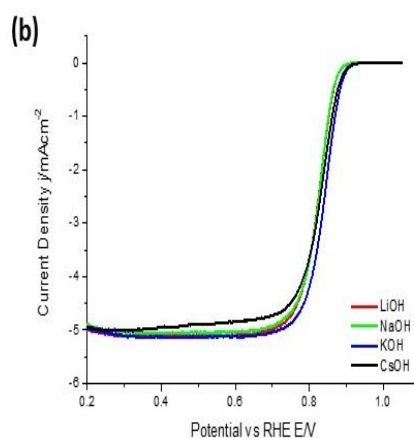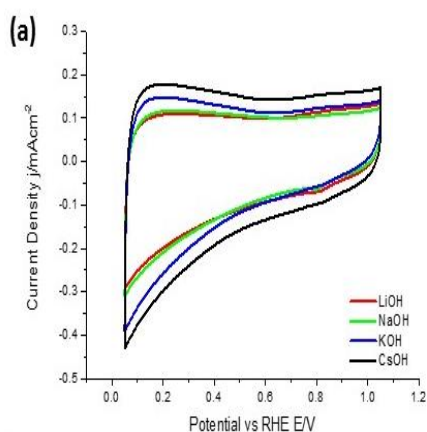
Figure 3.28. Cyclic voltammetry in an argon atmosphere (a) as well as ORR polarization curves (b) heat treated copper phthalocyanine loaded on Vulcan XC-72 using different electrolytes. ORR polarization curve comparisons for heat treated copper phthalocyanine loaded on Vulcan XC-72 before and after heat treatment in KOH (c)

Figure 3.29. ORR polarization curves taken at different rotation rates for heat treated copper phthalocyanine loaded on Vulcan XC-72 in LiOH (a), NaOH (b), KOH (c), and CsOH (d).
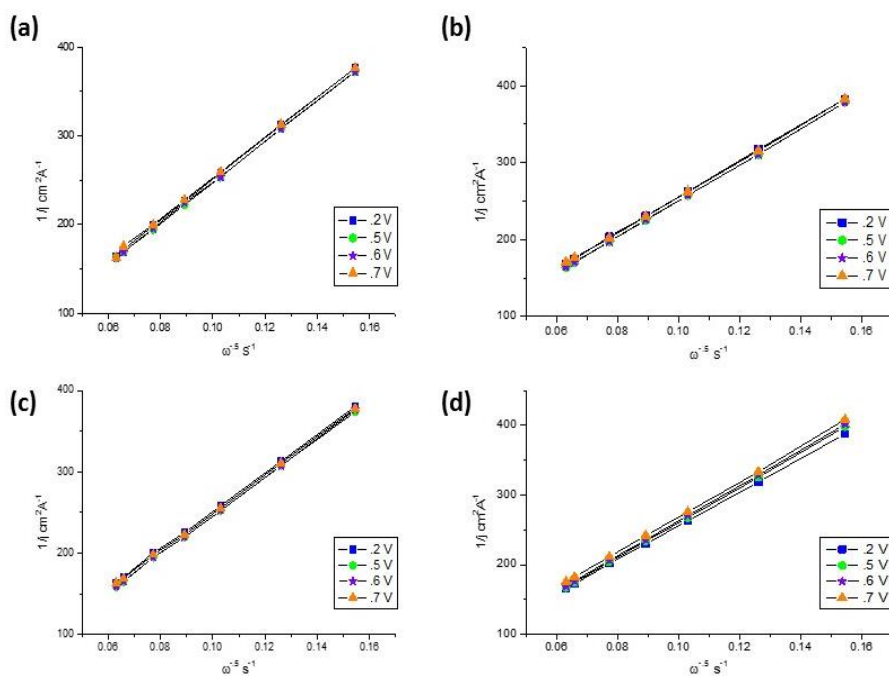
Figure 3.30. Koutecky-Levich plots for heat treated copper phthalocyanine loaded on Vulcan XC-72 in LiOH (a), NaOH (b), KOH (c), and CsOH (d).
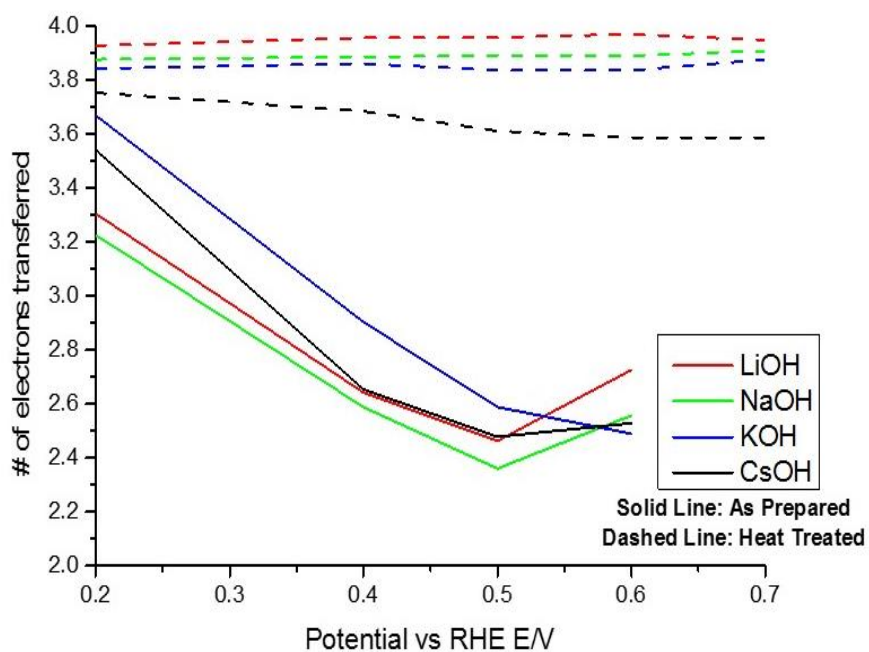
Figure 3.31. Number of electrons transferred for heat treated copper phthalocyanine loaded on Vulcan XC-72 at different voltages and in different electrolytes before (solid lines) and after (dashed lines) heat treatment.

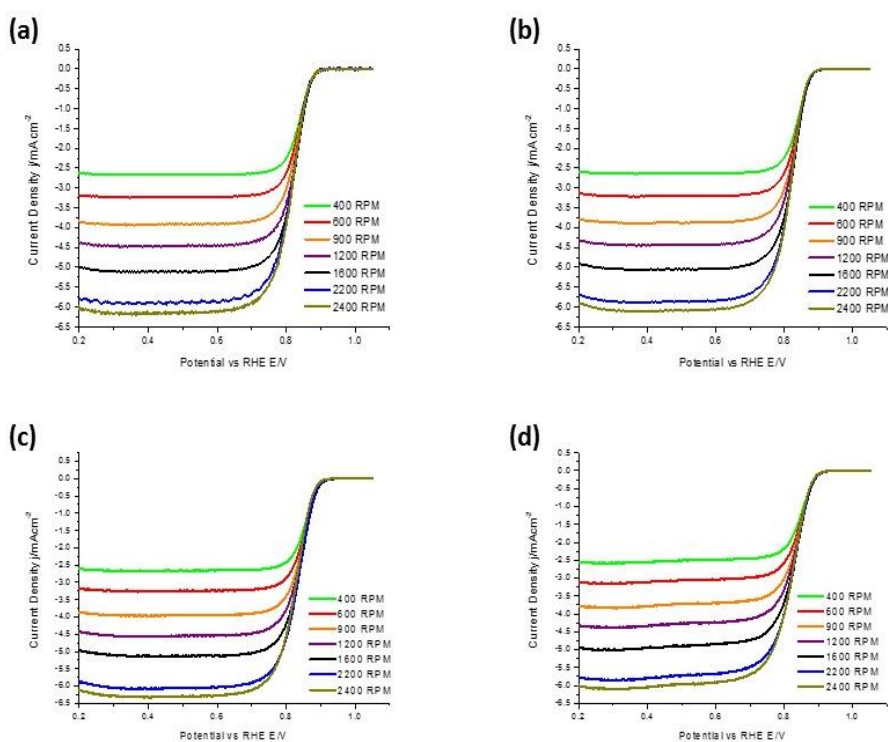Vulcan XC-72 were heat treated.   To start, the redox peak for $Co^{+2/+3}$ disappeared after heat treatment and the resulting CV profile has a similar shape to that of carbon (figure 3.32(a)).   In addition, although the onset potential didn't necessarily improve (figure 3.32(c)), the limiting current region showed a downward sloping trend after heat treatment.   This was in contrast to before heat treatment since the limiting current region was sloping upwards.   An upward sloping curve usually signifies that the overpotential is still playing a major role in hindering reaction kinetics. Therefore, changes that occurred with heat treatment seemed to have facilitated reaction kinetics and improved overall performance.   Similar to heat treated copper phthalocyanine on Vulcan XC-72, further analysis of the Koutecky-Levich graphs and calculations showed that the ORR proceeded for the majority through the four electron transfer mechanism as opposed to the two electron transfer method before heat treatment (figures 3.33, 3.34 and 3.35).

As mentioned earlier in this section, density functional theory calculations concluded that the Co^{+2}-N-C structure had an oxygen binding energy strong enough to facilitate the two electron reduction of oxygen. Likewise, the resulting experimental data supported this notion and before heat treatment, no evidence refuting this theory was present.   However, after heat treatment, many of the characteristics (XRD, UV-Vis spectra, CV) that are associated with the Co^{+2}-N-C structure are no longer visible. In addition, the ORR performance across different electrolytes before heat treatment showed random, different performances.   However, after heat treatment, the mixed kinetics and onset potential were unifom, and with the exception of KOH, the limiting current region have were similar as well. Cumulating these results, the conclusions allude that Co^{+2}-N-C sites no longer exist or exist in minute amounts after heat treatment.   If this is the case, the Co^{+2}-N-C sites can no longer be the active sites for the ORR and therefore, the ORR must proceed through a different pathway.

(a)

(b)

(c)
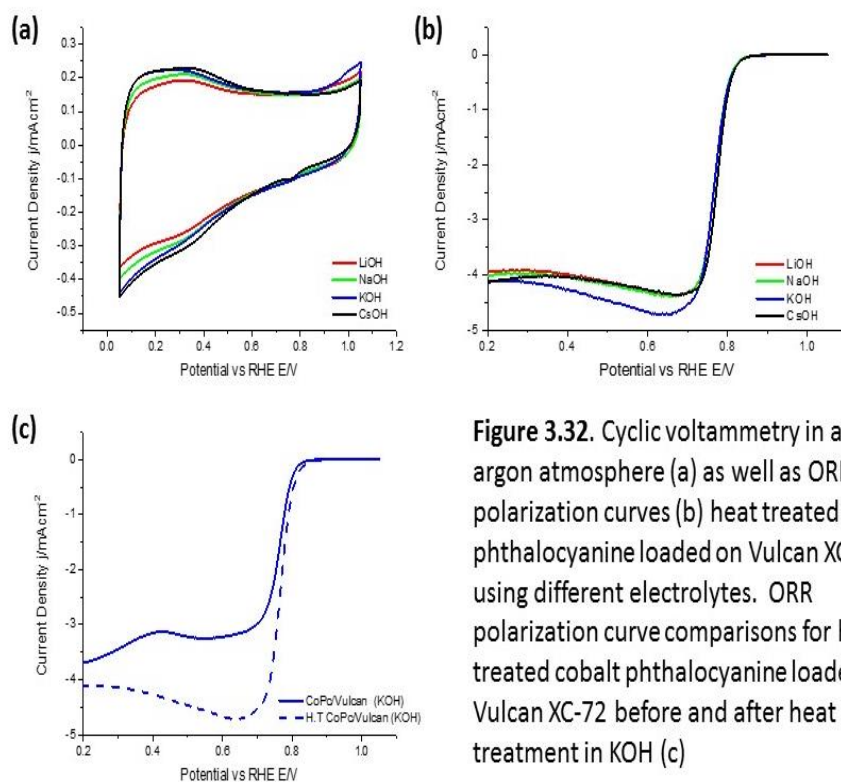
Figure 3.32. Cyclic voltammetry in an argon atmosphere (a) as well as ORR polarization curves (b) heat treated cobalt phthalocyanine loaded on Vulcan XC-72 using different electrolytes. ORR polarization curve comparisons for heat treated cobalt phthalocyanine loaded on Vulcan XC-72 before and after heat treatment in KOH (c)

Figure 3.33. ORR polarization curves taken at different rotation rates for heat treated cobalt phthalocyanine loaded on Vulcan XC-72 in LiOH (a), NaOH (b), KOH (c), and CsOH (d).
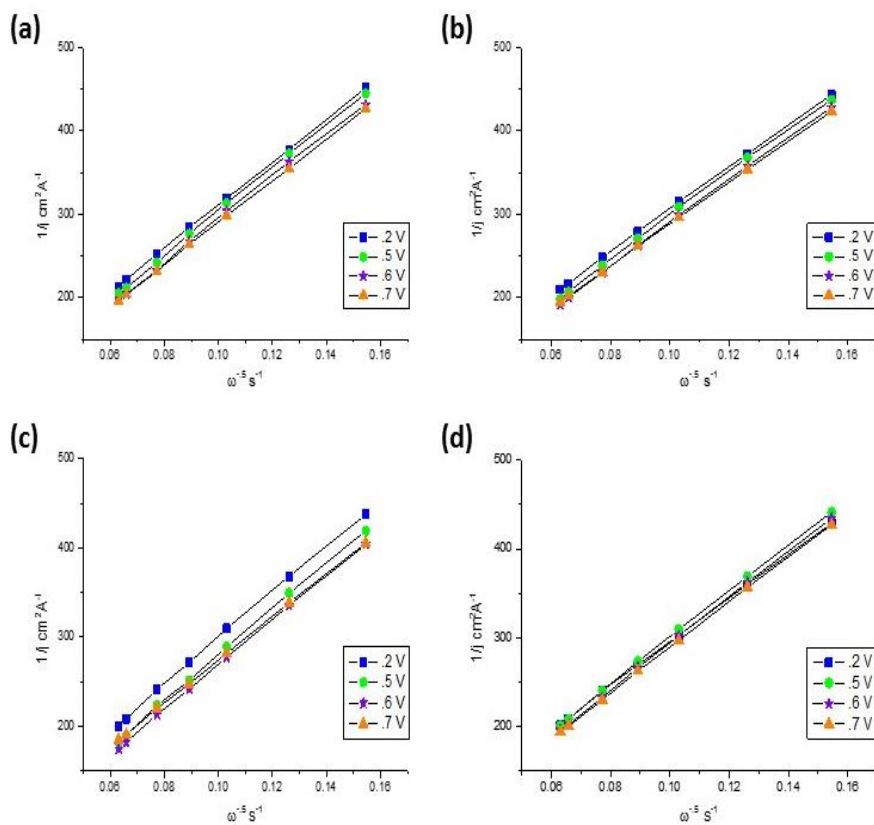
Figure 3.34. Koutecky-Levich plots for heat treated cobalt phthalocyanine loaded on Vulcan XC-72 in LiOH (a), NaOH (b), KOH (c), and CsOH (d).
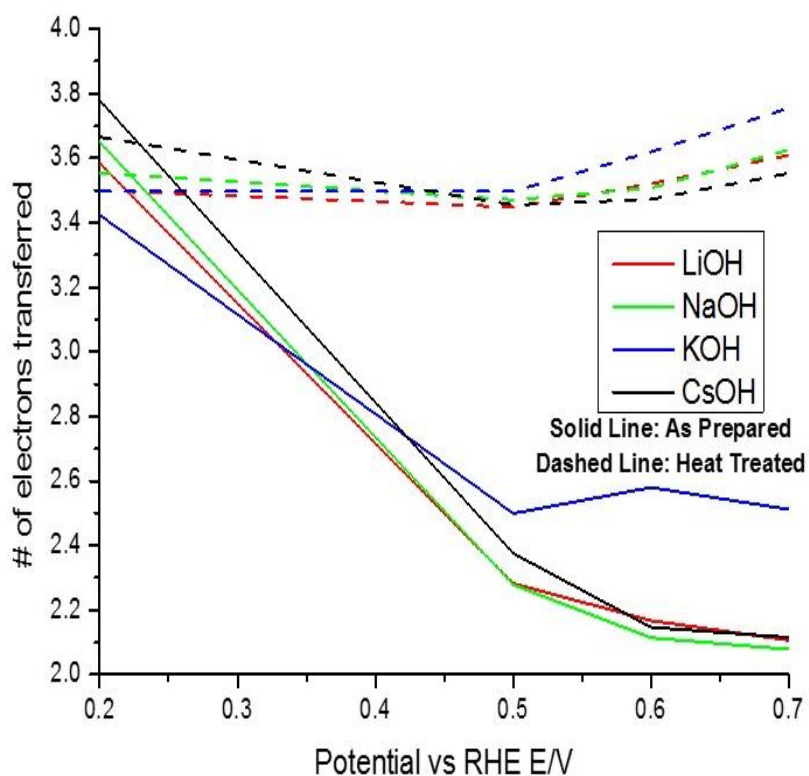
Figure 3.35. Number of electrons transferred for heat treated cobalt phthalocyanine loaded on Vulcan XC-72 at different voltages and in different electrolytes before (solid lines) and after (dashed lines) heat treatment.
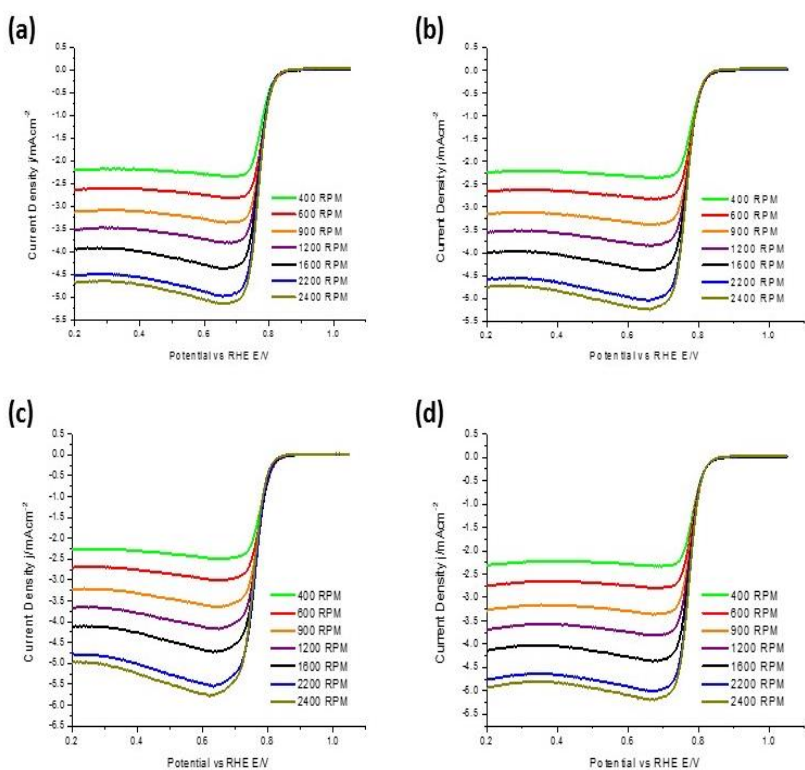
This hypothesis will be discussed further in the next segment.

Contrary to the other catalysts, a slight decrease in overall ORR activity was observed for iron phthalocyanine loaded on Vulcan XC-72 after heat treatment (figure 3.36(c)).   Analysis of the cyclic voltammetry profiles showed a drastic decrease in the intensity of the redox peaks that were distinctly present before heat treatment (figure 3.36(a)).   The redox peak that correlates to the $Fe^{+2/+3}$ redox still existed after heat treatment, but were nowhere near as intense as before.   In addition, when the ORR performance across different electrolytes was evaluated, differences could be discerned. ORR performance increased in the order of LiOH < KOH < NaOH < CsOH (figure 3.36(b)).   This trend is distinctly different from the trend before heat treatment when no noticeable changes were seen across different electrolytes. Koutecky-Levich calculations showed that the heat treated catalyst still favored the four electron transfer pathway for oxygen reduction (figures 3.37, 3.38 and 3.39).   However, though all of the approximate transfer numbers were four, the values of electron transfer were slightly lower across all electrolytes after heat treatment when compared to the transfer numbers before heat treatment (figure 3.39).   Similar to the results obtained with heat treated cobalt phthalocyanines loaded on Vulcan XC-72, data analysis of heat treated iron phthalocyanines on Vulcan XC-72 seems to imply that the Fe^{+2}-N-C coordinated sites are no longer the active sites for the ORR.

ORR polarization curve measurements taken in the presence of cyanide ions provided further evidence for this hypothesis.   As shown in figure 3.18(d), the cyanide ions created a significantly detrimental effect on the ORR by blocking the Fe ion sites.   However, although a decrease in performance was seen in the presence of heat treated iron phthalocyanine samples, the degree of performance drop off was nowhere near that of what it was before heat treatment.   Similar results reporting this unusual occurrence have been reported elsewhere but an explanation for this anomaly has yet to be found.[48]   Also, as figure 3.40 shows, the ORR
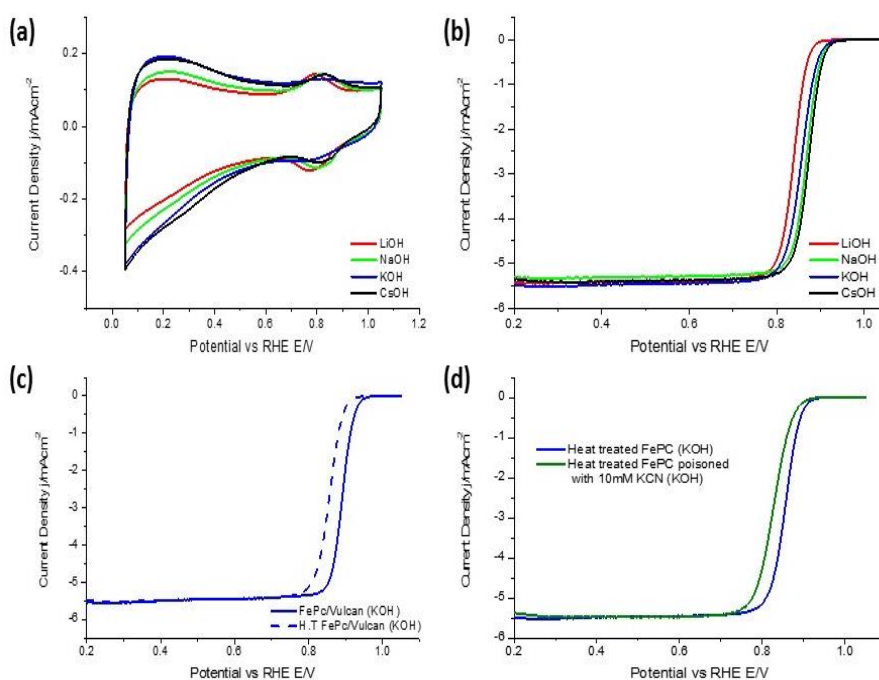
Figure 3.36. Cyclic voltammetry in an argon atmosphere (a) as well as ORR polarization curves (b) heat treated iron phthalocyanine loaded on Vulcan XC-72 using different electrolytes. ORR polarization curve comparisons for heat treated iron phthalocyanine loaded on Vulcan XC-72 before and after heat treatment in KOH (c) and the effect of KCN poisoning on iron phthalocyanine loaded on Vulcan XC-72 (d).

Figure 3.37. ORR polarization curves taken at different rotation rates for heat treated iron phthalocyanine loaded on Vulcan XC-72 in LiOH (a), NaOH (b), KOH (c), and CsOH (d).
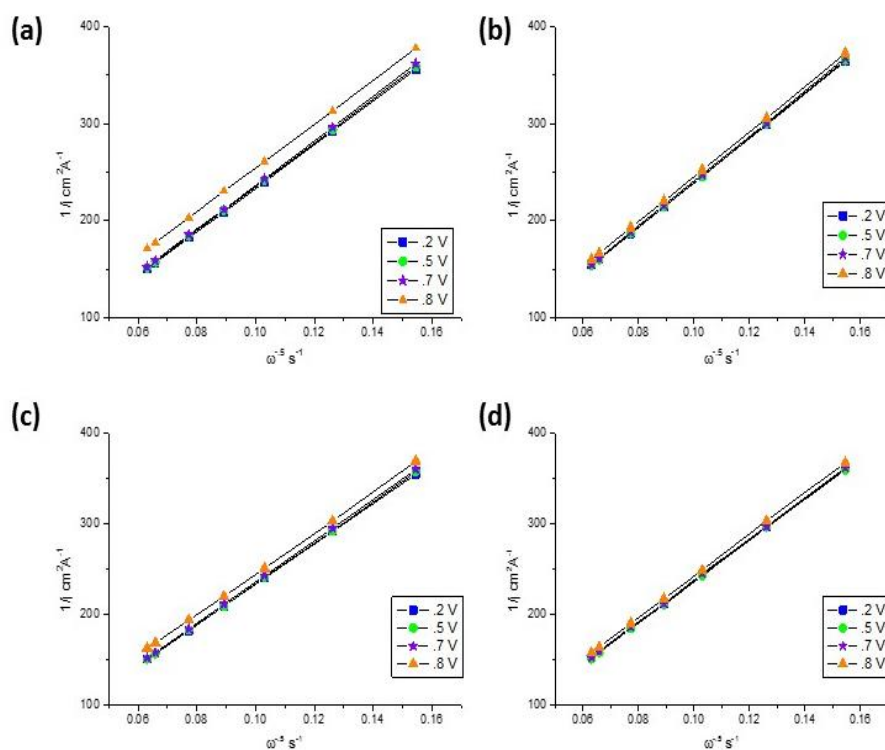
Figure 3.38. Koutecky-Levich plots for heat treated iron phthalocyanine loaded on Vulcan XC-72 in LiOH (a), NaOH (b), KOH (c), and CsOH (d).
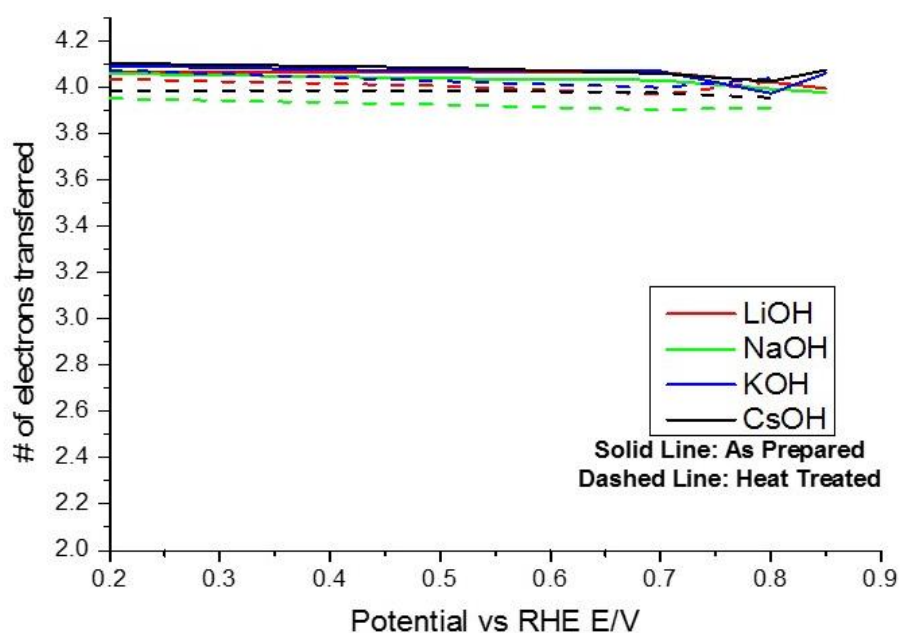
Figure 3.39. Number of electrons transferred for heat treated iron phthalocyanine loaded on Vulcan XC-72 at different voltages and in different electrolytes before (solid lines) and after (dashed lines) heat treatment.

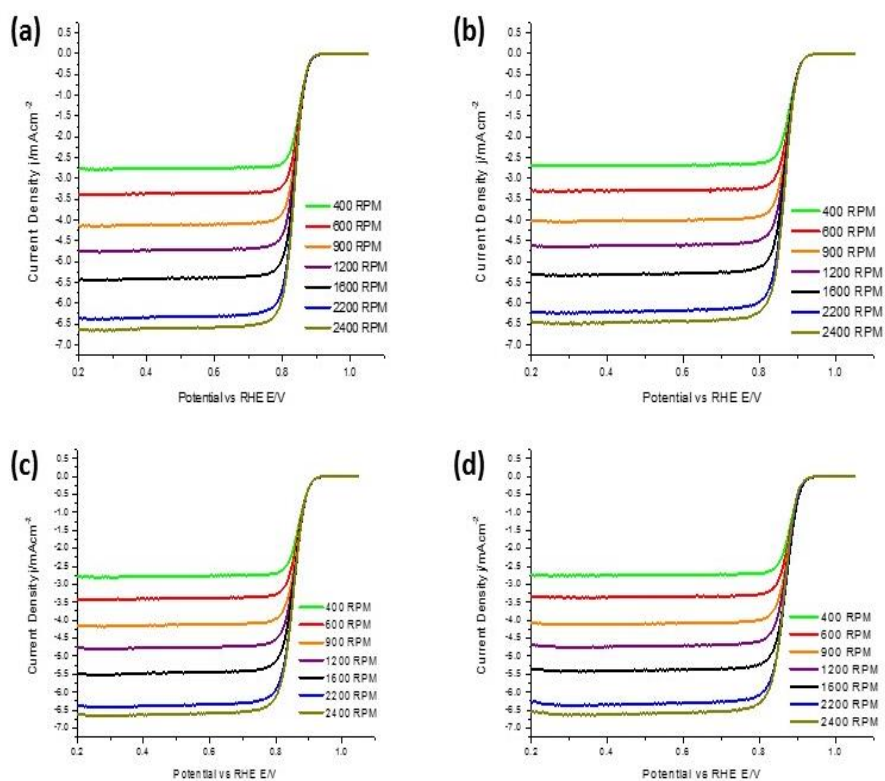activity of the poisoned heat treated iron phthalocyanine and heat treated copper phthalocyanine are nearly identical.   This surprising result could be explained if poisoning by cyanide eliminates the activity of the Fe^{+2}-N-C active sites that survived the heat treatment process.   The nearly identical ORR performance suggests that factors other than adsorption energy onto the catalyst surface influence the ORR reaction kinetics after heat treatment.

Figure 3.40 shows the ORR activity of the heat treated metal phthalocyanines on Vulcan XC-72. Vast improvement in ORR catalytic performance were seen for copper and cobalt phthalocyanines after heat treatment while pure Vulcan XC-72 and iron phthalocyanine showed performance degradation after heat treatment.   For the catalysts that are known to have a strong enough oxygen binding energy to catalyze the ORR through surface adsorption reactions in the inner Helmholtz plane, the trends in catalytic activity across different electrolytes changed before and after heat treatment.   However, for catalysts that are not known to bind oxygen to its surface, trends in ORR performance across difference electrolytes remained for the most part, the same before and after heat treatment.   All these results suggest that the pathway through which the ORR mechanism is proceeding after heat treatment is not reliant on the reactions at the inner Helmholtz plane.   In addition, heat treated copper and iron phthalocyanines poisoned with cyanide have nearly identical ORR polarization curves, implying that other influences may be determining the ORR kinetics.   Heat treated cobalt phthalocyanine possibly showed less activity than the two previously mentioned catalysts because different coordinated structures can hypothetically form during heat treatment.[59]   Structures where cobalt is coordinated to one or more nitrogen functional groups are found to be possible using density functional theory.[59]   These different coordinated structures could influence the characteristics, and in turn the ORR performance of heat treated cobalt phthalocyanine loaded on Vulcan XC-72.
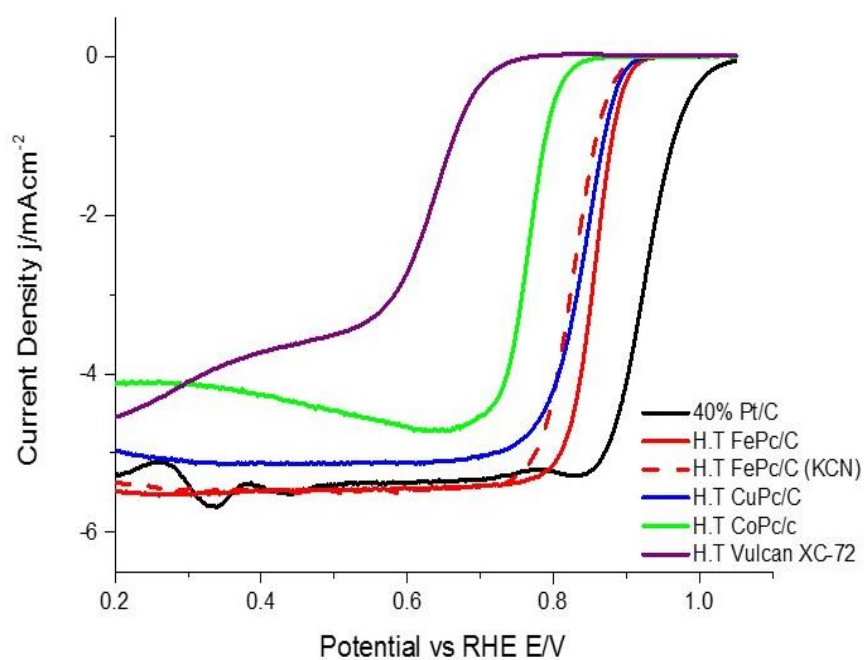
Figure 3.40. ORR polarization curves comparing 40% Johnson-Matthey Pt/C with heat treated Vulcan XC-72, copper phthalocyanine, cobalt phtalocyanine, iron phthalocyanine poisoned with KCN and iron phthalocyanine loaded on Vulcan XC-72.

3.4 Differences Due to Heat Treatment

3.4.1 The Role of Nitrogen

Numerous reports regarding non-precious metal catalysts all seem to agree that nitrogen needs to be present for a catalyst to have high catalytic activity.[74-76]   However, a controversy still remains in regards to what role the presence of nitrogen plays in catalyzing the reaction.   Reports that support the role of nitrogen as a stabilizing agent for metal ions[28], as a facilitator for the formation of the actual active site during heat treatment [77], as not being part of the active site but manipulating the carbon adjacent to the nitrogen to becoming the active site [30], and even as being the active site itself [17] have all been published.   Other reports have stressed the importance of the location of the nitrogen in determining the catalytic activity.[34] However, using a combination of experimental data and density functional theory calculations, Choi et al. concluded that although the oxygen binding energy was not enough to completely facilitate the complete reduction of oxygen to water, the presence of nitrogen doped sites on the catalyst surface can assist in facilitating the ORR in alkaline solutions.[17]   Specifically, they concluded that if the one electron reduction of oxygen to superoxide (O_2^-) was possible, superoxide adsorption onto the nitrogen doped sites and subsequent reduction to water would be possible.[17]   These novel and innovative conclusions are realistically possible since superoxide, once formed, is stable in alkaline solutions [14] and it is generally accepted that heat treatment leads to nitrogen doping of the carbon surface.[78]

X-ray photoelectron spectroscopy (XPS) spectra of the N 1s orbital before (figure 3.41) and after (figure 3.42) heat treatment showed that nitrogen enrichment occurred for the metal phthalocyanines loaded on Vulcan XC-72.   As expected, for Vulcan XC-72, no traces of nitrogen were
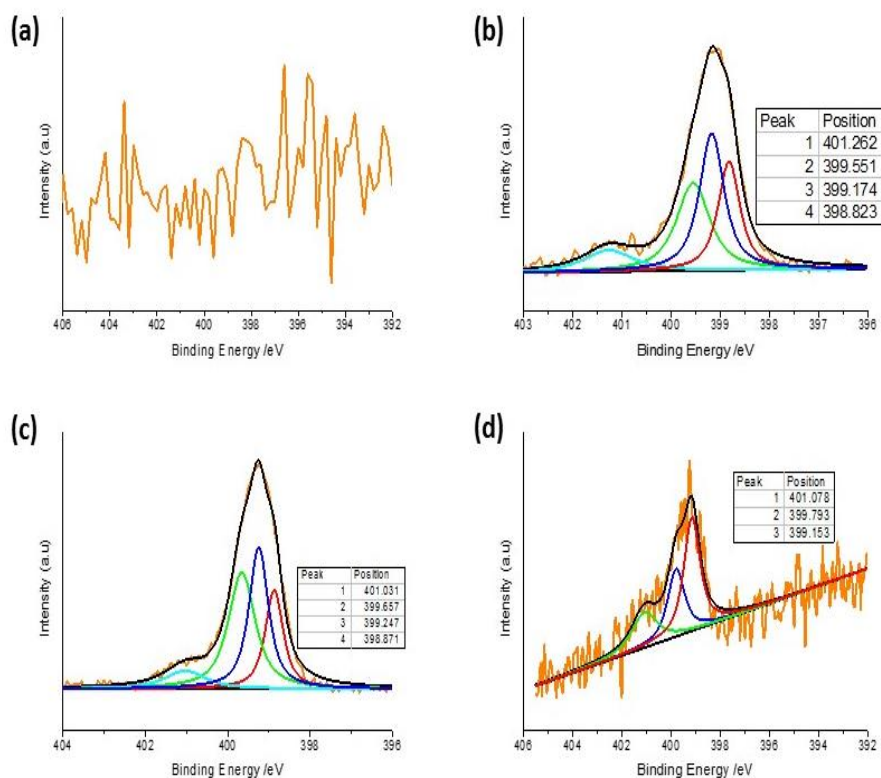
Figure 3.41. Nitrogen 1s spectra for Vulcan XC-72 (a), copper phthalocyanine on Vulcan XC-72 (b), cobalt phthalocyanine on Vulcan XC-72 (c), and iron phthalocyanine on Vulcan XC-72 (d).
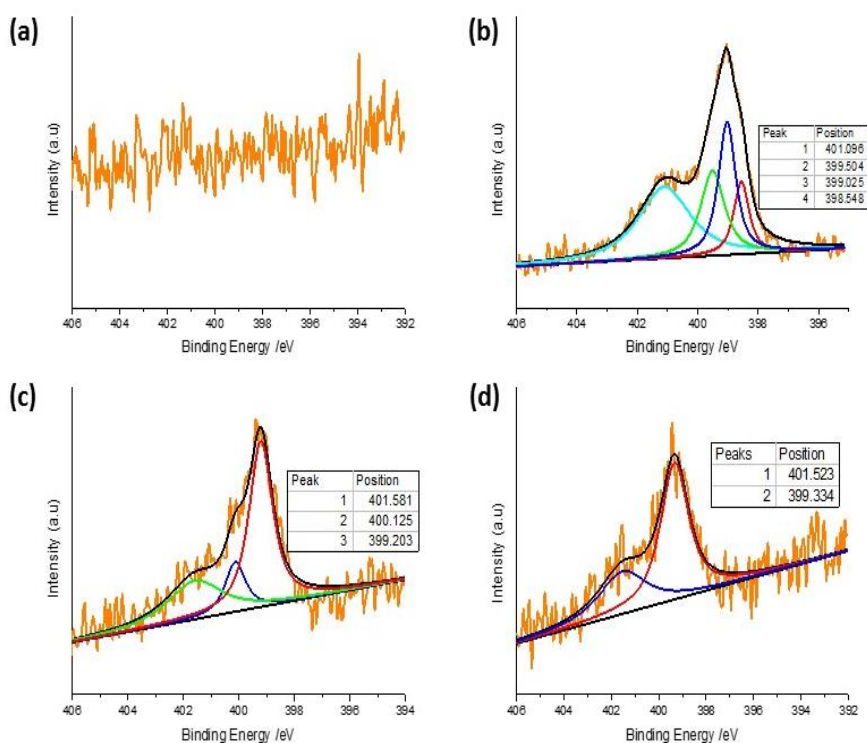
Figure 3.42. Nitrogen 1s spectra for heat treated Vulcan XC-72 (a), copper phthalocyanine on Vulcan XC-72 (b), cobalt phthalocyanine on Vulcan XC-72 (c), and iron phthalocyanine on Vulcan XC-72 (d).

detected (figure 3.41(a)).   Deconvolution of the nitrogen spectra for the metal phthalocyanines loaded on Vulcan XC-72 showed peaks that could be associated to pyridinic (≈398.6 eV), pyrrolic (≈ 400 eV) and graphitic nitrogen (≥ 401.3 eV).[34]   It is hard to say with conviction that the peaks before 400 eV are truly pyridinic and pyrrolic nitrogen peaks though because the nitrogen found in phthalocyanines exhibits peaks at similar electron volts.[79, 80].   Therefore, since graphitic nitrogen peaks arise past 401 eV and thus, could be directly linked to nitrogen doping of the carbon surface, a ratio of the area of nitrogen peaks found after 400 eV to the area of nitrogen peaks found before 400 eV were compared before and after heat treatment. As table 3.5 shows, this ratio increased after heat treatment for all the metal phthalocyanines loaded on Vulcan XC-72.

From the XPS data results, certain conclusions could be made. First, the increase in ratio of graphitic nitrogen after heat treatment suggested that the metal phthalocyanines do break down during heat treatment and the originally coordinated nitrogen proceeds to enrich the carbon surface. Second, the nitrogen doped carbon sites seem to play an integral role in the catalysis of oxygen since pure Vulcan XC-72, which had no nitrogen content, proceeded through the two electron reduction pathway after heat treatment. It is not likely that the complete oxygen reduction reaction occurs on N-doped carbons because both density functional theory calculations[17] and experimental results showing that even "metal-free" catalysts probably are influenced by trace metal impurities[29], conclude that these sites do not have a strong enough oxygen binding energy.   However, although the exact role is still unknown, experimental data shown here and numerous published reports prove that these nitrogen sites are part of the oxygen reduction reaction scheme in heat treated catalysts.   As mentioned earlier, Choi et al calculated that these N-doped carbons would be able to facilitate superoxide reduction to water[17].   Coupled with the fact that superoxide ions are more stable in alkaline mediums than acidic mediums[14], it is hard to refute the

Name	Pyridinic and Pyrrolic (Less than 400 ev) Nitrogen Peak Area		Graphitic (401-402 ev) Nitrogen Peak Area		Graphitic Nitrogen — (Pyridinic + Pyrrolic Nitrogen)	
	As prepared	Heat Treated	As prepared	Heat Treated	As prepared	Heat Treated
CuPc Vulcan	1.928	2.258	1.203	2.05	.624	.908
CoPc Vulcan	1.857	1.905	1.188	2.358	.640	1.238
FePc Vulcan	1.597	1.418	1.239	2.404	.776	1.695

Table 3.5. Peak areas and the ratio of graphitic to pyridinic and pyrrolic nitrogen present before and after heat treatment for metal phthalocyanines loaded on Vulcan XC-72.

notion that the enhanced ORR performance of non-precious metal catalysts in alkaline electrolytes is heavily influenced by superoxide ion stability and nitrogen doped carbon sites.

3.4.2 Possible Reaction Pathways

Based off of the results extracted from this study, the following model for the ORR on non-precious metal catalysts in alkaline mediums is proposed. As figure 3.43 shows, for catalysts able to bind oxygen (cobalt and iron phthalocyanine), oxygen diffuses into the inner layer and adsorbs onto the surface. The reaction then proceeds either through the two or four electron reduction method depending on adsorption strength. For catalysts that cannot adsorb oxygen onto its surface (Vulcan XC-72 and copper phthalocyanine), single electron transfer from the electrode to oxygen in solution at the outer layer occurs either through surface functional groups present on the carbon surface or through the phthalocyanine material itself, creating a superoxide ion. If no other catalytic sites are present, the superoxide ion is converted into a peroxide intermediate and subsequently reduced to peroxide in solution. Electron transfer from the electrode to the outer Helmholtz plane have also been supported in other reports and the Mukerjee group even stated that the inner Helmholtz plane catalyst is non-specific for the two electron reduction reaction in alkaline solutions.[15] This reaction scheme also explains why similarities and differences are seen between Vulcan XC-72, copper phthalocyanine, and cobalt phthalocyanine (figure 3.44). Even though they all catalyze the two electron reduction of oxygen to peroxide, copper phthalocyanine on Vulcan XC-72 and pure Vulcan XC-72 show similar catalytic behavior since they both utilize electron transfer to the outer Helmholtz plane and the formation of superoxide to reduce oxygen. Cobalt phthalocyanine shows different behavior because oxygen reduction occurs through an inner Helmholtz plane

Figure 3.43. Schematic illustration of the electron transfer processes occurring before heat treatment.
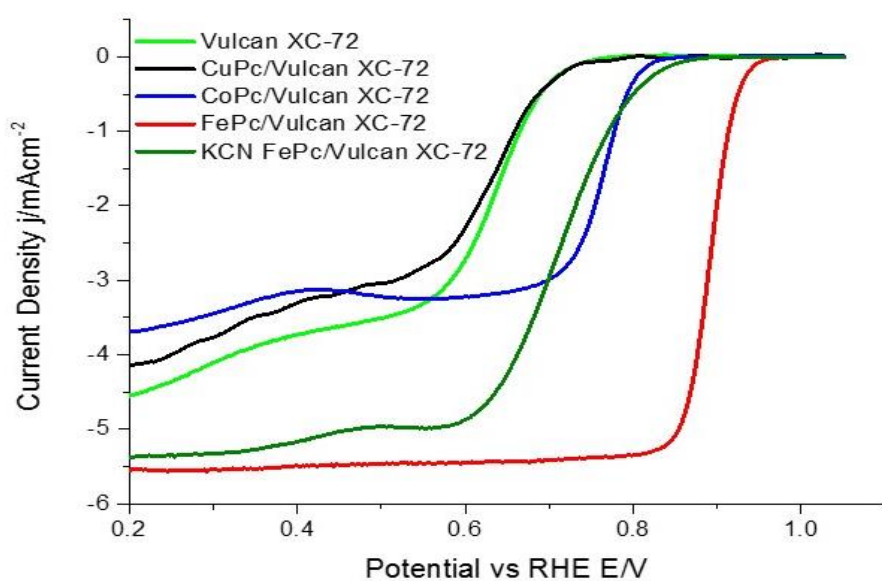
Figure 3.44. Comparison of catalytic ORR activity before heat treatment.

reaction, meaning that different reaction kinetics influence the overall performance.   Iron phthalocyanine loaded on Vulcan XC-72 facilitates the complete reduction of oxygen to water through an inner Helmholtz plane reaction.   The optimal or near optimal oxygen adsorption strength of Fe^{+2}-N-C sites allow oxygen to bind and remain adsorbed until it is completely reduced.   Therefore, before heat treatment, the only pathway for the complete four electron reduction of oxygen is through the well-known reactant adsorption onto a catalyst surface pathway.

Figure 3.45 shows the reaction pathways that are present after heat treatment.   Based off of the experimental results, heat treatment causes decomposition of the metal phthalocyanines and subsequent transformation of the metal ions to either metal particles or metal oxides.   In addition, the nitrogen that was originally coordinated to the metal ion is released and proceeds to dope the carbon surface, creating a nitrogen rich carbon surface. Although some M^+-N-C or derivatives of M^+-N-C sites may survive the heat treatment process, the concentration of sites that survive is probably minute and therefore cannot play a major factor in the overall ORR performance. Instead, the formation of oxides and or metal particles on the catalyst surface favor the electron transfer pathway across the oxide or particle from the electrode to the outer Helmholtz plane.   Similar to before heat treatment, this electron transfer leads to the formation of superoxide ions.   However, the presence of nitrogen sites on the carbon sites provide active sites for superoxide ions to bind to and undergo further reduction.   Giving credence to this theory is that reactions occurring over multiple sites with reaction intermediates being able to migrate or diffuse to different catalyst sites have been shown in previously published reports.[63, 81]

Comparing the ORR performance across different electrolytes before and after heat treatment gave further support of the proposed reaction pathway.   Copper phthalocyanine and Vulcan XC-72 exhibited the same trends in performance before and after heat treatment since both catalysts
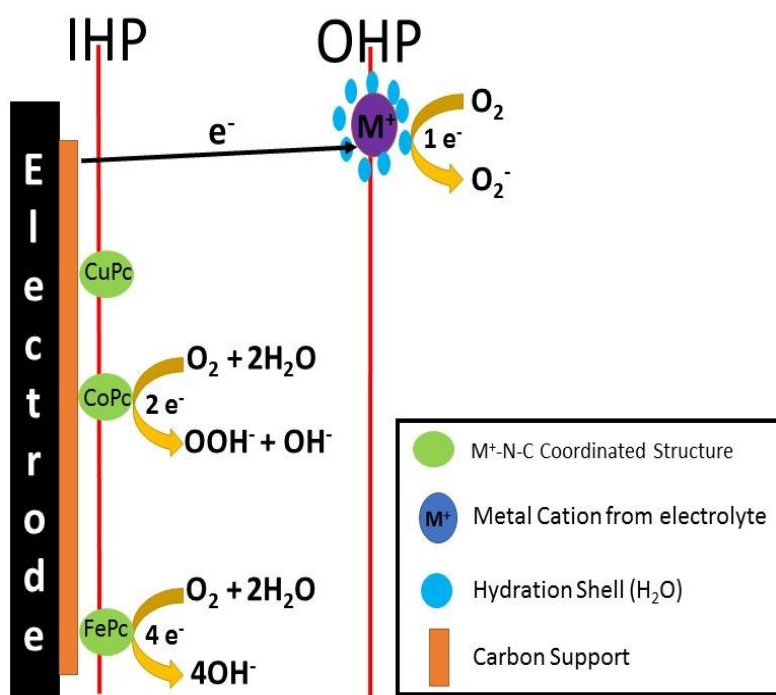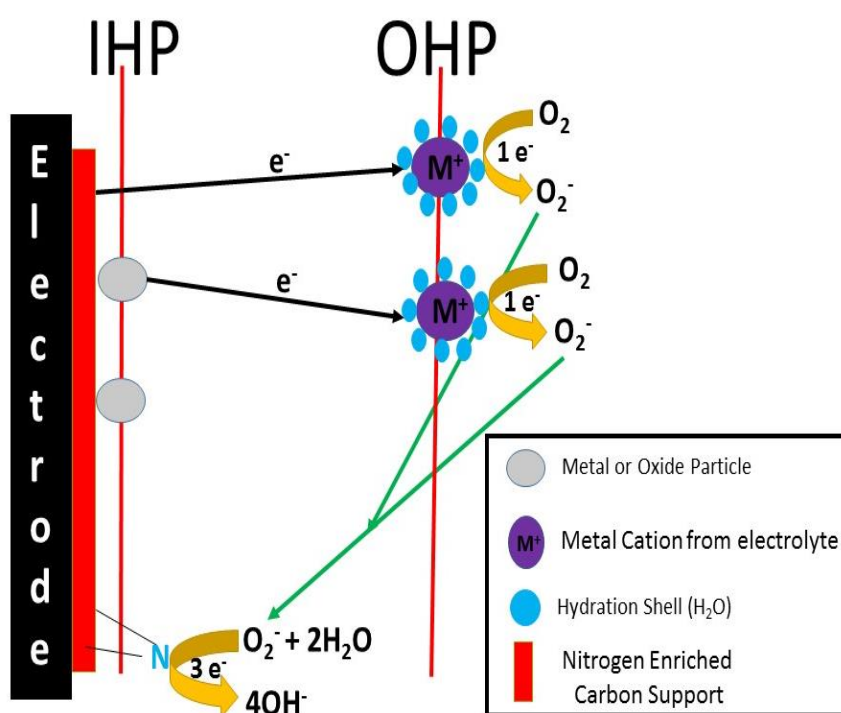
Figure 3.45. Schematic illustration of the electron transfer processes occurring after heat treatment.
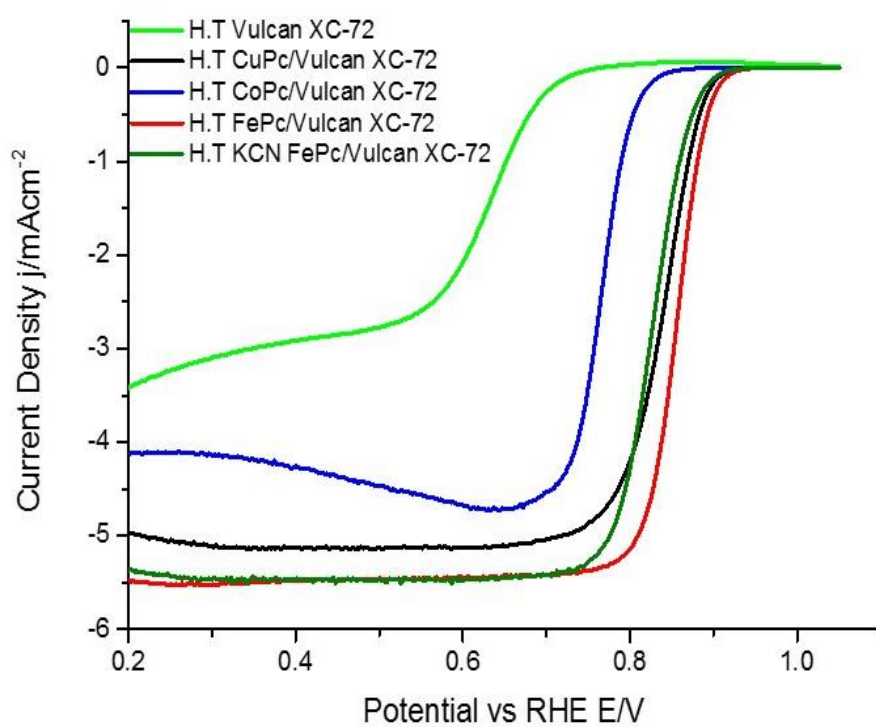
Figure 3.46. Comparison of catalytic ORR activity after heat treatment.

utilize the outer Helmholtz plane reaction in both situations. The only differences between the two catalysts after heat treatment are that the copper phthalocyanine loaded on Vulcan XC-72 contains a nitrogen enriched surface. The absence of these nitrogen doped sites seems to be the reason why Vulcan XC-72 can only catalyze the two electron reduction of oxygen even after heat treatment while copper phthalocyanine on Vulcan XC-72 shows four electron reduction kinetics. Cobalt and iron phthalocyanine loaded on Vulcan XC-72 showed different trends in performance across different electrolytes before and after heat treatment. This is likely due to the catalysts operating through the inner Helmholtz plane reaction before heat treatment and through the outer Helmholtz plane reaction after heat treatment. Assuming that the cyanide poisoning, removes the surviving M^+-N-C sites, the ORR performance of heat treated iron phthalocyanine loaded on Vulcan XC-72 poisoned with KCN should be similar to that of heat treated copper phthalocyanine loaded on Vulcan XC-72. This was the case as shown in figure 3.46. Based on these results, heat treated cobalt phthalocyanine should also exhibit catalytic activity similar to that of heat treated copper and iron phthalocyanine. However, this anomaly is probably due to cobalt phthalocyanine being able to form many Co^{+x}-N-C derivatives during the heat treatment process.[59] The similar onset potential and mixed kinetics region before and after heat treatment implies that the inner Helmholtz plane reaction may still be playing a major role even after heat treatment for cobalt phtalocyanines loaded on Vulcan XC-72. However, Koutecky-Levich calculations showed that the heat treated cobalt phthalocyanine operating through a four electron transfer reaction. In addition, XPS measurements suggest that nitrogen enrichment occurred as well. Therefore, it can be concluded that even if the inner Helmholtz plane reaction is still favored over the outer Helmholtz plane reaction in heat treated cobalt phthalocyanine loaded on Vulcan XC-72, the peroxide intermediates from the reaction might be migrating to the nitrogen sites on

the carbon surface and being reduced further.   Although, both iron phthalocyanine and heat treated iron phthalocyanine proceed through the transfer of four electrons, different pathways likely led to different kinetic influences.   Factors such as reactant loss during migration between active sites, could explain the slightly lower performance of heat treated iron phthalocyanine catalysts when compared with as prepared iron phthalocyanine catalysts.   Also, due to methods for directly observing the double layer not being available, it is difficult to explain exactly why differences in performances are seen across different alkaline electrolytes. However, differences in hydration energy of the metal cations offer a possible explanation.   A higher hydration energy results in a larger hydration shell around the cation.[82]   Therefore, metal cations that have a high hydration energy, and thus a larger hydration shell, would not be able to approach the catalyst surface as close as a metal cation with a lower hydration energy.   Assuming this hypothesis is true, the distance of metal cations from closest to the surface would be in the order of $Cs^+ < K^+ < Na^+ < Li^+$.   At high overpotentials, the differences in distance does not play a major role in the kinetics of the reaction.   However, if electron tunneling to the outer Helmholtz plane is vital toward the reduction of oxygen, lower overpotentials will lead to a greater repulsion between the electrode surface and the metal cations in the outer Helmholtz plane.   This greater distance between the outer Helmholtz plane and the electrode could lead to difficulties in electron tunneling to create the superoxide at the outer Helmholtz plane.   Therefore, the cation furthest away from the surface (Li+) would be affected first, which is evidenced in the ORR polarization curves.   As previously mentioned, it is impossible to confirm that this scenario is taking place, but the trends in performance across different electrolytes for all the heat treated catalysts follow the trends in hydration energy, which in turn, correlates to the distance away from the electrode.

Chapter 4: Conclusions

4.1 Conclusions

Analysis of the experimental data combined with information from previously published reports shows that the oxygen reduction reaction in alkaline mediums does not necessarily have to occur through surface adsorption.   Instead, many factors in both the inner and outer Helmholtz plane determine the overall catalytic performance toward the oxygen reduction reaction.

The overall lower potentials at the electrode in alkaline electrolytes allow for the outer Helmholtz plane to approach closer to the catalyst surface than what would be possible in acidic electrolytes.   For catalysts requiring reactant adsorption upon its surface to catalyze the reaction (i.e. platinum), the closer outer Helmholtz plane is detrimental to overall catalytic activity since the solvated metal cations present at the outer Helmholtz plane can hinder reactant diffusion to the catalyst surface.

Contrary to the previous notion though, the outer Helmholtz plane is vital for facilitating oxygen reduction after heat treatment.   Heat treatment was found to destroy many of the coordinated structures that serve as the active sites for inner Helmholtz plane catalysis.   However, the formation of nitrogen enriched carbon surfaces along with the conversion of metal ions to metal particles or metal oxides provide another pathway for the complete four electron reduction of oxygen.   The shorter distance between the electrode and outer Helmholtz plane allows for electron transfer from the electrode to the solvated cation in the outer Helmholtz plane via the newly formed metal particle or metal oxide.   Oxygen in the solution can then be reduced to the superoxide ion, which can then migrate to a nitrogen site and undergo further reduction.   Thus, though the influence of the outer

Helmholtz plane could be detrimental for non-precious metal catalysts that rely on binding of oxygen to its surface, the reactions that occur through the outer Helmholtz plane are vital after heat treatment and provide a practical explanation for the drastic increase in catalytic activity observed for most catalysts after heat treatment.

4.2 Implications for Future Research

The phthalocyanines used in this study showed very competitive activity with that of platinum and therefore may beg the question of why aren't they currently used as fuel cell catalysis.   Unfortunately, though technically a non-precious metal catalyst, the cost of metal phthalocyanines is comparable to that of platinum.   As a result, commercialization of fuel cells using a phthalocyanine catalyst would not be practical.   However, the findings from this study can be applied toward finding a viable alternative to platinum in the future.

Figure 3.47 shows the ORR polarization curves for 40% Johnson-Matthey Pt/C as well as some of the better performing catalysts from this study.   As seen in the graph, iron phthalocyanine loaded on Vulcan XC-72 showed the closest activity to platinum.   It was concluded from experimental analysis and information from other published reports that the Fe^{+2}/Fe^{+3} redox peak controls the ORR activity.   Therefore, methods to add functional groups or substitute in groups that would shift the redox peak to higher potentials could hypothetically improve the ORR performance.   Ates et al. applied a similar concept to lithium-ion batteries with successful results, which show that this concept may be realistically possible.[83]

Although heat treatment leads to nitrogen enrichment of the carbon surface, an overall loss of nitrogen content occurs as well.[78]   Elemental analysis confirmed that heat treated metal phthalocyanines are no exception to this loss(table 3.6).   A high loss in nitrogen concentration during heat

treatment could diminish the number of superoxide adsorption sites necessary for further reduction.   Therefore, methods for enriching the carbon surface with nitrogen and facilitating electron transfer without the use of heat treatment could lead to catalysts that could be tailor made toward the oxygen reduction reaction.   Once again, methods to add functional groups that can facilitate the electron transfer to the outer Helmholtz plane as well as provide adsorption sites for superoxide ions could result in true metal free catalysts that possess high catalytic activity coupled with safe and economically friendly synthesis methods.   The energy demands of society have been and will continue to rise. However, advancements in renewable energy sources provide hope that clean, renewable energy sources will be able to supply these energy demands sooner rather than later.
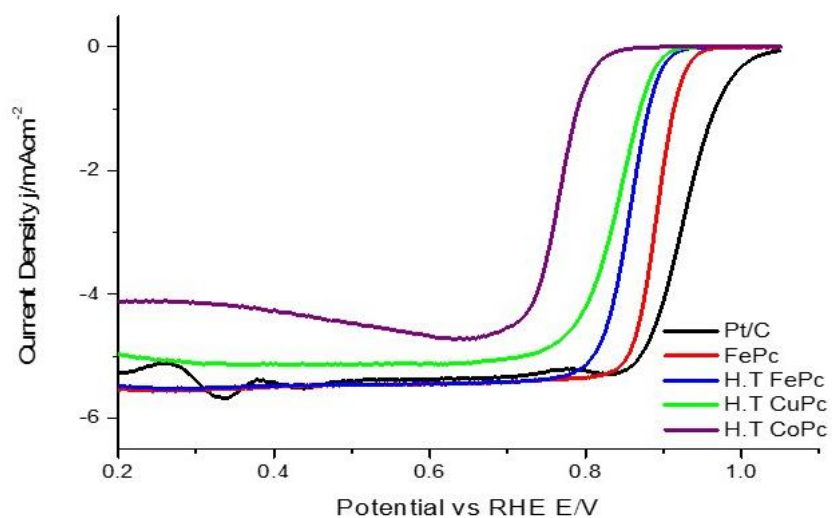
Figure 3.47. ORR polarization curves of the non-precious metal catalysts used in this study that had the highest catalytic activity.

Sample	Carbon %		Nitrogen %	
	Before Heat Treatment	After Heat Treatment	Before Heat Treatment	After Heat Treatment
Vulcan XC-72	98.83	100	0	0
Copper phthalocyanine on Vulcan XC-72	97.58	99.33	2.91	.56
Cobalt phthalocyanine on Vulcan XC-72	93.09	98.20	3.06	1.06
Iron phthalocyanine on Vulcan XC-72	97.31	98.65	1.315	.35

Table 3.6. Weight percent of carbon and nitrogen present in the catalysts before and after heat treatment as determined by elemental analysis.

References

[1] L. Carrette, K. Friedrich, U. Stimming, Fuel Cells-Fundamentals and Applications, Fuel Cells, 1 (2001) 5-39.

[2] R. O'Hayre, S.-W. Cha, F.B. Prinz, W. Colella, Fuel Cell Fundamentals, Wiley 2005.

[3] J. Zhang, PEM Fuel Cell Electrocatalysts and Catalyst Layers: Fundamentals and Applications, Springer 2008.

[4] X.Y. Zhou, Z. Chen, F. Delgado, D. Brenner, R. Srivastava, Atomistic Simulation of Conduction and Diffusion Processes in Nafion Polymer Electrolyte and Experimental Validation, Journal of the Electrochemical Society, 154 (2007) B82-B87.

[5] A.A. Gewirth, M.S. Thorum, Electroreduction of Dioxygen for Fuel-Cell Applications: Materials and Challenges, Inorganic Chemistry, 49 (2010) 3557-3566.

[6] G. Girishkumar, B. McCloskey, A.C. Luntz, S. Swanson, W. Wilcke, Lithium-Air Battery: Promise and Challenges, The Journal of Physical Chemistry Letters, 1 (2010) 2193-2203.

[7] A.J. Bard, M.A. Fox, Artificial Photosynthesis - Solar Splitting of Water to Hydrogen and Oxygen, Accounts of Chemical Research, 28 (1995) 141-145.

[8] J.K. Nørskov, J. Rossmeisl, A. Logadottir, L. Lindqvist, J.R. Kitchin, T. Bligaard, H. Jonsson, Origin of the Overpotential for Oxygen Reduction at a Fuel-Cell Cathode, Journal of Physical Chemistry B, 108 (2004) 17886-17892.

[9] T.H. Yu, T. Hofmann, Y. Sha, B.V. Merinov, D.J. Myers, C. Heske, W.A. Goddard, Finding Correlations of the Oxygen Reduction Reaction Activity of Transition Metal Catalysts with Parameters Obtained from Quantum Mechanics, Journal of Physical Chemistry C, 117 (2013) 26598-26607.

[10] C. Lu, I.C. Lee, R.I. Masel, A. Wieckowski, C. Rice, Correlations Between the Heat of Adsorption and the Position of the Center of the d-band: Differences Between Computation and Experiment, Journal of Physical Chemistry A, 106 (2002) 3084-3091.

[11] T. Hofmann, T.H. Yu, M. Folse, L. Weinhardt, M. Bar, Y.F. Zhang, B.V. Merinov, D.J. Myers, W.A. Goddard, C. Heske, Using Photoelectron Spectroscopy and Quantum Mechanics to Determine d-Band Energies of Metals for Catalytic Applications, Journal of Physical Chemistry C, 116 (2012) 24016-24026.

[12] F. Abild-Pedersen, A. Nilsson, J.K. Nørskov, Comment on "Using Photoelectron Spectroscopy and Quantum Mechanics to Determine d-Band Energies of Metals for Catalytic Applications", Journal of Physical Chemistry C, 117 (2013) 6914-6915.

[13] P. Quaino, N.B. Luque, R. Nazmutdinov, E. Santos, W. Schmic

kler, Why is Gold Such a Good Catalyst for Oxygen Reduction in A lkaline Media?, Angewandte Chemie - International Edition, 51 (201 2) 12997-13000.

[14] B.B. Blizanac, P.N. Ross, N.M. Markovic, Oxygen eEectroredu ction on Ag(111): The pH Effect, Electrochimica Acta, 52 (2007) 2 264-2271.

[15] N. Ramaswamy, S. Mukerjee, Influence of Inner- and Outer-S phere Electron Transfer Mechanisms during Electrocatalysis of Oxy gen Reduction in Alkaline Media, Journal of Physical Chemistry C, 115 (2011) 18015-18026.

[16] N. Ramaswamy, S. Mukerjee, Fundamental Mechanistic Unders tanding of Electrocatalysis of Oxygen Reduction on Pt and Non-Pt Surfaces: Acid versus Alkaline Media, Advances in Physical Chemis try, 2012 (2012) 1-17.

[17] C.H. Choi, H.K. Lim, M.W. Chung, J.C. Park, H. Shin, H. Kim, S.I. Woo, Long-Range Electron Transfer over Graphene-Based Cat alyst for High-Performing Oxygen Reduction Reactions: Importance of Size, N-doping, and Metallic Impurities, Journal of the America n Chemical Society, 136 (2014) 9070-9077.

[18] A.J. Bard, L.R. Faulkner, Electrochemical Methods: Fundament als and Applications, 2nd ed., Wiley New York2001.

[19] C.-J. Yang, An Impending Platinum Crisis and its Implications

for the Future of the Automobile, Energy Policy, 37 (2009) 1805-1 808.

[20] Q. Li, R. He, J.-A. Gao, J.O. Jensen, N.J. Bjerrum, The CO Po isoning Effect in PEMFCs Operational at Temperatures up to 200°C , Journal of The Electrochemical Society, 150 (2003) A1599.

[21] J.J. Baschuk, X.G. Li, Carbon Monoxide Poisoning of Proton E xchange Membrane Fuel Cells, International Journal of Energy Rese arch, 25 (2001) 695-713.

[22] A. Kolics, A. Wieckowski, Adsorption of Bisulfate and Sulfate Anions on a Pt (111) Electrode, Journal of Physical Chemistry B, 1 05 (2001) 2588-2595.

[23] J. Mostany, E. Herrero, J.M. Feliu, J. Lipkowski, Thermodyna mic Studies of Anion Adsorption at Stepped Platinum (hkl) Electrod e Surfaces in Sulfuric Acid Solutions, Journal of Physical Chemistry B, 106 (2002) 12787-12796.

[24] R. Subbaraman, D. Strmcnik, V. Stamenkovic, N.M. Markovic, Three Phase Interfaces at Electrified Metal—Solid Electrolyte Syste ms 1. Study of the Pt(hkl)—Nafion Interface, Journal of Physical Ch emistry C, 114 (2010) 8414-8422.

[25] K. Kodama, R. Jinnouchi, T. Suzuki, H. Murata, T. Hatanaka, Y. Morimoto, Increase in Adsorptivity of Sulfonate Anions on Pt (1 11) Surface with Drying of Ionomer, Electrochemistry Communicati

ons, 36 (2013) 26-28.

[26] K. Gong, F. Du, Z. Xia, M. Durstock, L. Dai, Nitrogen-Doped Carbon Nanotube Arrays with High Electrocatalytic Activity for Oxygen Reduction, Science, 323 (2009) 760-764.

[27] Y. Li, W. Zhou, H. Wang, L. Xie, Y. Liang, F. Wei, J.C. Idrobo, S.J. Pennycook, H. Dai, An Oxygen Reduction Electrocatalyst Based on Carbon Nanotube-Graphene Complexes, Nature Nanotechnology, 7 (2012) 394-400.

[28] G. Wu, K.L. More, C.M. Johnston, P. Zelenay, High-Performance Electrocatalysts for Oxygen Reduction Derived from Polyaniline, Iron, and Cobalt, Science, 332 (2011) 443-447.

[29] L. Wang, A. Ambrosi, M. Pumera, "Metal-free" Catalytic Oxygen Reduction Reaction on Heteroatom-Doped Graphene is Caused by Trace Metal Impurities, Angewandte Chemie - International Edition, 52 (2013) 13818-13821.

[30] L. Yu, X.L. Pan, X.M. Cao, P. Hu, X.H. Bao, Oxygen Reduction Reaction Mechanism on Nitrogen-Doped Graphene: A Density Functional Theory Study, Journal of Catalysis, 282 (2011) 183-190.

[31] F. Cheng, J. Chen, Metal-Air Batteries: From Oxygen Reduction Electrochemistry to Cathode Catalysts, Chemical Society Reviews, 41 (2012) 2172-2192.

[32] H. Zhu, S.J. Paddison, T.A. Zawodzinski Jr, The Effects of the Ligand, Central Metal, and Solvent on the O2 Binding of Non-Precious Metal Catalyst Model Systems: An ab initio Study, Electrochimica Acta, 101 (2013) 293-300.

[33] Z. Shi, J.J. Zhang, Density Functional Theory Study of Transitional Metal Macrocyclic Complexes' Dioxygen-Binding Abilities and their Catalytic Activities toward Oxygen Reduction Reaction, Journal of Physical Chemistry C, 111 (2007) 7084-7090.

[34] T. Sharifi, G. Hu, X. Jia, T. Wågberg, Formation of Active Sites for Oxygen Reduction Reactions by Transformation of Nitrogen Functionalities in Nitrogen-Doped Carbon Nanotubes, ACS Nano, 6 (2012) 8904-8912.

[35] D. Strmcnik, K. Kodama, D. van der Vliet, J. Greeley, V.R. Stamenkovic, N.M. Markovic, The Role of Non-Covalent Interactions in Electrocatalytic Fuel-Cell Reactions on Platinum, Nature Chemistry, 1 (2009) 466-472.

[36] D. Strmcnik, D.F. van der Vliet, K.C. Chang, V. Komanicky, K. Kodama, H. You, V.R. Stamenkovic, N.M. Marković, Effects of Li+, K+, and Ba2+ Cations on the ORR at Model and High Surface Area Pt and Au Surfaces in Alkaline Solutions, The Journal of Physical Chemistry Letters, 2 (2011) 2733-2736.

[37] I. Katsounaros, K.J. Mayrhofer, The Influence of Non-Covalent Interactions on the Hydrogen Peroxide Electrochemistry on Platin

um in Alkaline Electrolytes, Chemical Communications, 48 (2012) 6
660-6662.

[38] N. Danilovic, R. Subbaraman, D. Strmcnik, A. Paulikas, D. Mye
rs, V. Stamenkovic, N. Markovic, The Effect of Noncovalent Intera
ctions on the HOR, ORR, and HER on Ru, Ir, and Ru0. 50Ir0. 50 M
etal Surfaces in Alkaline Environments, Electrocatalysis, 3 (2012) 2
21-229.

[39] I.S. Park, K.S. Lee, J.H. Choi, H.Y. Park, Y.E. Sung, Surface S
tructure of Pt-Modified Au Nanoparticles and Electrocatalytic Activi
ty in Formic Acid Electro-oxidation, Journal of Physical Chemistry
C, 111 (2007) 19126-19133.

[40] K.J. Mayrhofer, B.B. Blizanac, M. Arenz, V.R. Stamenkovic, P.
N. Ross, N.M. Markovic, The Impact of Geometric and Surface Ele
ctronic Properties of Pt-Catalysts on the Particle Size Effect in Ele
ctrocatalysis, Journal of Physical Chemistry B, 109 (2005) 14433-1
4440.

[41] M. Wakisaka, Y. Udagawa, H. Suzuki, H. Uchida, M. Watanabe
, Structural Effects on the Surface Oxidation Processes at Pt Singl
e-Crystal Electrodes Studied by X-ray Photoelectron Spectroscopy,
 Energy & Environmental Science, 4 (2011) 1662-1666.

[42] N.M. Markovic, T.J. Schmidt, V. Stamenkovic, P.N. Ross, Oxy
gen Reduction Reaction on Pt and Pt Bimetallic Surfaces: A Selecti
ve Review, Fuel Cells, 1 (2001) 105-116.

[43] M.J.T.C. van der Niet, N. Garcia-Araez, J. Hernández, J.M. Feliu, M.T.M. Koper, Water Dissociation on Well-Defined Platinum Surfaces: The Electrochemical Perspective, Catalysis Today, 202 (2013) 105-113.

[44] K.J. Schouten, M.J. van der Niet, M.T. Koper, Impedance Spectroscopy of H and OH adsorption on Stepped Single-Crystal Platinum Electrodes in Alkaline and Acidic Media, Physical Chemistry Chemical Physics, 12 (2010) 15217-15224.

[45] C. Stoffelsma, P. Rodriguez, G. Garcia, N. Garcia-Araez, D. Strmcnik, N.M. Markovic, M.T. Koper, Promotion of the Oxidation of Carbon Monoxide at Stepped Platinum Single-Crystal Electrodes in Alkaline Media by Lithium and Beryllium Cations, Journal of the American Chemical Society, 132 (2010) 16127-16133.

[46] D.F. van der Vliet, M.T.M. Koper, Electrochemistry of Pt (100) in Alkaline Media: A Voltammetric Study, Surface Science, 604 (2010) 1912-1918.

[47] F. Ghani, J. Kristen, H. Riegler, Solubility Properties of Unsubstituted Metal Phthalocyanines in Different Types of Solvents, Journal of Chemical and Engineering Data, 57 (2012) 439-449.

[48] M.S. Thorum, J.M. Hankett, A.A. Gewirth, Poisoning the Oxygen Reduction Reaction on Carbon-Supported Fe and Cu Electrocatalysts: Evidence for Metal-Centered Activity, The Journal of Physical Chemistry Letters, 2 (2011) 295-298.

[49] R.R. Chen, H.X. Li, D. Chu, G.F. Wang, Unraveling Oxygen Reduction Reaction Mechanisms on Carbon-Supported Fe-Phthalocyanine and Co-Phthalocyanine Catalysts in Alkaline Solutions, Journal of Physical Chemistry C, 113 (2009) 20689-20697.

[50] V. Bambagioni, C. Bianchini, J. Filippi, A. Lavacchi, W. Oberhauser, A. Marchionni, S. Moneti, F. Vizza, R. Psaro, V. Dal Santo, A. Gallo, S. Recchia, L. Sordelli, Single-Site and Nanosized Fe-Co Electrocatalysts for Oxygen Reduction: Synthesis, Characterization and Catalytic Performance, Journal of Power Sources, 196 (2011) 2519-2529.

[51] T. Nagaoka, T. Sakai, K. Ogura, T. Yoshino, Oxygen Reduction at Electrochemically Treated Glassy-Carbon Electrodes, Analytical Chemistry, 58 (1986) 1953-1955.

[52] J.A. Menéndez, J. Phillips, B. Xia, L.R. Radovic, On the Modification and Characterization of Chemical Surface Properties of Activated Carbon: In the Search of Carbons with Stable Basic Properties, Langmuir : The ACS Journal of Surfaces and Colloids, 12 (1996) 4404-4410.

[53] P. Trogadas, T.F. Fuller, P. Strasser, Carbon as Catalyst and Support for Electrochemical Energy Conversion, Carbon, 75 (2014) 5-42.

[54] S.J. Percival, B. Zhang, Electrocatalytic Reduction of Oxygen at Single Platinum Nanowires, Journal of Physical Chemistry C, 117

(2013) 13928-13935.

[55] W. Bian, Z. Yang, P. Strasser, R. Yang, A CoFe2O4/Graphene Nanohybrid as an Efficient Bi-Functional Electrocatalyst for Oxygen Reduction and Oxygen Evolution, Journal of Power Sources, 250 (2014) 196-203.

[56] R. Silva, D. Voiry, M. Chhowalla, T. Asefa, Efficient Metal-Free Electrocatalysts for Oxygen Reduction: Polyaniline-Derived N- and O-Doped Mesoporous Carbons, Journal of the American Chemical Society, 135 (2013) 7823-7826.

[57] S. Kundu, T.C. Nagaiah, W. Xia, Y.M. Wang, S. Van Dommele, J.H. Bitter, M. Santa, G. Grundmeier, M. Bron, W. Schuhmann, M. Muhler, Electrocatalytic Activity and Stability of Nitrogen-Containing Carbon Nanotubes in the Oxygen Reduction Reaction, Journal of Physical Chemistry C, 113 (2009) 14302-14310.

[58] K.C. Honeychurch, J.P. Hart, The Chronoamperometric and Voltammetric Behaviour of Glutathione at Screen-Printed Carbon Micro-Band Electrodes Modified with Cobalt Phthalocyanine, Advances in Analytical Chemistry, 2 (2012) 46-52.

[59] Z. Shi, H.S. Liu, K. Lee, E. Dy, J. Chlistunoff, M. Blair, P. Zelenay, J.J. Zhang, Z.S. Liu, Theoretical Study of Possible Active Site Structures in Cobalt- Polypyrrole Catalysts for Oxygen Reduction Reaction, Journal of Physical Chemistry C, 115 (2011) 16672-16680.

[60] S. Baranton, C. Coutanceau, E. Garnier, J.M. Léger, How Does α-FePc Catalysts Dispersed onto High Specific Surface Carbon Support Work Towards Oxygen Reduction Reaction (ORR)?, Journal of Electroanalytical Chemistry, 590 (2006) 100-110.

[61] C.H. Barlow, J.C. Maxwell, W.J. Wallace, W.S. Caughey, Elucidation of the Mode of Binding of Oxygen to Iron in Oxyhemoglobin by Infrared Spectroscopy, Biochemical and Biophysical Research Communications, 55 (1973) 91-95.

[62] M.F. Perutz, Regulation of Oxygen Affinity of Hemoglobin: Influence of Structure of the Globin on the Heme Iron, Annual Review of Biochemistry, 48 (1979) 327-386.

[63] U. Tylus, Q. Jia, K. Strickland, N. Ramaswamy, A. Serov, P. Atanassov, S. Mukerjee, Elucidating Oxygen Reduction Active Sites in Pyrolyzed Metal-Nitrogen Coordinated Non-Precious-Metal Electrocatalyst Systems, Journal of Physical Chemistry C, 118 (2014) 8999-9008.

[64] N. Ramaswamy, U. Tylus, Q. Jia, S. Mukerjee, Activity Descriptor Identification for Oxygen Reduction on Nonprecious Electrocatalysts: Linking Surface Science to Coordination Chemistry, Journal of the American Chemical Society, (2013).

[65] A.B. Anderson, R.A. Sidik, Oxygen Electroreduction on Fe II and Fe III Coordinated to N4 Chelates. Reversible Potentials for the Intermediate Steps from Quantum Theory, Journal of Physical Che

mistry B, 108 (2004) 5031-5035.

[66] W.M. Li, J. Wu, D.C. Higgins, J.Y. Choi, Z.W. Chen, Determination of Iron Active Sites in Pyrolyzed Iron-Based Catalysts for the Oxygen Reduction Reaction, ACS Catalysis, 2 (2012) 2761-2768.

[67] B. Stöhr, H.P. Boehm, R. Schlögl, Enhancement of the Catalytic Activity of Activated Carbons in Oxidation Reactions by Thermal Treatment with Ammonia or Hydrogen Cyanide and Observation of a Superoxide Species as a Possible Intermediate, Carbon, 29 (1991) 707-720.

[68] C.W.B. Bezerra, L. Zhang, K.C. Lee, H.S. Liu, A.L.B. Marques, E.P. Marques, H.J. Wang, J.J. Zhang, A Review of Fe-N/C and Co-N/C Catalysts for the Oxygen Reduction Reaction, Electrochimica Acta, 53 (2008) 4937-4951.

[69] I.T. Bae, D.A. Tryk, D.A. Scherson, Effect of Heat Treatment on the Redox Properties of Iron Porphyrins Adsorbed on High Area Carbon in Acid Electrolytes: An in situ Fe K-edge X-ray Absorption Near-Edge Structure Study, Journal of Physical Chemistry B, 102 (1998) 4114-4117.

[70] F. Jaouen, M. Lefèvre, J.-P. Dodelet, M. Cai, Heat-treated Fe/N/C Catalysts for O2 Electroreduction: Are Active Sites Hosted in Micropores?, Journal of Physical Chemistry B, 110 (2006) 5553-5558.

[71] H.P. Boehm, Some Aspects of the Surface-Chemistry of Carbon-Blacks and Other Carbons, Carbon, 32 (1994) 759-769.

[72] D.R. Dreyer, S. Park, C.W. Bielawski, R.S. Ruoff, The Chemistry of Graphene Oxide, Chemical Society Reviews, 39 (2010) 228-240.

[73] D.R. Dreyer, A.D. Todd, C.W. Bielawski, Harnessing the Chemistry of Graphene Oxide, Chemical Society Reviews, 43 (2014) 5288-5301.

[74] K. Parvez, S. Yang, Y. Hernandez, A. Winter, A. Turchanin, X. Feng, K. Mullen, Nitrogen-Doped Graphene and its Iron-Based Composite as Efficient Electrocatalysts for Oxygen Reduction Reaction, ACS Nano, 6 (2012) 9541-9550.

[75] L.T. Qu, Y. Liu, J.B. Baek, L.M. Dai, Nitrogen-Doped Graphene as Efficient Metal-Free Electrocatalyst for Oxygen Reduction in Fuel Cells, ACS Nano, 4 (2010) 1321-1326.

[76] G. Lalande, R. Cote, D. Guay, J. Dodelet, L. Weng, P. Bertrand, Is Nitrogen Important in the Formulation of Fe-based Catalysts for Oxygen Reduction in Solid Polymer Fuel Cells?, Electrochimica Acta, 42 (1997) 1379-1388.

[77] P.H. Matter, L. Zhang, U.S. Ozkan, The Role of Nanostructure in Nitrogen-Containing Carbon Catalysts for the Oxygen Reduction Reaction, Journal of Catalysis, 239 (2006) 83-96.

[78] G. Wu, P. Zelenay, Nanostructured Nonprecious Metal Catalysts for Oxygen Reduction Reaction, Accounts of Chemical Research, 46 (2013) 1878-1889.

[79] S. Kera, M.B. Casu, K.R. Bauchspiess, D. Batchelor, T. Schmidt, E. Umbach, Growth Mode and Molecular Orientation of Phthalocyanine Molecules on Metal Single Crystal Substrates: A NEXAFS and XPS study, Surface Science, 600 (2006) 1077-1084.

[80] P. Zhao, L.H. Niu, L. Huang, F.S. Zhang, Electrochemical and XPS investigation of Phthalocyanine Oligomer Sulfonate as a Corrosion Inhibitor for Iron in Hydrochloric Acid, Journal of the Electrochemical Society, 155 (2008) C515-C520.

[81] T.S. Olson, S. Pylypenko, J.E. Fulghum, P. Atanassov, Bifunctional Oxygen Reduction Reaction Mechanism on Non-Platinum Catalysts Derived from Pyrolyzed Porphyrins, Journal of the Electrochemical Society, 157 (2010) B54-B63.

[82] W.R. Fawcett, Examination of the Role of Ion Size in Determining Double Layer Properties on the Basis of a Generalized Mean Spherical Approximation, Journal of Electroanalytical Chemistry, 500 (2001) 264-269.

[83] M.N. Ates, C.J. Allen, S. Mukerjee, K.M. Abraham, Electronic Effects of Substituents on Redox Shuttles for Overcharge Protection of Li-ion Batteries, Journal of the Electrochemical Society, 159 (2012) A1057-A1064.

국 문 초 록

알칼리 전해질에서 비귀금속 촉매의
산소환원반응에 대한 외부 헬름홀츠면 영향의
전기화학적 조사

이영원
화학생물공학부
서울대학원

화석연료의 지속적인 고갈과 우리 사회의 에너지 수요 증가는 계속해서 대체 에너지원에 대한 연구를 가속화시키고 있다. 이런 연구를 통해 만들어진 에너지 소자들은 에너지 수요를 충족시킬만한 충분한 가능성을 가지고 있지만 대부분의 경우 희귀하거나 고가인 물질들이 높은 효율의 소자를 구동하기 위해서 필요하다는 단점이 있다. 이러한 전기화학적 에너지 소자를 대표적으로 잘 보여주는 것이 바로 연료전지이다. 산화환원반응을 통해 화학에너지를 전기에너지로 변환하는 연료전지는 청정하고 재이용이 가능하며 무독성의 에너지원이라는 장점이 있으며, 이러한 점에서 잠재적으로 미래 에너지 수요를 충족하는데 중요한 역할을 할 수 있다고 평가된다. 그러나 연료전지의 공기극에서 일어나는 산소환원반응은 높은 과전압을 가지고 있고, 종종 연료전지 상용화의 가장 큰 문제로 보여진다. 그 결과, 알맞은 가격과 내구성이 있는 촉매들을 개발하여

과전압을 줄이고 연료전지의 효율을 높이는 연구가 지속적으로 핵심 주제로서 진행이 되고 있다.

최근 연구들은 질소화합물에 금속이온을 결합하여 열처리한 물질들의 알칼리 전해질에서 산소환원에 대한 높은 촉매 활성을 보고해왔다. 이러한 촉매들은 백금을 대체할만한 물질들로 각광받지만 그 활성 부위에 대한 정보, 또는 어떻게 산소환원반응이 진행되는지는 아직도 의문점이 남아 있다. 결론적으로 이러한 점들이 밝혀지지 않는 한 촉매들의 최적화 역시 힘들다고 볼 수 있다.

이 연구는 산소환원반응의 활성부위와 가능한 반응경로를 구리, 코발트, 철 금속 프탈로시아닌을 이용하여 조사하는 것에 초점을 맞추었다. 이런 금속 이온들은 서로 다른 산소 흡착 에너지를 가지기 때문에 그에 따라 다른 산소환원반응 활성이 관찰되었다. 추가로, 피독 실험에서는 매우 큰 활성 감소가 나타났고 이로 인해 열처리 전 촉매들에 대해서는 M^+-N-C 구조가 활성 부위라는 것과 산소환원반응이 2전자 반응 또는 4전자 반응경로로 진행되는 것이 산소 흡착 세기에 영향을 받는다는 것을 보이고자 한다.

그러나 이런 구조들은 열처리를 통해 분해 될 수 밖에 없고 산소환원반응의 반응경로를 변화시킬 수 밖에 없다. 이런 가설을 확인하기 위해 수산화 리튬, 수산화 나트륨, 수산화 칼륨 그리고 수산화 세슘 전해질을 이용해 열처리 전후의 프탈로시아닌 촉매들에 대해 전기화학적 측정을 수행하였다. 열처리 전과 후의 코발트와 철 프탈로시아닌에서 산소환원반응 활성의 경향이 변하였고 이것은 서로 다른 반응경로가 선호된다는 것을 보여준다. 열처리 후의 변화를 살펴보기 위해 X선 회절 실험, X선 광전자 분광법 그리고 자외선/가시선 분광법을 이용해 물리적 특성 측정을 수행하였다. 이 열처리 후 촉매의 실험결과에서, 산소는 외부헬름홀츠면 반응으로 초과산화물로 먼저 변화하고 추가적으로 질소가 도핑 된 부위에서 완전히

환원되는 것으로 나타났다. 이런 결과들은 열처리 후 관찰되는 높은 수준의 촉매활성과 그 높은 활성이 알칼리 전해질에서만 관찰되는 것에 대한 어느 정도 타당한 설명이라고 할 수 있다.

주요어: 비귀금속 촉매, 산소환원반응, 알칼리 연료전지, 내부 및 외부 헬름홀츠면 반응

학번: 2013-22533